Załącznik nr 1/1
do Zarządzenia Rektora PG nr 30/2022 z 14 kwietnia 2022 r.

POLITECHNIKA GDAŃSKA

Imię i nazwisko autora rozprawy: **Karolina Milewska**
Dyscyplina naukowa: **Inżynieria Materiałowa**

ROZPRAWA DOKTORSKA

Tytuł rozprawy w języku polskim: **Wytwarzanie, struktura i właściwości luminescencyjne szkieł i szkło-ceramik boranowo-bizmutowych domieszkowanych jonami ziem rzadkich**

Tytuł rozprawy w języku angielskim: **Synthesis, structure and luminescence properties of borate-bismuth glasses and glass-ceramics doped with rare earth ions**

Promotor *podpis*
prof. dr hab. inż. Barbara Kościelska

Gdańsk, rok 2024

Załącznik nr 1/2
do Zarządzenia Rektora PG nr 30/2022 z 14 kwietnia 2022 r.

GDAŃSK UNIVERSITY OF TECHNOLOGY

The author of the doctoral dissertation: **Karolina Milewska**
Scientific discipline: **Material Engineering**

DOCTORAL DISSERTATION

Title of doctoral dissertation: **Synthesis, structure and luminescence properties of borate-bismuth glasses and glass-ceramics doped with rare earth ions**

Title of doctoral dissertation (in Polish): **Wytwarzanie, struktura i właściwości luminescencyjne szkieł i szkło-ceramik boranowo-bizmutowych domieszkowanych jonami ziem rzadkich**

Supervisor *signature*
prof. dr hab. inż. Barbara Kościelska

Gdańsk, year 2024

POLITECHNIKA GDAŃSKA

OŚWIADCZENIE

Autor rozprawy doktorskiej: Karolina Milewska

Ja, niżej podpisany(a), oświadczam, iż jestem świadomy(a), że zgodnie z przepisem art. 27 ust. 1 i 2 ustawy z dnia 4 lutego 1994 r. o prawie autorskim i prawach pokrewnych (t.j. Dz.U. z 2021 poz. 1062), uczelnia może korzystać z mojej rozprawy doktorskiej zatytułowanej:
„Wytwarzanie, struktura i właściwości luminescencyjne szkieł i szkło-ceramik boranowo-bizmutowych domieszkowanych jonami ziem rzadkich" do prowadzenia badań naukowych lub w celach dydaktycznych.[1]

Świadomy(a) odpowiedzialności karnej z tytułu naruszenia przepisów ustawy z dnia 4 lutego 1994 r. o prawie autorskim i prawach pokrewnych i konsekwencji dyscyplinarnych określonych w ustawie Prawo o szkolnictwie wyższym i nauce (Dz.U.2021.478 t.j.), a także odpowiedzialności cywilno-prawnej oświadczam, że przedkładana rozprawa doktorska została napisana przeze mnie samodzielnie.

Oświadczam, że treść rozprawy opracowana została na podstawie wyników badań prowadzonych pod kierunkiem i w ścisłej współpracy z promotorem prof. dr hab. inż. Barbarą Kościelską.

Niniejsza rozprawa doktorska nie była wcześniej podstawą żadnej innej urzędowej procedury związanej z nadaniem stopnia doktora.

Wszystkie informacje umieszczone w ww. rozprawie uzyskane ze źródeł pisanych i elektronicznych, zostały udokumentowane w wykazie literatury odpowiednimi odnośnikami, zgodnie z przepisem art. 34 ustawy o prawie autorskim i prawach pokrewnych.

Potwierdzam zgodność niniejszej wersji pracy doktorskiej z załączoną wersją elektroniczną.

Gdańsk, dnia ....
podpis doktoranta

Ja, niżej podpisany(a), wyrażam zgodę na umieszczenie ww. rozprawy doktorskiej w wersji elektronicznej w otwartym, cyfrowym repozytorium instytucjonalnym Politechniki Gdańskiej.

Gdańsk, dnia ....
podpis doktoranta

[1] Art. 27. 1. Instytucje oświatowe oraz podmioty, o których mowa w art. 7 ust. 1 pkt 1, 2 i 4–8 ustawy z dnia 20 lipca 2018 r. – Prawo o szkolnictwie wyższym i nauce, mogą na potrzeby zilustrowania treści przekazywanych w celach dydaktycznych lub w celu prowadzenia działalności naukowej korzystać z rozpowszechnionych utworów w oryginale i w tłumaczeniu oraz zwielokrotniać w tym celu rozpowszechnione drobne utwory lub fragmenty większych utworów.
2. W przypadku publicznego udostępniania utworów w taki sposób, aby każdy mógł mieć do nich dostęp w miejscu i czasie przez siebie wybranym korzystanie, o którym mowa w ust. 1, jest dozwolone wyłącznie dla ograniczonego kręgu osób uczących się, nauczających lub prowadzących badania naukowe, zidentyfikowanych przez podmioty wymienione w ust. 1.

POLITECHNIKA GDAŃSKA

STATEMENT

The author of the doctoral dissertation: Karolina Milewska

I, the undersigned, declare that I am aware that in accordance with the provisions of Art. 27 (1) and (2) of the Act of 4th February 1994 on Copyright and Related Rights (Journal of Laws of 2021, item 1062), the university may use my doctoral dissertation entitled:
"Synthesis, structure and luminescence properties of borate-bismuth glasses and glass-ceramics doped with rare earth ions" for scientific or didactic purposes.[1]

Gdańsk,..... .....
signature of the PhD student

Aware of criminal liability for violations of the Act of 4th February 1994 on Copyright and Related Rights and disciplinary actions set out in the Law on Higher Education and Science(Journal of Laws 2021, item 478), as well as civil liability, I declare, that the submitted doctoral dissertation is my own work.

I declare, that the submitted doctoral dissertation is my own work performed under and in cooperation with the supervision of prof. dr hab. inż. Barbara Kościelska.

This submitted doctoral dissertation has never before been the basis of an official procedure associated with the awarding of a PhD degree.

All the information contained in the above thesis which is derived from written and electronic sources is documented in a list of relevant literature in accordance with Art. 34 of the Copyright and Related Rights Act.

I confirm that this doctoral dissertation is identical to the attached electronic version.

Gdańsk,..... .....
signature of the PhD student

I, the undersigned, agree to include an electronic version of the above doctoral dissertation in the open, institutional, digital repository of Gdańsk University of Technology.

Gdańsk,..... .....
signature of the PhD student

[1] Art 27. 1. Educational institutions and entities referred to in art. 7 sec. 1 points 1, 2 and 4–8 of the Act of 20 July 2018 – Law on Higher Education and Science, may use the disseminated works in the original and in translation for the purposes of illustrating the content provided for didactic purposes or in order to conduct research activities, and to reproduce for this purpose disseminated minor works or fragments of larger works.

2. If the works are made available to the public in such a way that everyone can have access to them at the place and time selected by them, as referred to in para. 1, is allowed only for a limited group of people learning, teaching or conducting research, identified by the entities listed in paragraph 1.

Podziękowania

Składam serdeczne podziękowania mojej Pani Promotor, ***prof. dr hab. inż. Barbarze Kościelskiej*** *za nieocenione wsparcie, cierpliwość, zaangażowanie oraz cenne rady i pomoc w realizacji niniejszej rozprawy doktorskiej.*

Stokrotnie dziękuję również mgr. Witoldowi Lizakowi, który wprowadził mnie w świat wytopu szkła i cierpliwie dzielił się ze mną swoją ogromną wiedzą. Dziękuję także wszystkim innym, którzy wnieśli swój wkład w powstanie tej pracy.

Podziękowania kieruję także do Koleżanek i Kolegów z Instytutu Nanotechnologii i Inżynierii Materiałowej za miłą współpracę, pomoc oraz życzliwość. W szczególności dziękuję zespołowi Fizyki Nanomateriałów za owocną współpracę.

Rodzinie i Przyjaciołom dziękuję za towarzyszenie mi w trudnych i radosnych chwilach oraz wiarę we mnie.

W szczególności dziękuję mojemu Mężowi za nieustające wsparcie, cierpliwość i zrozumienie, które mi okazywał w trakcie mojego doktoratu.

Table of Contents

List of important abbreviations and symbols

Abbreviations:

CCT Correlated Color Temperature

CRI Color Rendering Index

DSC Differential Scanning Calorimetry

DTA Differential Thermal Analysis

FTIR Fourier-Transform Infrared Spectroscopy

J-O Judd-Ofelt Parameter

LED Light Emitting Diode

RE Rare-Earths

TRES Time-Resolved Emission Spectroscopy

UV-Vis Ultraviolet-Visible Spectroscopy

WLED White Light Emitting Diode

XPS X-Ray Photoelectron Spectroscopy

XRD X-Ray Diffraction

Symbols:

S	Saad-Poulain parameter
T_c	crystallization temperature
T_g	glass transition temperature
T_m	melting temperature
T_x	onset of crystallization peak temperature
ΔT	thermal stability
x	x chromaticity parameter
y	y chromaticity parameter
λ_{em}	emission wavelength
λ_{exc}	excitation wavelength
τ	luminescence decay timed
Ω_λ	Judd-Ofelt parameter

Streszczenie

Materiały luminescencyjne, zwłaszcza luminofory domieszkowane jonami ziem rzadkich RE^{3+}, przyciągają znaczną uwagę w ostatnich latach ze względu na swój szeroki zakres zastosowań. Mogą być one wykorzystane w urządzeniach optoelektronicznych, takich jak wyświetlacze, lasery, wzmacniacze światłowodowe czy luminofory do diod elektroluminescencyjnych (LED). W szczególności badania nad diodami elektroluminescencyjnymi emitującymi światło białe (WLED) cieszą się dużym zainteresowaniem, ponieważ stają się one nową generacją źródeł światła. Charakteryzują się wysoką wydajnością, długą żywotnością oraz niskim napięciem zasilania. Są również przyjazne dla środowiska i kompaktowe. Powszechnie stosowane, komercyjne diody elektroluminescencyjne emitujące światło białe (WLEDs) składają się z żółtego fosforu $Y_3Al_5O_{12}:Ce^{3+}$ (YAG: Ce^{3+}) i emitującej w zakresie UV diody z azotku indu i galu (InGaN) umieszczonych w żywicy epoksydowej. Charakteryzują się one jednak niskim współczynnikiem oddawania barw (CRI) i wysokimi wartościami temperatur barwowych (CCT), słabą stabilnością materiału epoksydowego oraz brakiem komponentu czerwonego, co skutkuje emisją światła o nienaturalnym, niebieskawo-zimnym odcieniu. Rozwiązaniem może być dodanie składowej koloru czerwonego, co skutkowałoby emisją światła zbliżoną do barwy światła dziennego, co jest bardziej preferowane. Aby sprostać tym wymaganiom, badania nad nowymi, trwałymi luminoforami są niezwykle pożądane. Dużą uwagą cieszy się koncepcja uzyskania światła białego za pomocą jonów RE^{3+} osadzonych w szklanym luminoforze, oparta na mieszaniu się kolorów zgodnie z modelem RGB (czerwony, zielony, niebieski). Kluczowym dla tego podejścia jest staranny dobór odpowiedniej matrycy do ich wprowadzenia. Powinna ona zapewniać zarówno stabilność mechaniczną, jak i chemiczną, oraz optymalne parametry emitowanego światła. Wśród wielu rodzajów szkieł, szkła boranowo-bizmutowe wydają się być obiecującymi kandydatami. Wykazują one szereg pożądanych właściwości, takich jak: stabilność mechaniczna i chemiczna, wysoki współczynnik załamania światła, niska energia fononów oraz szeroki zakres transmisji zarówno w widzialnej, jak i podczerwonej części widma. Te cechy czynią je wartymi zbadania jako potencjalne matryce dla jonów RE^{3+}. Właściwości szklanej matrycy można poprawić poprzez dodatek fluorków, takich jak AlF_3 i SrF_2. Modyfikacja szkła fluorkami może prowadzić do polepszenia ich właściwości jako matryc dla optycznie aktywnych jonów RE^{3+}.

W niniejszej rozprawie doktorskiej przedstawiono wyniki badań nad nowymi szkłami i szkło-ceramikami zawierającymi odpowiednio AlF_3 i SrF_2. Przeprowadzono szereg eksperymentów w celu określenia odpowiednich warunków syntezy przezroczystych szkieł i szkło-ceramik. Zwrócono uwagę na analizę struktury i właściwości luminescencji w obu układach. Wprowadzenie AlF_3 do matrycy boranowo-bizmutowej spowodowało wzrost intensywności luminescencji jonów RE^{3+} w szkłach zawierających 10% mol AlF_3. Wykazano, że barwę emitowanego koloru można regulować poprzez zmianę proporcji jonów RE^{3+}. Lokalna symetria jonów Eu^{3+} mogła zostać zmniejszona ze względu na obecność jonów Al^{3+}, natomiast spadek intensywności Eu^{3+} przy wyższym stężeniu Al^{3+} może wskazywać na większą symetrię wokół jonów RE^{3+}. W układzie domieszkowanych szkło-ceramik, uzyskano pomyślną krystalizację nanokryształów SrF_2. Udowodniono, że modyfikacje strukturalne wyjściowego szkła, prowadzące do krystalizacji nanostruktur SrF_2, zależą silnie od ilości fluorku strontu. Wzrost intensywności luminescencji zaobserwowano po wygrzewaniu w próbkach zawierających 20% mol SrF_2. Czasy życia luminescencji uzyskany dla tej ceramiki szklanej wskazują, że część jonów Eu^{3+} była zlokalizowana w nanokryształach SrF_2. Potwierdza to także analiza parametrów Judda–Ofelta (Ω_2 i Ω_4) oraz współczynnika intensywności luminescencji (R). Uzyskane wyniki, zgodnie z tezą przyjętą w niniejszej rozprawie doktorskiej, wskazują, że proponowane szkła i szkło-ceramiki boranowo-bizmutowe mogą być odpowiednimi matrycami dla optycznie aktywnych jonów RE^{3+} i potencjalnymi kandydatami na luminofory.

Abstract

Luminescent materials, particularly phosphors doped with RE^{3+} ions, have attracted considerable attention in recent years owing to their wide range of applications. In particular, they can be used in optoelectronic devices, such as displays, lasers, fiber amplifiers or phosphors for light-emitting diodes (LEDs). Especially, research on white light emitting diodes (WLEDs) is of great interest, as they become the new generation of light sources. They are characterized by high efficiency, long lifetime, low applied voltage, environmental friendliness and compactness. Typical, commercial WLEDs are combine of $Y_3Al_5O_{12}:Ce^{3+}$ (YAG: Ce^{3+}) yellow phosphor and blue-emitting indium gallium nitride (InGaN) chip in an epoxy resin. However, they are characterized by a low color rendering index (CRI) and high correlated color temperatures (CCT), poor stability of an epoxy material, and lack of red color component, resulting in unnatural, bluish-cold light. The solution can be the addition of red color component, resulting in light emission close to daylight, which is more preferable. To meet these requirements, research on new, durable phosphors are highly desirable. The concept of obtaining white light emission by using RE^{3+} ions embedded in glass phosphor based on the concept of mixing colors according to the RGB model (Red, Green, Blue) gained much attention. Crucial to this approach is the careful selection of the host matrix for embedded RE^{3+} ions. Such a matrix should offer both mechanical and chemical stability, along with optimal parameters for light emission. Among various glasses, borate-bismuth glasses appear to be a promising candidates, exhibiting a number of desirable properties including mechanical and chemical stability, high refractive index, low phonon energy, and, wide transmission in both the visible and infrared regions of the spectrum. These properties make them worthy of examination as potential hosts for RE^{3+} ions. The properties of glass matrix can be improved by the addition of fluorides, such as AlF_3 and SrF_2. The incorporation of fluorides into the glass matrix can lead to increase they properties as a matrices for optically active RE^{3+}.

In this doctoral dissertation, the results of studies on new borate-bismuth glasses and glass-ceramics containing AlF_3 and SrF_2 respectively, have been examined and presented as potential hosts for RE^{3+} ions. A series of experiments were conducted to determine appropriate conditions for the synthesis of transparent glasses and glass-ceramics. Attention was focused on the analysis of the structure and luminescence properties in both systems. The introduction of AlF_3 into the borate-bismuth matrix

resulted in an increase in the luminescence intensity of RE^{3+} ions in glasses containing 10 mol% AlF_3. It was demonstrated that the emitted color can be tuned by varying the RE^{3+} ions ratios. The local symmetry of Eu^{3+} ions could be reduced due to the presence of Al^{3+} ions, while the decrease in Eu^{3+} intensity at higher Al^{3+} concentration could indicate higher symmetry around RE^{3+} ions. In studies glass ceramics system doped with, successful crystallization of SrF_2 nanocrystals has been obtained. It has been proven that the structural modifications of parental glass, leading to SrF_2 nanostructure crystallization, depend strongly on the initial amount of strontium fluoride. The increase in luminescence intensity was observed after annealing in samples containing 20 mol% SrF_2. The luminescence lifetimes obtained for these glass-ceramics indicate that some of the Eu^{3+} ions were located in SrF_2 nanocrystals. This was also confirmed by the analysis of the Judd–Ofelt parameters Ω_2 and Ω_4, and luminescence intensity ratio R. The obtained results, in accordance with the thesis assumed in this doctoral dissertation, indicate that the proposed borate-bismuth glasses and glass-ceramics could be suitable matrices for optically active RE^{3+} ions and potential candidates for phosphors.

Scientific achievements

The list of publications constituting a scientific achievements referred to in Art. 186, section 1 p. 3 of the Act, of this doctoral dissertation entitled "Synthesis, structure and luminescent properties of borate-bismuth glasses and glass-ceramics doped with rare earth metal ions":

1. **Karolina Milewska**, Michał Maciejewski, Marcin Łapiński, Anna Synak, Mirosław Behrendt, Wojciech Sadowski, Barbara Kościelska, *Structural and luminescence properties of B_2O_3-Bi_2O_3-AlF_3 glass doped with Eu^{3+}, Tb^{3+} and Tm^{3+} ions*, Journal of Non Crystalline Solids, Vol. 605, (2023), 122169.
   (IF = **4,458**)

My contribution to this publication involved the synthesizing glasses with various molar ratios of the chemical compositions. To obtain the final sample compositions, I conducted a series of experiments. These experiments involved synthesizing glasses with different molar ratios of components and varying synthesis parameters to achieve the desired optical properties of the glasses. While the method of melting two-component borate-bismuth glasses is known from the literature, however, the addition of AlF_3 and RE^{3+} ions required experimental determination of new synthesis conditions and sample compositions. After determining the glass compositions and melting conditions, I synthesized samples with appropriate optical properties for further testing, involving structure, thermal, and luminescence analyses. I analyzed the obtained results and was involved in interpreting the data generated from the experiments. I actively participated in the discussion of the obtained results. I was responsible for communication with reviewers and preparation of the final version of the manuscript.

<u>My percentage contribution is **55%**</u>

The percentage contribution of others co-authors: Michał Maciejewski (10%), Marcin Łapiński (10%), Anna Synak (10%), Mirosław Behrendt (5%), Wojciech Sadowski (5%), Barbara Kościelska (5%).

2. **Karolina Milewska**, Michał Maciejewski, Michal Žitňan, José J. Velázquez, Dušan Galusek, Wojciech Sadowski, Barbara Kościelska, *Tunable emission and energy transfer of B_2O_3–Bi_2O_3–AlF_3 glass system doped with Eu^{3+}/Dy^{3+}*, Journal of Luminescence, Vol. 269, (2024) 120440. (IF = **3,6**)

My contribution to the publication involved synthesizing B_2O_3–Bi_2O_3–AlF_3 glasses, whose composition and synthesis conditions were determined by me in the previous

publication (I). Subsequently, I focused on selecting appropriate concentration ratios of RE^{3+} ions addition: Eu^{3+} and Dy^{3+}, to achieve white light emission. I prepared samples for structure, thermal, and luminescence analyses, conducting XRD, FTIR, Raman, luminescence, and luminescence decay times measurements (TRES). Additionally, I analyzed the obtained results, interpreted the data generated from the experiments, actively participating in the discussion of the obtained results. Moreover, I calculated the luminescence decay times based on conducted TRES measurements, prepared CIE diagrams, and determined color purity of emitted light. Furthermore, I was responsible for communication with reviewers and preparation of the final version of the manuscript.

My percentage contribution is **60%**

The percentage contribution of others co-authors: Michał Maciejewski (10%), Michal Žitňan (10%), José J. Velázquez (5%), Dušan Galusek (5%), Wojciech Sadowski (5%), Barbara Kościelska (5%).

3. **Karolina Milewska**, Michał Maciejewski, Anna Synak, Marcin Łapiński, Aleksandra Mielewczyk-Gryń, Wojciech Sadowski, Barbara Kościelska, *From Structure to Luminescent Properties of B_2O_3-Bi_2O_3-SrF_2 Glass and Glass-Ceramics Doped with Eu^{3+} Ions*. Materials, 14, 4490. (IF = **3,748**)

My role in preparing this publication involved determining the appropriate parameters for the synthesizing borate-bismuth glass ceramics doped with SrF_2 nanocrystals. Since there were no reports in the literature on attempts to obtain SrF_2 nanocrystals in these matrices, I conducted experimental investigations to establish the synthesis conditions. After synthesizing the samples, I conducted a series of measurements to investigate their structure, thermal, and luminescence properties. This included XRD, DSC, FTIR, and luminescence measurements. Additionally, I analyzed the obtained results and interpreted the data generated from the experiments. I actively participated in the discussion of the obtained results. Moreover, I calculated the luminescence decay times based on conducted TRES measurements, and Judd-Ofelt parameters. I also handled communication with reviewers and prepared the final version of the manuscript.

My percentage contribution is **55%**

The percentage contribution of others co-authors: Michał Maciejewski (20%), Anna Synak (5%), Marcin Łapiński (5%), Aleksandra Mielewczyk-Gryń (5%), Wojciech Sadowski (5%), Barbara Kościelska (5%).

In addition, I am a co-author of one publication listed in JCR List. The results of my scientific and research work were presented at 7 national and international conferences.

Other publication from the JCR List:

4. Michał Maciejewski, **Karolina Milewska**, Anna Synak, Wojciech Sadowski, Barbara Kościelska, *Influence of controlled crystallization and SrF_2 content on the structure and properties of Eu^{3+} doped phosphate glasses*, Journal of Non-Crystalline Solids, 616, (2023) 122473. (IF = **4,458**)

I. Total impact factor (IF) (according to the Scopus database as of 08.04.2024):
   a) Publications included in the presented cycle: **14**
   b) Total publications: **17,6**

II. Total number of citations of publications (according to the Scopus database as of 08.04.2024):
   a) Publications included in the presented cycle: **19**
   b) Total publications: **20**

III. Hirsch Index (according to the Scopus database as of 08.04.2024): **2**

1. Introduction

Luminescent materials have attracted considerable attention in recent years owing to their diverse range of applications. Among them, phosphors doped with rare-earth (RE) ions are a very interesting group. In particular, they can be used in optoelectronic devices, such as displays, lasers, fiber amplifiers or phosphors for light-emitting diodes (LEDs) [1]. Especially, research on white light emitting diodes (WLEDs) is of great interest, as they become the new generation of light sources, which gradually replace the traditional fluorescent lamps and bulbs [2]. This is primarily because they are characterized by high efficiency, long lifetime and low applied voltage [3]. Moreover, they are environmental friendly and compactness. With these advantages, they find applications not only as a point light sources, but also automotive headlights or back-lighting of TV sets.

Typical, commercial WLEDs are combine of $Y_3Al_5O_{12}:Ce^{3+}$ (YAG: Ce^{3+}) yellow phosphor and blue-emitting indium gallium nitride (InGaN) chip in an epoxy resin [4] [5]. However, light emitted in this way is characterized by a low color rendering index (CRI) and high correlated color temperatures (CCT). These are mainly the results of lack of red color component, resulting in unnatural, bluish-cold light, which is not desirable for applications as light sources in homes or workplaces [6]. The solution can be the addition of red color component, resulting in light emission close to daylight, which is more preferable. Another disadvantage is the poor thermal stability of epoxy material. To meet these requirements, research on new, durable phosphors are highly desirable.

The concept of obtaining white light emission by using RE^{3+} ions is based on the excitation of optically active centers with the appropriate wavelength, which are embedded in phosphor. This is primarily based on the concept of mixing colors according to the RGB model (Red, Green, Blue) [7] [8]. An example can be the simultaneous emission of Eu^{3+}, Tm^{3+}, and Tb^{3+} ions excited by single wavelength, emitting in red, blue and green color. Crucial to this approach is the careful selection of the host matrix for embedded RE^{3+} ions. Such a matrix should offer both mechanical and chemical stability, along with optimal parameters for light emission. Currently, glasses is being considered as a suitable material for host matrix. This research primarily focuses on selecting the appropriate glass composition to achieve the desired light parameters.

Among various glasses, borate-bismuth glasses appear to be a promising candidates, exhibiting a number of desirable properties including mechanical and chemical stability [9] [10]. Notably, they are characterized by a high refractive index and

low phonon energy and, importantly, they offer wide transmission in both the visible and infrared regions of the spectrum. The possibility of formation of borate-bismuth glass system is confirmed by the equilibrium phase diagram created by A. V. Egorysheva et al. [11] This proves that two-component glass can be obtained in a stable form. The notable advantage of this two-component glass system is its ease of synthesis using conventional melt-quenching technique. Borate-bismuth glasses are characterized by a wide glass formation region from 20 to 80 mol % Bi_2O_3 and a relatively low melting point. Diboron trioxide (B_2O_3) is a basic glass-forming compound and flux material. It is responsible for the decrease of melt viscosity in high temperatures, increase of glass resistance, and improved its thermal and chemical properties. The boron atom typically coordinate with three or four oxygen atoms to form [BO_3] and [BO_4] structural units. The addition of Bi_2O_3 as a modifier to boron oxide enhances its optical properties. Glasses containing Bi_2O_3 are characterized by high density, transparency in wide a range of frequencies, and high refractive index. Combining boron oxide with bismuth oxide enables the tuning of the optical properties depending on the composition. These properties make them worthy of examination as potential hosts for RE^{3+} ions. Borate glasses were often used as matrices for RE^{3+} ions [12][13]. Lead borate glasses doubly doped with Dy^{3+}-Tb^{3+} and Tb^{3+}-Eu^{3+} were investigated using optical spectroscopy [14]. Additionally, glasses in a Bi_2O_3-B_2O_3 system doped with Eu_2O_3 were successfully obtained [15]. However, there is a research gap regarding two-component B_2O_3-Bi_2O_3 glasses aimed at achieving white light emission and exploring the impact of this matrix on the luminescence properties of RE ions.

Furthermore, it is possible to adjust the luminescence properties of ions by changing the local environment around them. Studies have revealed that modifying the local surroundings of optically active centers embedded in a glassy environment can influence the luminescence properties of emitted light.

The properties of glass matrix can be improved by the addition of fluorides, such as PbF_2, SrF_2, CaF_2, BaF_3, and AlF_3 [16] [17] [18] [19]. However, PbF_2 and CdF_2 are not preferred due to their toxicity. The incorporation of fluorides into the glass matrix can lead to changes in the optical and thermal properties of the glass. For example, the presence of Al^{3+} ions reduces nonradiative decay rates and increases radiative transition probabilities [20]. It was found that Al^{3+} ions addition increased the luminescence intensity of RE^{3+} ions in tellurite-based glasses doped with Eu^{3+}, Tb^{3+}, and Tm^{3+} [21]. In the $BaO–B_2O_3–P_2O_5$: Eu_2O_3 glass system, the highest intensity of luminescence

transitions was observed for glasses mixed with 3.0 mol% of Al_2O_3 [22]. Early studies on the influence of Al^{3+} ions on luminescence properties indicated that, Al^{3+} ions improves the solubility of RE^{3+} ions in glass matrix, thereby preventing dopants from clustering and reducing ion-ion energy migration and cross-relaxation. Another explanation for the influence of Al^{3+} ions on the luminescence properties is presented in [23] [24] publications. According to these studies, a low concentration of Al^{3+} lowers the RE site symmetry and increases radiative transitions. With higher Al^{3+} concentrations, RE dopants preferentially occupy positions near Al^{3+}, where the phonon energy is lower than in the glass matrix. This, leads to a decrease in the probability of nonradiative transitions of RE^{3+}.

Fluorides can also be introduced into glass matrices as nanocrystals to form glass ceramics materials [25]. Nanocrystals such as CaF_2 [26], BaF_2 [27], and LaF_3 [28] have been widely studied and have shown high potential for photonic applications. Glass ceramics are an interesting alternative to glasses because they combine the properties of both glass and crystals. It is well-known that the luminescence properties of RE doped glass and glass ceramics depend on the local environment of RE ions. The crystalline phases embedded in the glass matrix can significantly affect the luminescent properties of the material. Numerous experiments have confirmed that, during controlled crystallization, RE^{3+} ions can be embedded into the fluoride nanocrystals distributed in the glass matrix [29] [30]. The presence of the crystalline phase in the glassy matrix prevents luminescence concentration quenching and enhances the luminescence properties of the matrix, which is attributed to the formation of clusters of RE^{3+} ions [31]. Fluoride nanocrystals can reduce the phonon energy of glass, resulting in enhanced fluorescence emission. Additionally, combining the glass host and crystal phases can lead to improved optical, mechanical, thermal, and electrical properties [32]. It should be mentioned, that the transparency of the achieved glass ceramics is crucial, for luminescence materials. Optical transparency can be achieved if the diameter of the crystallites does not exceed 30 nm [33]. The size of the crystalline phase can be controlled by selecting appropriate crystallization conditions, such as time and temperature. Among the various fluoride nanocrystals, much attention has been focused on glass ceramics containing SrF_2 nanocrystals [34]. Strontium fluoride is an attractive material due to its optical properties, such as wide bandgap and low phonon energy, as well as favorable physical properties including a low refraction index, high radiation resistance, mechanical resistivity, and low hygroscopic properties [35]. The addition of SrF_2 to the glass matrix

can have a noticeably impact the emission properties of RE^{3+} ions due to the presence of Sr-F bonds. These bonds influence the radiative transitions and reduce the probability of phonon relaxation [36]. Additionally, it is known that lanthanide ions can form clusters in SrF_2 due to charge compensation when divalent strontium is substituted by trivalent RE^{3+} ions [37]. Research on materials containing RE^{3+} ions and doped with SrF_2 nanocrystals has garnered considerable attention [38] [39]. For instance, the synthesis of tellurite glass ceramics with SrF_2 and Eu^{3+} ions has been successfully achieved [36]. In a study by Luo et al., the luminescence of Eu^{3+} ions was investigated in $50SiO_2$-$22Al_2O_3$-$20SrF_2$-$6NaF$-$2EuF_3$ glass ceramics [40]. Transparent glass ceramics with SrF_2 nanocrystals were synthesized with a composition of $50SiO_2$–$10Al_2O_3$–$20ZnF_2$–$20SrF_2$, and it was found that the SrF_2 nanocrystals were homogeneously precipitated within the glass matrix, with an average size of approximately 20 nm. After crystallization, a significant enhancement in Eu^{3+} ions luminescence was observed [41].

Nevertheless, there is a notable absence of research concerning the modification of two-component B_2O_3-Bi_2O_3 glass and glass ceramics for optical applications. This suggest the need for further research to deepen the current state of knowledge, as they seem to be good candidate for RE^{3+} ions matrices.

2. Research goals and study objectives

The aim of the scientific research conducted in this doctoral dissertation was to design novel borate-bismuth glass and glass-ceramics doped with fluorides to be used as matrices for optically active rare-earth ions (RE^{3+}). Attention was focused on the analysis of the structure and luminescence properties for their potential use as phosphors. According to the thesis, using borate-bismuth glass as a precursor material should provide good mechanical and chemical stability. Further modification of this matrix by adding the fluorides, should provide enhancement in luminescence of RE^{3+} ions, while maintaining the stability and transparency of the precursor matrix. The next goal is to achieve white light generation from borate-bismuth glass and glass ceramics doped with RE^{3+} ions.

The scope of research carried out in this doctoral dissertation included the following aspects:

1. Synthesis of borate-bismuth glass matrix with appropriate properties for optical purposes.
2. Modification of borate-bismuth glass matrix by addition of fluorides: AlF_3 and SrF_2, to obtain new glass and glass-ceramics matrices:
    a. Synthesis transparent borate-bismuth glasses doped with AlF_3 and studied the influence of AlF_3 on glass structure.
    b. Synthesis transparent borate-bismuth glass and glass-ceramics with SrF_2 and studied influence of SrF_2 on glass matrix.
3. Doping the proposed borate-bismuth glass and glass ceramics matrices with selected RE^{3+} rare-earth ions: Eu^{3+}, Tm^{3+}, Tb^{3+}, and Dy^{3+} - introduced individually, in double, and triple combinations, to analyze the luminescence properties and obtain white light as a result of changing the ratio of RE^{3+} ions and excitation wavelength.
4. Investigation and discussing the influence of the environment on the luminescent properties of RE^{3+} ions in the presence AlF_3 and SrF_2 nanocrystals in synthesized glass and glass ceramics.

To conduct the aforementioned research, a variety of research techniques were used. The X-ray Diffraction (XRD) technique was employed to determine the presence or absence of crystalline phases in the samples. Thermal properties were investigated using differential thermal analysis (DTA) and differential scanning calorimetry (DSC).

Fourier transform infrared spectroscopy (FTIR) and Raman spectroscopy were utilized to identify the structural units present in the glass matrices. X-ray photoelectron spectroscopy (XPS) analysis was conducted to determine the valence states of ions present in the samples. Photoluminescence (PL) and Time-resolved emission spectra (TRES) were used to characterize the luminescent properties of prepared samples. Using these research techniques, it was possible to comprehensively characterize the structure and properties of borate-bismuth glasses and glass ceramics.

The results of the scientific research were collected in the form of three publications in journals from the JCR list. These publications provide the detailed descriptions of the synthesis and research on the structure, optical, and luminescent properties of materials. Based on the presented results, an assessment of borate-bismuth glasses and glass ceramics was conducted concerning the influence of the environment on the luminescent properties of RE^{3+} ions. Specifically, the effects related to the introduction of AlF_3 into borate-bismuth glasses and the crystallization of SrF_2 in glass ceramics were examined. These publications also represent the first reports on the production of borate-bismuth glasses and glass ceramics containing metal fluorides as new and interesting matrices for optically active rare-earth ions.

3.Guide to publications comprising a doctoral dissertation

1.1. "Structural and luminescence properties of B_2O_3-Bi_2O_3-AlF_3 glass doped with Eu^{3+}, Tb^{3+} and Tm^{3+} ions"

The first publication in the series constituting this doctoral dissertation, titled *"Structural and luminescence properties of B_2O_3-Bi_2O_3-AlF_3 glass doped with Eu^{3+}, Tb^{3+} and Tm^{3+} ions"* [I], describes the synthesis and research results on the structure and luminescence of glasses based on borate and bismuth oxides doped with RE^{3+} ions. The publication presents an analysis of the influence of adding of aluminum fluoride (AlF_3) on the structure of the glassy matrix and the luminescent properties of RE^{3+} ions. The research related to the publication's topic included the designing a borate-bismuth glassy matrix suitable for optical applications. A two-component matrix composed of boron oxide and bismuth oxide was proposed, considering literature reports that suggested such a system could be prepared by conventional melt quenching technique. However, the potential of use these oxides-based glasses as matrices for optically active RE^{3+} ions, along with their further modifications thorough the addition of other compounds (e.g. fluorides), remained unexplored. Therefore, in the initial phase, research work was focused on selecting the appropriate glass composition and synthesis parameters. While the conditions for the synthesizing borate-bismuth glasses are known from the literature, there are no reports about these glasses doped with AlF_3. Therefore, a series of synthesis attempts were conducted in order to determine the appropriate doping ratios and synthesis parameters, such time and temperature, while ensuring that the glass remains transparent.

As a result of a series of experiments, the following compositions and synthesis conditions were established. Borate-bismuth glasses with the nominal composition (in mol%): $50B_2O_3$–$50Bi_2O_3$ (BBO), $45B_2O_3$–$45Bi_2O_3$–$10AlF_3$ (BBO+$10AlF_3$), and $40B_2O_3$–$40\ Bi_2O_3$–$20AlF_3$ (BBO+$20AlF_3$) were synthesized using the conventional melt-quenching technique in an air atmosphere. Subsequently, to study the influence of AlF_3 addition on luminescent properties, samples singly doped with Ln^{3+} ions (BBO+Eu, BBO+$10AlF_3$+Eu, BBO+$10AlF_3$+Tb, BBO+$10AlF_3$+Tm) were prepared. Based on the obtained results, the BBO+$10AlF_3$ was chosen, to be modified by the addition of Ln^{3+} ions, where Ln^{3+}=$0.5Eu^{3+}$+$0.5Tb^{3+}$+$1Tm^{3+}$ (BBO+$10AlF_3$:Ln1), Ln^{3+}=$0.7Eu^{3+}$+$0.5Tb3^{3+}$+$0.8Tm^{3+}$ (BBO+$10AlF_3$:Ln2), Ln^{3+}=$0.05Eu^{3+}$+$0.95Tb^{3+}$+$1Tm^{3+}$ (BBO+$10AlF_3$:Ln3). Moreover, to investigate the

possibility of energy transfer between Tb^{3+} and Eu^{3+} ions, BBO+10AlF_3+1Eu+1Tb glass was prepared. The compositions of the samples are presented in Table 1. Mixed raw materials (H_3BO_3, $Bi_5OH(OH)_9(NO_3)_4$, AlF_3, Eu_2O_3, Tm_2O_3, $Tb(NO_3)_3$ were melted in porcelain crucibles at 950 ˚C for 20 min. Next, the melts were poured onto a hot steel plate at a temperature of 250 ˚C, pressed by another plate immediately, and then cooled down to room temperature. According to the research stated in this thesis, by selecting appropriate parameters of the synthesis process, homogeneous, transparent glasses with a slightly yellow color were obtained.

Table 1. Compositions of synthesized samples.

Name	**Sample composition (molar ratios)**					
	B_2O_3	Bi_2O_3	AlF_3	Eu_2O_3	Tb_2O_3	Tm_2O_3
BBO	50	50		-	-	-
BBO+Eu	49	49		2	-	-
BBO+10AlF_3	45	45	10	-	-	-
BBO+20AlF_3	40	40	20	-	-	-
BBO+20AlF_3+Eu	39	39	10	2	-	-
BBO+10AlF_3+Eu	44	44	10	2	-	-
BBO+10AlF_3+Tb	44	44	10	-	2	-
BBO+10AlF_3+Tm	44	44	10	-	-	2
BBO+10AlF_3+Eu/Tb	44	44	10	1	1	-
BBO+10AlF_3+Ln1	44	44	10	0.5	0.5	1
BBO+10AlF_3+Ln2	44	44	10	0.5	0.7	0.8
BBO+10AlF_3+Ln3	44	44	10	0.05	0.95	1

The Differential Thermal Analysis (DTA) technique was used to determine the glass transition (T_g) and glass crystallization (T_c) temperatures of the as-prepared glasses (Fig. 1). The DTA curves show changes in T_g and T_c due to presence of AlF_3. The T_g of the samples doped with AlF_3 were found to be higher than T_g of the undoped one. This can be explained by the correlation between the T_g and the enthalpy of bonds in the glass matrix [42]. The addition of aluminum fluoride may lead to the formation of new linkages between glass components, resulting in a higher energy barrier for molecule motion to overcome and increasing the thermal stability of the glass matrix. The T_c was also found to have higher value after introduction of AlF_3. The presence of strong bonds could lead to an increase in the stability of glass matrix, resulting in a higher value of crystallization temperatures. However, the stability of the glasses decreases after the introduction of AlF_3. This conclusion is based on the calculated parameters of glass stability (ΔT) and resistance against devitrification (S) (Table 2), according to the following equations [43]:

$$\Delta T = T_x - T_g \qquad (1)$$

$$S = \frac{(T_c - T_x)(T_c - T_g)}{T_g} \quad (2)$$

With the addition of aluminum fluoride, both ΔT and S parameters decrease. The addition of AlF_3 to the basic glass matrix (BBO) results in the lower stability of the borate-bismuth glass matrix and a higher tendency to crystallize.

Table 2. Thermal parameters of BBO, BBO+10AlF_3, and BBO+20AlF_3 glasses.

Sample	T_g (˚C)	T_x (˚C)	T_c (˚C)	Δ T (˚C)	S (˚C)
BBO	425.9	428	503.5	56.1	3.62
BBO+10AlF_3	433.6	487.1	507.4	53.5	3.45
BBO+20AlF_3	428.7	484.5	503.2	55.8	3.14

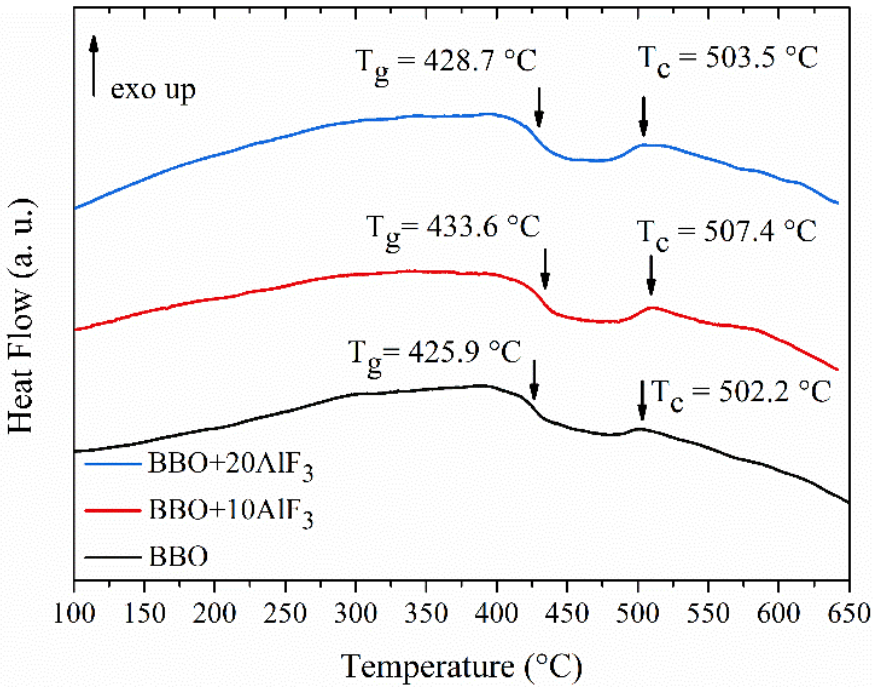

Figure 1. DTA curves of BBO, BBO+10AlF_3 and BBO+20AlF_3 [I].

The amorphous character of the prepared samples was confirmed by the X-Ray Diffraction (XRD) method (Fig. 2). No differences due to the addition of AlF_3 can be observed. Only two board humps in the range of 20-40 (2θ) and 40-65 (2θ) indicate the lack of long-range order in the glass matrices are present.

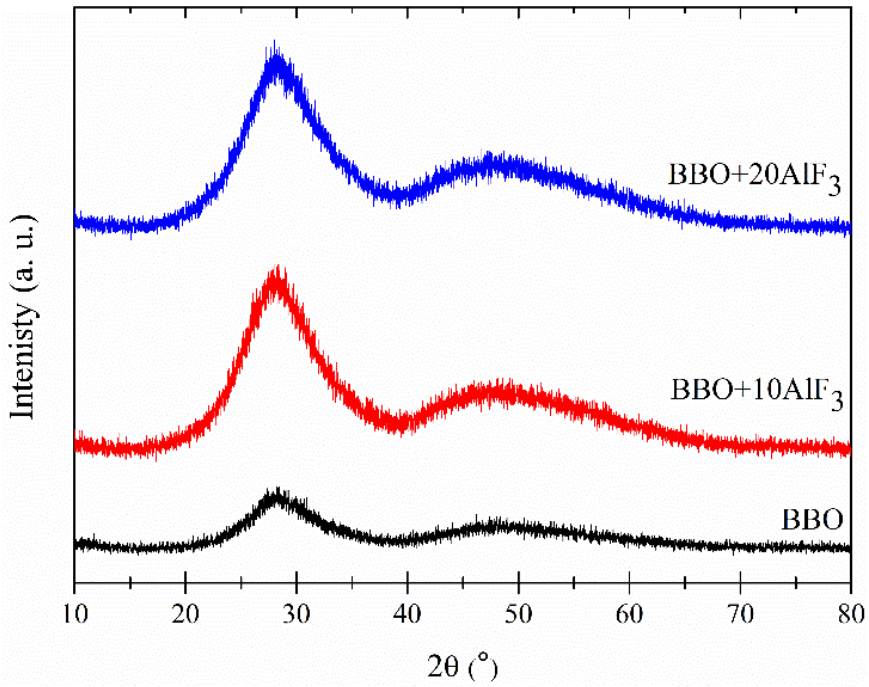

Figure 2. XRD patterns of as-prepared BBO, BBO+10AlF_3, and BBO+20AlF_3 [I].

Infrared spectroscopy (FTIR) measurements provide insight into the structural unit present in glass samples (Fig. 3). The broad absorption bands in the range 645–760 cm^{-1} and 1182–1356 cm^{-1} can be assigned to the deformation vibration of [BO_3] groups. Additionally, also band around 1356–1478 cm^{-1} is associated with the stretching vibrations of [BO_3] units. The tetrahedral units [BO_4] are visible in the spectrum at 790–1110 cm^{-1}. Despite changes in DTA result related to the addition of AlF_3, the stretching vibrations of Al-F bonds, which typically appear at 642 and 646 cm^{-1}, as well as the vibrations of Al-O bonds in AlO_4 units at around 1124 cm^{-1}, are not visible [44] [45]. These regions are dominated by broad bands from [BO_3] and [BO_4] units. Due to this fact, the presence of AlF_3 may be overlapped by them, resulting in no significant changes in spectra of glass samples doped with 10 and 20 mol% of AlF_3.

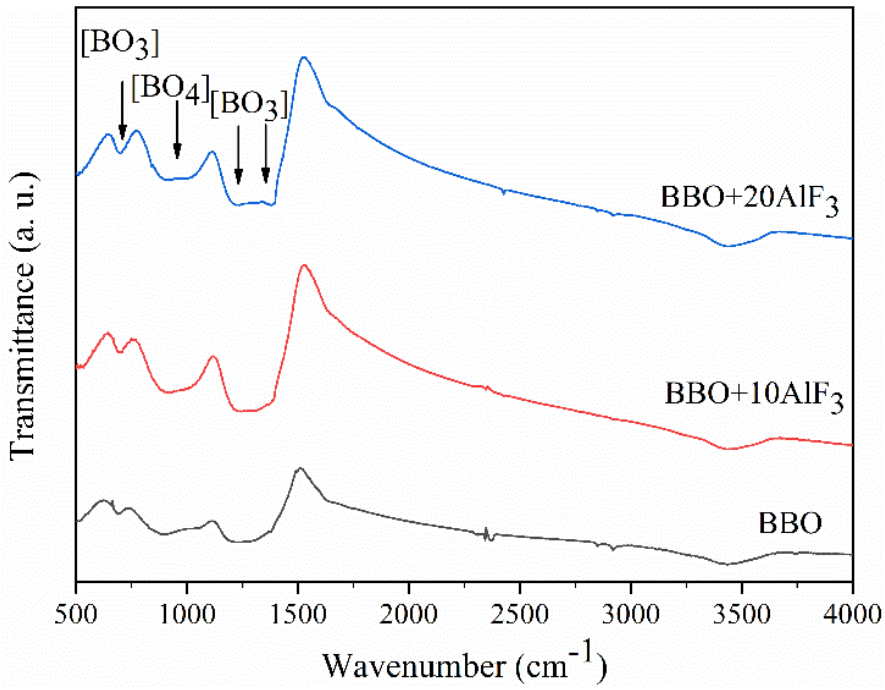

Figure 3 FTIR spectra of as-prepared BBO, BBO+10AlF_3, and BBO+20AlF_3 glasses [I].

To confirm the presence of AlF_3 and determine the valence states of ions, X-ray photoelectron spectroscopy (XPS) analysis was used (Fig. 4). The bands associated with the presence of aluminum fluoride and bismuth atoms were subjected to detailed analysis in the BBO+10AlF_3 glass. Two signals connected with the presence of Al^{3+} ions can be distinguished in the band observed in the 72–77 eV range. First, at 75,5 eV, it can be assigned to the presence of Al-F bonds in AlF_3. Second, at 74,5 may be associated with the Al-O bonds in Al_2O_3. The contribution of Al-F and Al-O bonds was established at 15% and 85%, respectively. The XPS analysis confirms the presence of AlF_3 in prepared glass samples. To gain a better insight into the structure of glass matrix, the investigation of Bi ions was performed. Measurements shows the presence Bi 4f spin-orbit doublet in the region 155–167 eV. After deconvolution four separate bands can be seen. Peaks at 159.0 and 165.0 eV can be attributed to Bi 4f $_{7/2}$ and Bi 4f $_{5/2}$ peaks of Bi^{3+}, whereas two peaks at 157 and 163 eV can be described to Bi f $_{7/2}$ and Bi f $_{5/2}$ of Bi^0, respectively.

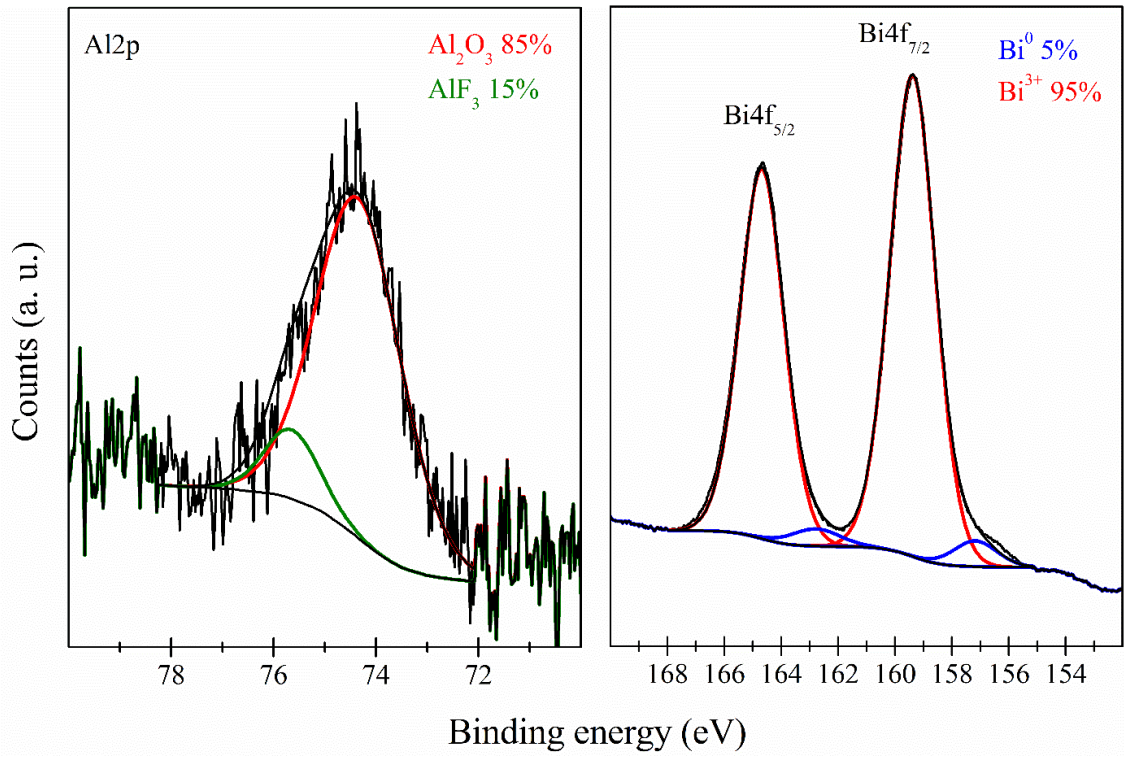

Figure 4 XPS spectra of BBO+10AlF_3 sample [I].

As a part of the research procedure for the proposed glasses, it was essential to evaluate their suitability as matrices for optically active RE^{3+} ions. The primary criterion for selecting a glass was the highest light emission. Firstly, the goal was to investigate whether AlF_3 doping has an effect on the emission of RE^{3+} ions. To achieve this, 2 mol% of Eu^{3+} ions were added to the as-prepared glasses: BBO, BBO+10ALF_3, and BBO+20AlF_3. The luminescence spectra of glasses were observed at λ_{em} = 615 nm, corresponding to the $^5D_0 \rightarrow {}^7F_2$ transition of Eu^{3+} ions (Fig. 5a). Several characteristic peaks for 4f-4f transitions can be seen in the spectrum, with excitation bands at: 363, 382, 395, 416, 465 and 533 nm, assigned to the $^7F_0 \rightarrow {}^5D_4$, $^5G_2$, $^5L_6$, $^5D_3$, $^5D_2$, $^5D_1$ transitions, respectively. The band at λ_{ex}= 465 nm, characterized by the highest intensity in the excitation spectrum, was selected as suitable for observing the emission spectra of the glasses (Fig. 5b). The emission spectra consisting of several bands at 578 nm ($^5D_0 \rightarrow {}^7F_0$), 591 nm ($^5D_0 \rightarrow {}^7F_1$), 615 nm ($^5D_0 \rightarrow {}^7F_2$), 652 nm ($^5D_0 \rightarrow {}^7F_3$) and 700 nm ($^5D_0 \rightarrow {}^7F_4$). The intensities of the excitation spectra change with the composition of the samples. The highest intensity is observed for glass doped with 10 mol% of AlF_3 addition. In contrast, for glass with 20 mol% AlF_3, the intensity is even lower than for the undoped matrix.

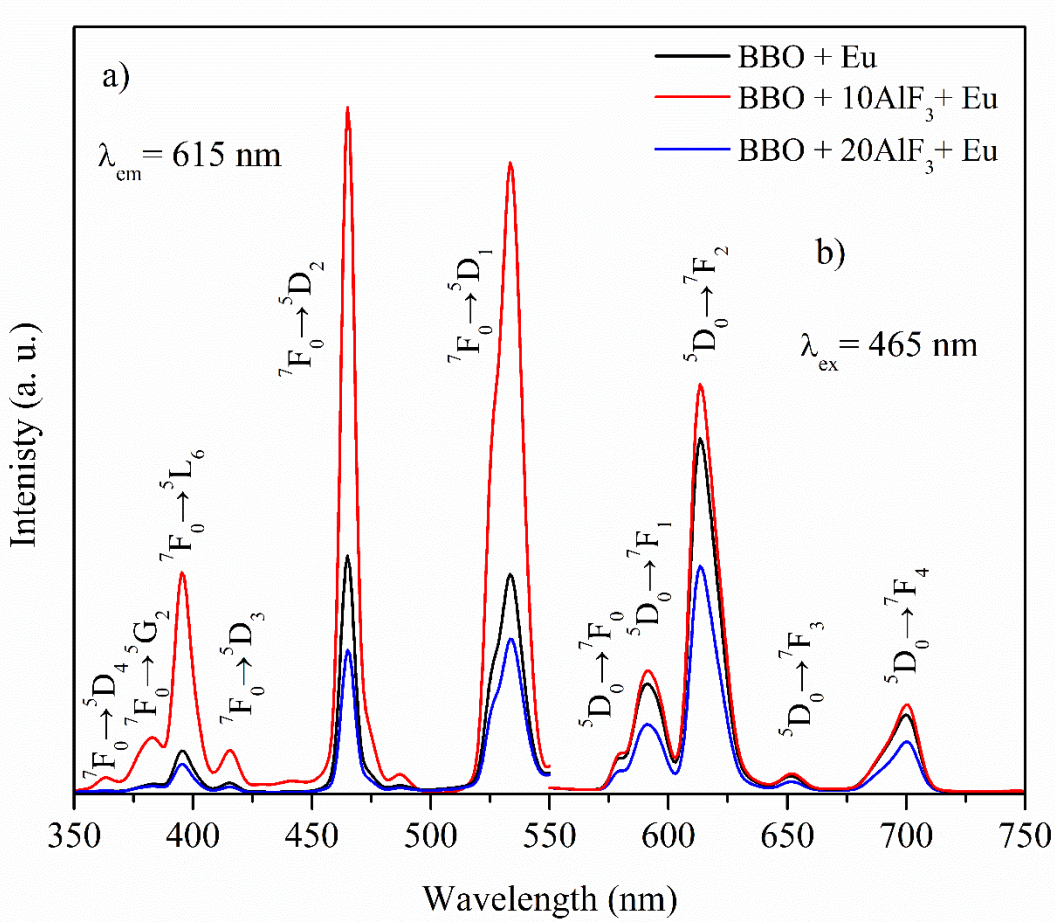

Figure 5 Excitation (a) and emission (b) spectra of samples doped with Eu^{3+} ions [I].

Due to the fact that the Eu^{3+} luminescence spectra are suitable probes for the study of local symmetry in glass matrices, studying their intensity can provide insight into how modification with AlF_3 affects their structure. Changes in the glass composition can influence their emission spectrum. Europium ions exhibit two characteristic bands in the emission spectrum corresponding to the $^5D_0 \rightarrow {}^7F_1$ and $^5D_0 \rightarrow {}^7F_2$ transitions. It was observed that the electric dipole transition intensity ($^5D_0 \rightarrow {}^7F_2$) is higher than the magnetic dipole transition in all glass samples. This suggests that Eu^{3+} ions are placed in the site without an inversion center. The ratio between the luminescence intensities of electric dipole and magnetic dipole transitions ($^5D_0 \rightarrow {}^7F_2/{}^5D_0 \rightarrow {}^7F_1$) is called the red to orange (R/O) ratio. In the studied glasses, the R/O ratios are 3.26 and 3.17 for BBO+10AlF_3+2Eu and BBO+20AlF_3+2Eu, respectively. The variation in this parameter confirms that the surrounding of RE^{3+} ions is affected by the addition of AlF_3. The dominance of the electric dipole transition in all samples results in the dominance of red color emission. When the intensity of the electric dipole is higher than the intensity of the magnetic dipole transition, Eu^{3+} ions occupy sites without inversion symmetry. It is evident that the addition of AlF_3

has a strong effect on the luminescence properties of studied borate-bismuth glasses doped with Eu^{3+} ions. The emission intensity varies with the concentration of AlF_3, reaching a maximum at 10 mol% of AlF_3 addition and then decreasing with a higher AlF_3 content. The local symmetry of Eu^{3+} ions could be reduced due to the presence of Al^{3+} ions, while the decrease in Eu^{3+} intensity at higher Al^{3+} concentration could indicate higher symmetry around RE^{3+} ions. Due to the highest intensity in the excitation spectra, the BBO+10AlF_3 composition was selected for further single and triple doping with Eu^{3+}, Tb^{3+}, and Tm^{3+} ions. They were introduced into the glass matrix in different proportions (Table 1) to investigate the possibility of achieving white light by simultaneously exciting their emission. First, the luminescence of Tb^{3+} and Tm^{3+} ions in BBO+10AlF_3 was examined separately. Under 544 nm observation, the excitation spectrum consists of three peaks at 354, 378, and 486 nm corresponding to $^7F_6 \rightarrow {}^5D_2$, $^5D_3$, $^5D_4$, of Tb^{3+} respectively (Fig. 6). The emission spectrum for the 378 nm excitation shows peaks at 496 nm ($^5D_4 \rightarrow {}^7F_6$), 549 ($^5D_4 \rightarrow {}^7F_5$), 594 nm ($^5D_4 \rightarrow {}^7F_4$) and 628 nm ($^5D_4 \rightarrow {}^7F_3$), which can be assigned to the 4f-4f transitions of Tb^{3+} ions. The excitation and emission spectra of the BBO+10AlF_3+Tm glass sample are presented in Fig. 7a and b respectively. The excitation spectra monitored at 455 nm wavelength consist of one peak at 358 nm due to $^3H_6 \rightarrow {}^1D_2$ transition of Tm^{3+} (Fig. 7a). Under 358 nm excitation, the emission spectrum shows peak at 455 nm, corresponding to the $^1D_2 \rightarrow {}^3F_4$ transition of Tm^{3+} ions (Fig. 7b).

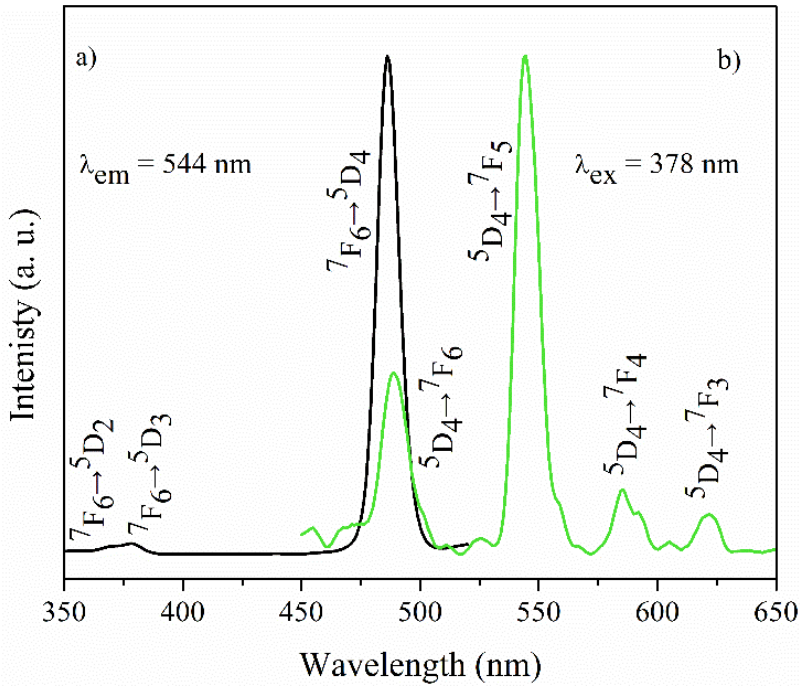

Figure 6 The excitation spectra monitored at 544 nm (a) and emission spectra monitored at 378 nm (b) of the BBO+10AlF_3+Tb^{3+} glass.

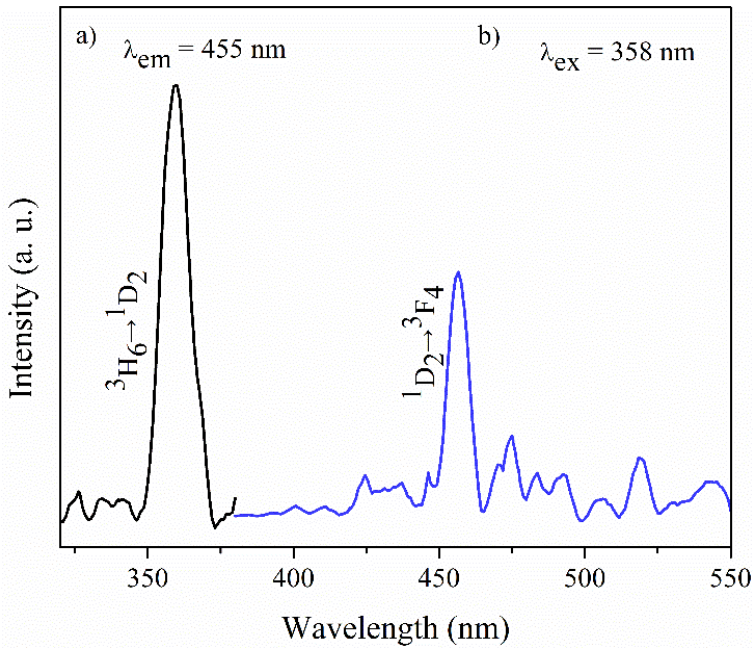

Figure 7 The excitation spectra monitored at 455 nm (a) and emission spectra monitored at 358 nm excitation (b) of the BBO+10AlF_3+Tm^{3+} sample.

Additionally, time-resolved emission spectra (TRES) were measured to obtain information on luminescence decay times for Eu^{3+}, Tb^{3+} and Tm^{3+} ions. The luminescence decays exhibit a one-exponential character, with lifetimes of about 1 ms for Eu^{3+} and Tb^{3+} ions (Fig. 8). However, the decay time for Tm^{3+} ions was on the order of microseconds.

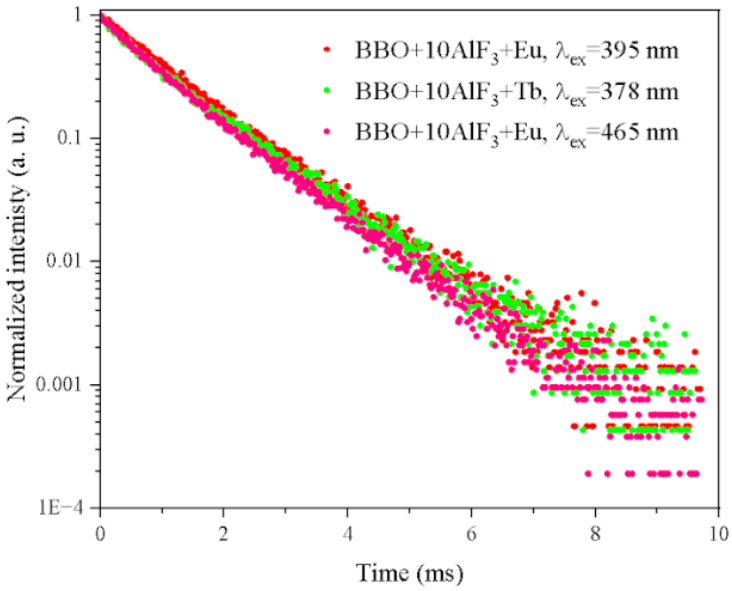

Figure 8 Luminescence decay curves of BBO+10AlF_3+2Eu obtained for λ_{ex}=395 nm, λ_{ex}=465 nm (observation at around λ_{em}=620 nm) and BBO+10AlF_3+2Tb at λ_{ex}=378 nm (observation at around λ=544 nm), respectively.

Next, The key objective was to investigate the possibility of sample excitation with one wavelength characteristic for Eu^{3+}, Tb^{3+}, and Tm^{3+} ions to achieve simultaneous emission from all added RE ions. They were introduced into the glass matrix in different proportions (Table 1) Based on the excitation spectra of glass samples singly doped with Eu^{3+}, Tb^{3+} and Tm^{3+} ions, measured at 454,544 and 615 nm, respectively (Fig. 9), three excitation wavelengths (355 nm, 378 nm, and 395 nm) have been chosen as adequate for exciting Eu^{3+}, Tb^{3+}, and Tm^{3+}.

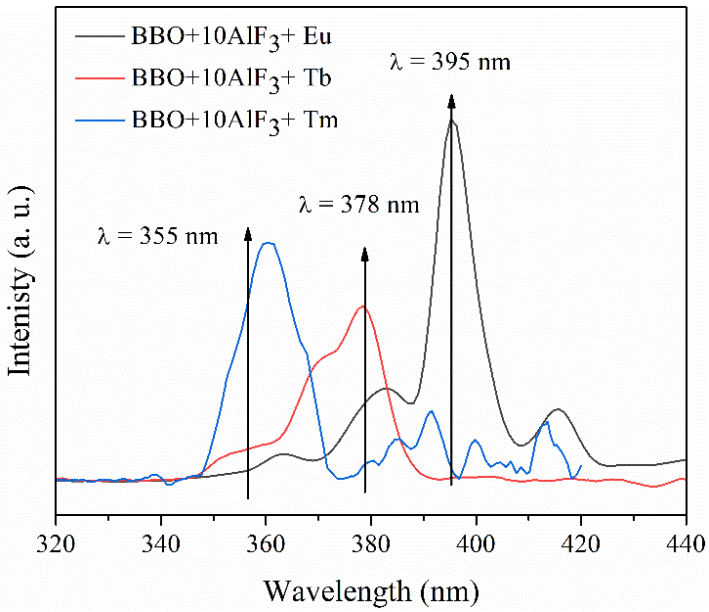

Figure 9 Excitation spectra of $BBO+10AlF_3+Re^{3+}$ ($Re=Eu^{3+}$, Tm^{3+}, Tb^{3+}) glass samples monitored at 455, 545, and 615 nm wavelengths.

They were used to excite the triply doped samples to investigate whether it is possible to use these lines to also excite other Ln^{3+} ions, for which the excitation line is not characteristic (Figs. 10–12). When the samples were excited at a wavelength of 378 nm (Fig. 10), only bands originating from Eu^{3+} and Tb^{3+} ions can be seen in the emission spectrum. No peaks assigned to the Tm^{3+} ions were recognized. The bands at 494 nm, 551 nm, 584 nm and 620 nm may be attributed to the Tb^{3+} ions corresponding to the $^5D_4 \rightarrow {}^7F_6$ and $^5D_4 \rightarrow {}^7F_5$, $^5D_4 \rightarrow {}^7F_4$, and $^5D_4 \rightarrow {}^7F_3$ transitions, respectively. The presence of Eu^{3+} ions is represented by several peaks: 584 nm ($^5D_0 \rightarrow {}^7F_0$), 597 nm ($^5D_0 \rightarrow {}^7F_1$), 619 nm ($^5D_0 \rightarrow {}^7F_2$), 658 nm ($^5D_0 \rightarrow {}^7F_3$), and 710 nm ($^5D_0 \rightarrow {}^7F_4$). The emission spectra under 395 nm excitation (Fig. 11), consist of several bands at 584 nm ($^5D_0 \rightarrow {}^7F_0$), 597 nm ($^5D_0 \rightarrow {}^7F_1$), 619 nm ($^5D_0 \rightarrow {}^7F_2$), 658 nm ($^5D_0 \rightarrow {}^7F_3$), and 706 ($^5D_0 \rightarrow {}^7F_4$), which can be assigned to Eu^{3+} ions. In the emission spectra of the samples excited with λ_{ex}=355 nm also lines corresponding to Eu^{3+} and Tb^{3+} ions (apart of the lines characteristic for Tm^{3+})

can also be seen (Fig. 12). Under 355 nm excitation, the emission spectrum (Fig. 12) shows bands at 459 nm, that can be assigned to the $^1D_2 \rightarrow {}^3F_4$ blue transition of Tm^{3+} ions. Peaks at 494 nm, 551 nm, 584 nm and 622 nm may be described to the Tb^{3+} ions, corresponding to the $^5D_4 \rightarrow {}_7F_6$, $^5D_4 \rightarrow {}^7F_5$, $^5D_4 \rightarrow {}^7F_4$, $^5D_4 \rightarrow {}^7F_3$ transitions, respectively. The presence of Eu^{3+} ions is represented by several peaks: 584 nm ($^5D_0 \rightarrow {}^7F_0$), 597 nm ($^5D_0 \rightarrow {}^7F_1$), 619 nm ($^5D_0 \rightarrow {}^7F_2$), 658 nm ($^5D_0 \rightarrow {}^7F_3$), and 710 nm ($^5D_0 \rightarrow {}^7F_4$). The obtained results indicate the possibility of emission in the red, green, and blue spectral range. In particular, the sample BBO+10AlF_3: Ln3 shows simultaneous emission from all added rare-earth ions at λ_{ex} = 355 nm.

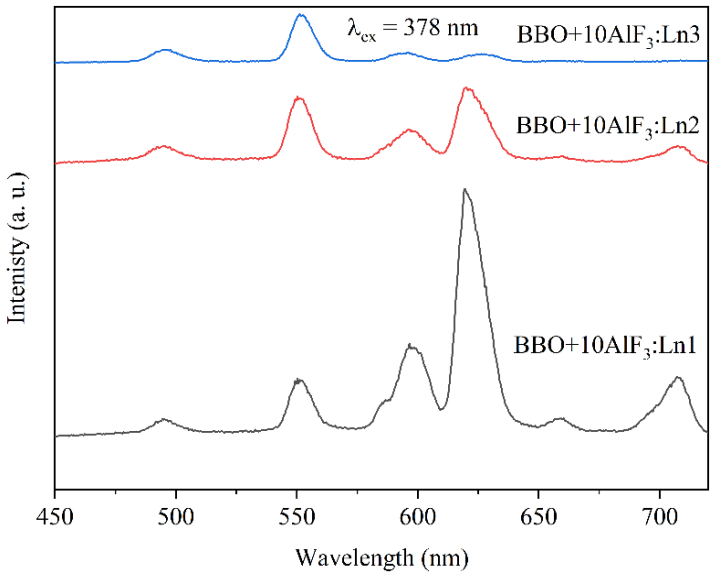

Figure 10 The emission spectra of BBO+10AlF_3:Ln1, Ln2, and Ln3 samples under 378 nm excitation.

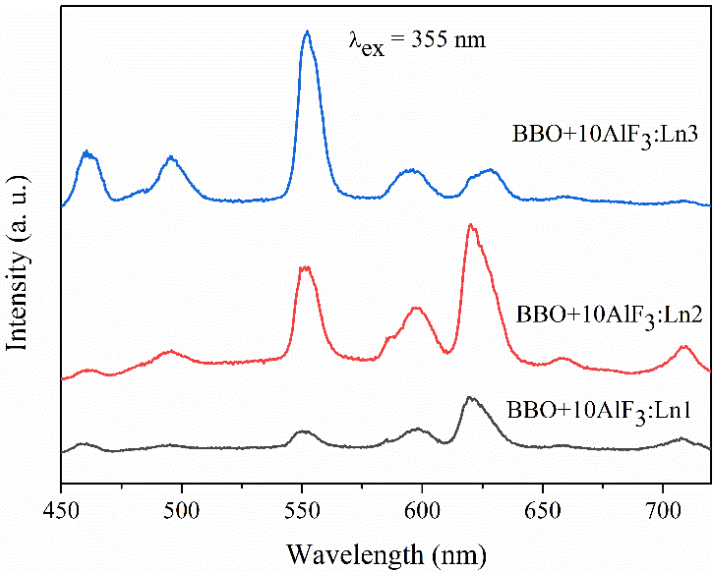

Figure 11 The emission spectra of BBO+10AlF_3:Ln1, Ln2, and Ln3 samples under 395 nm excitation.

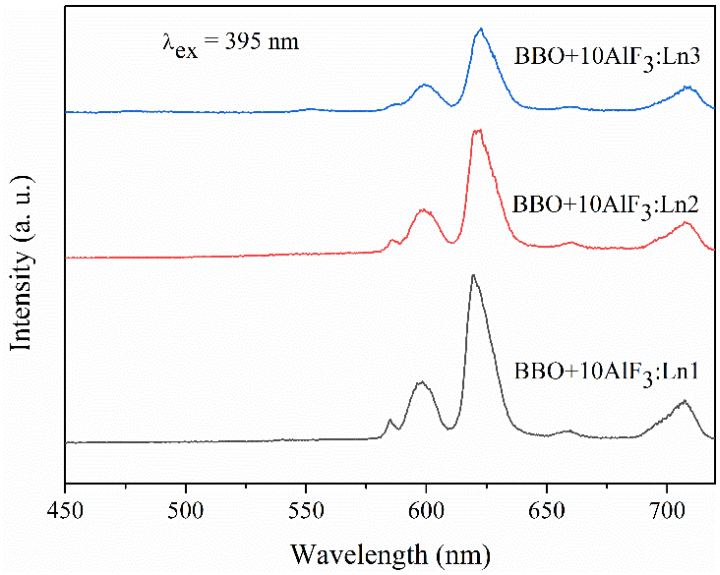

Figure 12 The emission spectra of BBO+10AlF_3:Ln1, Ln2, and Ln3 samples under 355 nm excitation.

In the case of glasses doped with RE ions, an additional aspect to investigate is the possibility of energy transfer between Tb^{3+} and Eu^{3+} ions. According to the Forster-Dexter theory, it can occur when the emission band of Tb^{3+} partially overlaps with the absorption band of the Eu^{3+} ions. Therefore the spectra of singly doped glasses with Tb^{3+} and Eu^{3+} ions were compared. When compare the excitation spectrum of the BBO+10AlF_3+Eu sample observed at λ_{em} = 615 nm wavelength, which corresponds to the $^5D_0 \rightarrow {}^7F_2$ transition of europium ions, and the emission spectrum of the BBO+10AlF_3+Tb glass at λ_{ex} = 378 nm assigned to the $^7F_6 \rightarrow {}^5D_3$ transition of Tb^{3+} ions (Fig. 13), in the 500–550 nm region, the partially overlapping of both spectra can be seen. Next, to study the energy transfer process, the luminescence spectra of double co-doped glasses were examined. The excitation spectra of the BBO+10AlF_3+1Eu+1 Tb sample under λ_{em} = 615 nm and λ_{em} = 544 nm are shown in Fig. 14a. At 544 nm ($^5D_4 \rightarrow {}^7F_5$: Tb^{3+}), only transitions of Tb^{3+} ions are present, but under 615 nm ($^5D_0 \rightarrow {}^7F_2$: Eu^{3+}) characteristic bands for both Eu^{3+} and Tb^{3+} ions are observed. This confirms that there is a possibility of obtaining the emission lines from europium using wavelength characteristics for both, Eu^{3+} (395 nm) and Tb^{3+} (378 nm) ions. Moreover, after excitation at λ_{ex} = 395 nm (Eu^{3+}), the emission spectrum consists of four bands assigned to the $^5D_0 \rightarrow {}^7F_{1-4}$ transitions of Eu^{3+} ions, but bands corresponding to Tb^{3+} ions were not detected. However, when the glass is excited at λ_{ex} = 378 nm, connected to the $^7F_6 \rightarrow {}^5D_3$ transition of Tb^{3+}, both emission lines corresponding to Tb^{3+} and Eu^{3+} ions are present in the emission spectrum.

This behavior confirms that the energy transfer process from Tb^{3+} ions to Eu^{3+} ions occurs in the borate-bismuth glass system [71,72, 73]. Based on the obtained results, the energy transfer (ET) mechanism in double doped glasses was proposed:

$$^5D_4\ (Tb^{3+}) + {}^7F_0\ (Eu^{3+}) \rightarrow {}^7F_5\ (Tb^{3+}) + {}^5D_1\ (Eu^{3+})$$

Upon λ_{ex} = 378 nm, Tb^{3+} ions are excited from $^7F_6$ ground state to the $^5D_3$ excited state (Fig. 15). Then, a non-radiative relaxation process to the $^5D_4$ state occurs. From $^5D_4$ state, the radiative transitions directly to the ground states at 496 nm ($^5D_4 \rightarrow {}^7F_6$), 549 ($^5D_4 \rightarrow {}^7F_5$), 594 nm ($^5D_4 \rightarrow {}^7F_4$) and 628 nm ($^5D_4 \rightarrow {}^7F_3$) take place. Part of the energy from $^5D_4$ energy level of Tb^{3+} can be transferred to the $^5D_1$ level of Eu^{3+} due to the existing overlap of the $^5D_4 \rightarrow {}^7F_5$ emission band of Tb^{3+} and $^7F_0 \rightarrow {}^5D_1$ excitation band of Eu^{3+} ions. Then, relaxed non-radiatively to the 5D0 and, subsequently, by radiative transitions to the $^7F_0$ (578 nm), $^7F_1$ (591 nm), $^7F_2$ (615 nm), $^7F_3$ (652 nm) and $^7F_4$ (700 nm) levels.

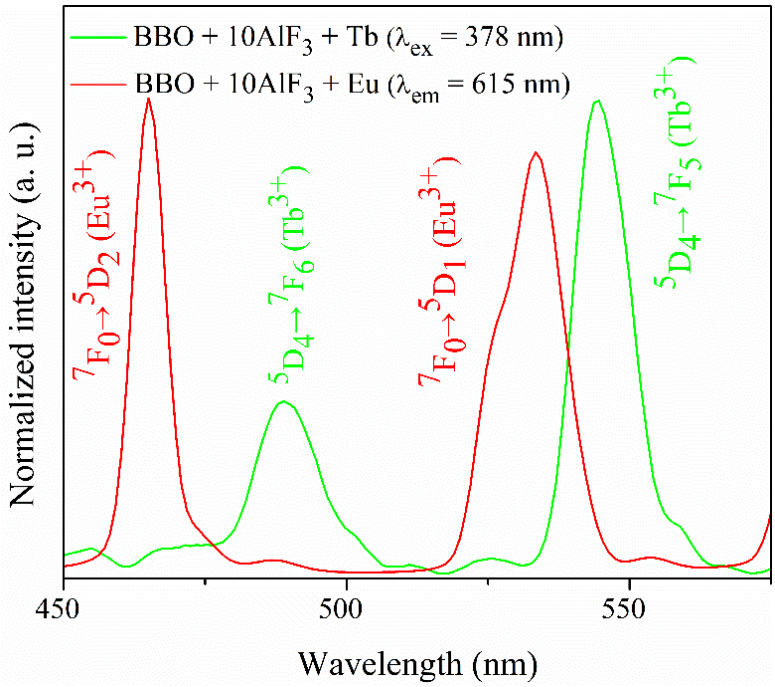

Figure 13 The excitation spectrum of BBO+10AlF_3+Eu glass at λ_{em} = 615 nm (Eu^{3+}), and the emission spectrum of the BBO+10AlF_3+Tb glass under λ_{exc} =378 nm (Tb^{3+}).

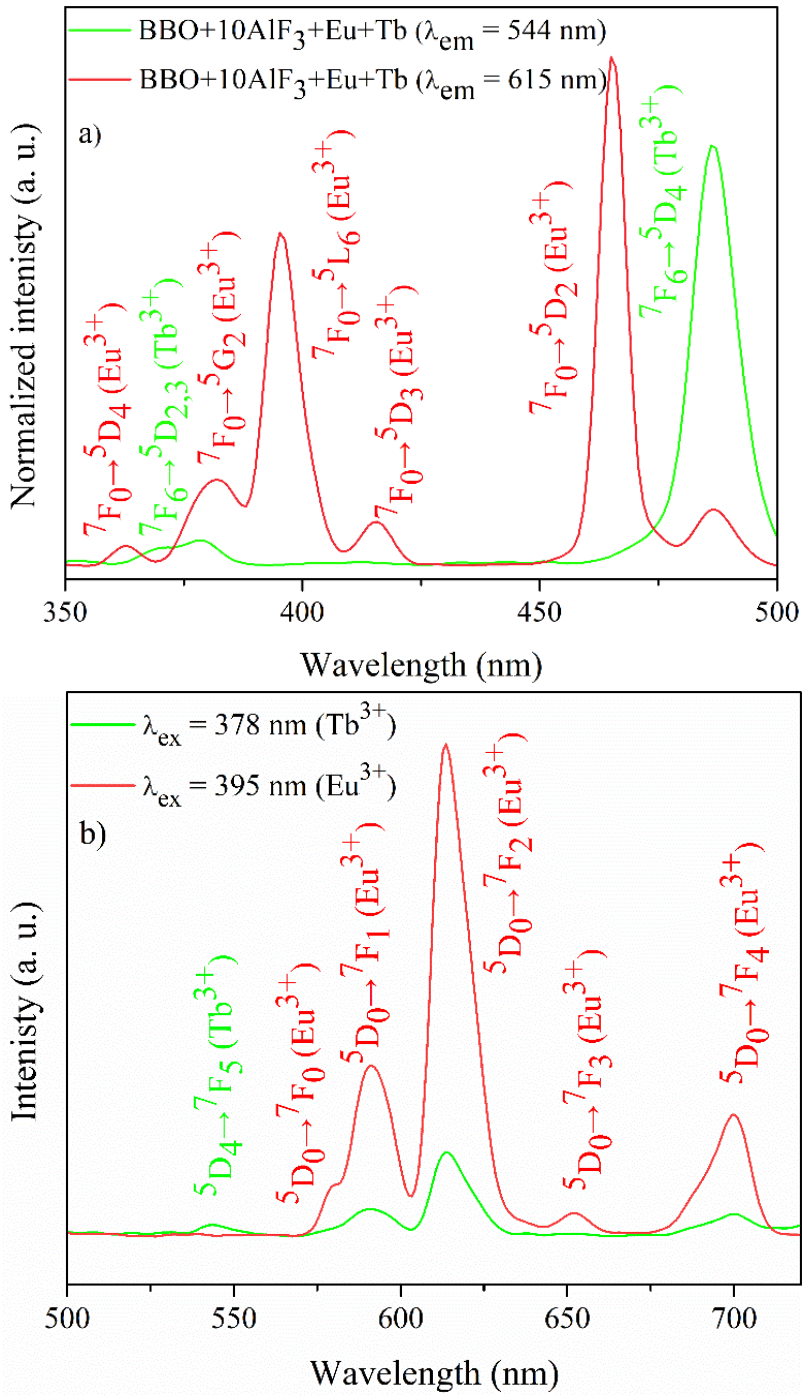

Figure 14 a) excitation spectra for BBO+10AlF_3+1Eu+1Tb sample under 544 nm, and 615 nm; b) emission spectra for BBO+10AlF_3+1Eu+1Tb at λ_{ex}= 395 nm and λ_{ex}= 387 nm.

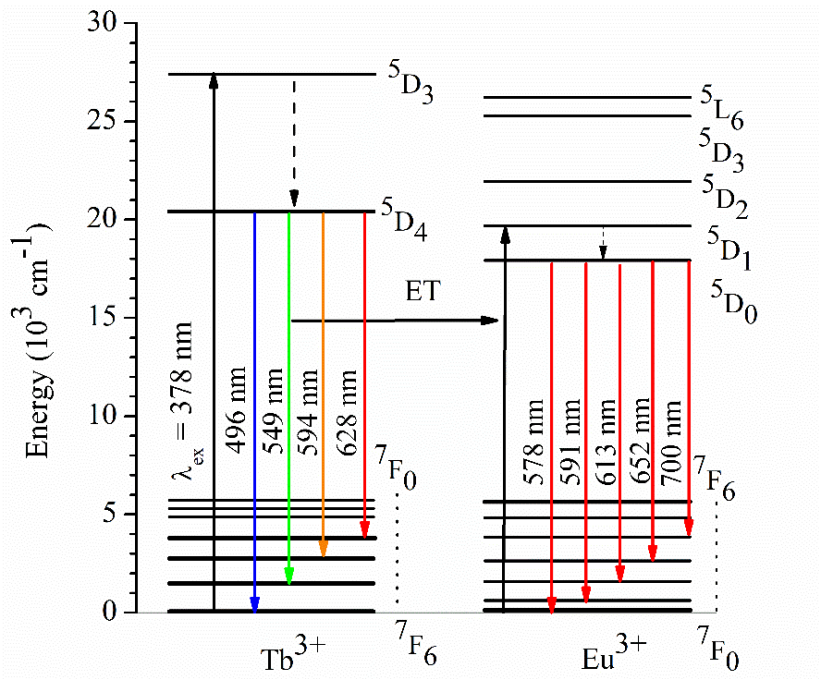

Figure 15 Partial energy level diagrams of Tb^{3+} and Eu^{3+}.

The colors of the emitted light were determined on the basis of CIE chromatic coordinates diagrams (Fig. 16). The proportions of RE ions and used excitation wavelengths influence the emitted colors. The samples triply co-doped with Eu^{3+}/ Tb^{3+}/Tm^{3+} ions were excited at λ_{exc} = 355 nm, a wavelength selected based on the luminescence spectra. The CIE chromatic coordinates for BBO+10AlF_3 glasses singly doped with Eu^{3+}, Tb^{3+}, Tm^{3+}, and triply doped with Eu^{3+}/Tb^{3+}/Tm^{3+} ions (BBO+10AlF3:Ln1, BBO+10AlF3:Ln2, BBO+10AlF3:Ln3) upon different excitations wavelengths are shown in Fig. 16. The emission of orange-yellowish light was achieved for BBO+10AlF3:Ln1 (a) and BBO+10AlF3:Ln2 (b). The color closest to white light was obtained at 355 nm excitation of the BBO+10AlF3:Ln3 (c) glass sample, where the addition of europium ions responsible for the reddish-orange color component was the lowest. Additionally, the singly doped samples with Eu^{3+}, Tb^{3+}, and Tm^{3+} ions were depicted, with emission in red, green, and blue color, respectively. The reason for such a difference in color change can be attributed to the presence of a new band in the emission spectrum. This sample reveals the peaks of all three added rare earth ions. It can be seen, that emitted color can be tuned by varying the rare-earth ions ratios. However, in order to achieve the generation of white light in the proposed bismuth-borate glass system, further studies are required, to consider an appropriate ratio of rare-earth ions and excitation wavelength. The detailed

corresponding chromaticity parameters (x, y) and correlated color temperature CCT values calculated according to Eq. (3) are shown in Table 3 [74].

$$CCT = -449n^3 + 3525n^2 - 6823n + 5520.33 \quad (3)$$

Where $n = (x-x_e)/(y-y_e)$ with $x_e = 0.332$ and $y_e = 0.186$.

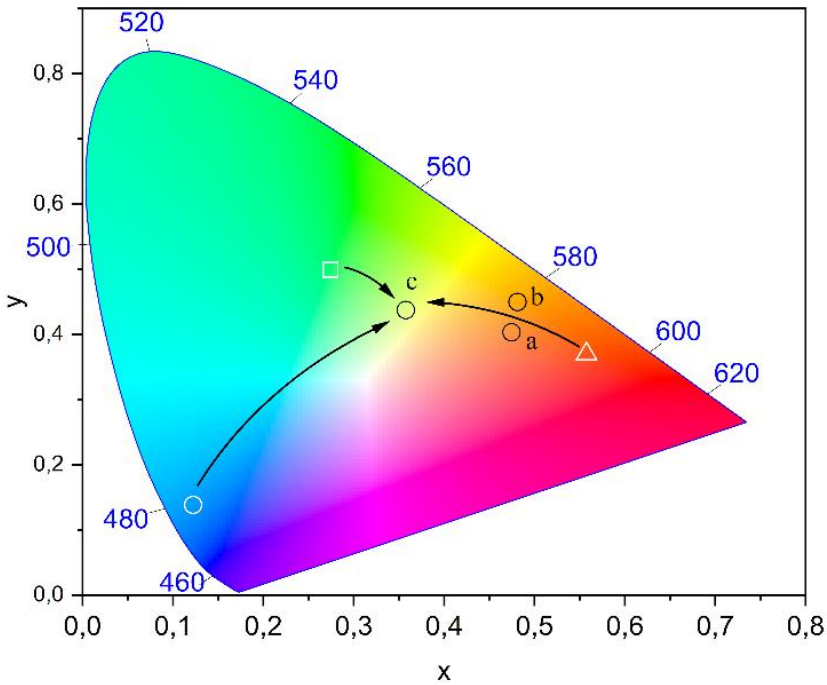

Figure 16 CIE chromaticity diagram of BBO+10AlF_3 glasses singly doped with Eu^{3+} at λ_{exc}= 395 nm (white triangle), Tb^{3+} at λ_{exc}= 378 nm (white square), Tm^{3+} at λ_{exc}= 355 nm (white circle) and triply doped with $Eu^{3+}/Tb^{3+}/Tm^{3+}$ samples at λ_{exc}= 355 nm: BBO+10AlF_3:Ln1 (a), BBO+10AlF_3:Ln2 (b), BBO+10AlF_3:Ln3 (c).

Table 3. Calculated x, y and CCT parameters.

Sample	λ_{ex} [nm]	x	y	CCT (K)
BBO+10AlF_3:Ln1	355	0.47	0.40	2475
BBO+10AlF_3:Ln2	355	0.48	0.45	2727
BBO+10AlF_3:Ln3	355	0.36	0.44	4804
Standard white [46]	-	0.33	0.33	5455
YAG+blue chips (II)[47]	-	0.29	0.30	5610
CdO-GeO_2-TeO_2: Dy^{3+}/Eu^{3+} glass [48]	382	0.41	0.40	3435
B_2O_3-TeO_2-PbO-ZnO-Li_2O-Na_2O-Er^{3+}/Dy^{3+} glass [49]	-	0.36	0.43	4753

The obtained results, in accordance with the thesis assumed in this doctoral dissertation, indicate that the proposed borate-bismuth glasses doped with AlF_3 could be suitable matrices for optically active RE^{3+} ions. The prepared samples were amorphous and consisted of [BO_3] triangular and [BO_4] tetrahedral structural units. The XPS studies

confirmed the presence of Al^{3+} ions in the form of AlF_3 and Al_2O_3 in the glass matrix. The introduction of AlF_3 into the borate-bismuth matrix resulted in an increase in the luminescence intensity of RE^{3+} ions in glasses containing 10 mol% AlF_3 compared to glasses without the addition of AlF_3 and those with the addition of 20 mol% AlF_3. It was demonstrated that the emitted color can be tuned by changing the proportions of RE^{3+} ions. The local symmetry of Eu^{3+} ions could be reduced due to the presence of Al^{3+} ions, while the decrease in Eu^{3+} intensity at higher Al^{3+} concentration could indicate higher symmetry around RE^{3+} ions.

The described results are consistent with the thesis presented in this doctoral dissertation and allow for a positive assessment of the proposed borate-bismuth glasses containing AlF_3 as new matrices for optically active RE^{3+} ions. The goals of this doctoral dissertation have been achieved. Optimal conditions for the synthesis of borate-bismuth glass matrices were established, allowing for obtaining transparent glasses. The RE^{3+} ions were successfully dissolve in the obtained glasses. Their luminescent properties were analyzed. Subsequently, the matrices were successfully modified by adding AlF_3, and its effect on the properties of glasses was examined.

The presented glassy matrix with composition (in mol%) $45B_2O_3$–$45Bi_2O_3$–$10AlF_3$ was used in further research on luminescent materials, particularly to obtain white light from RE^{3+} ions. Results of work carried out in this direction are described in the next part of the dissertation.

3.2. "Tunable emission and energy transfer of B_2O_3–Bi_2O_3–AlF_3 glass system doped with Eu^{3+}/Dy^{3+} "

Publication titled „Tunable emission and energy transfer of B_2O_3–Bi_2O_3–AlF_3 glass system doped with Eu^{3+}/Dy^{3+} " [II] is the continuation of research work on borate-bismuth glasses doped with AlF_3 to be use as matrices for RE^{3+} ions. It describes the results of research on the structure of glasses with Al^{3+} ions and RE^{3+} luminescence. This study provides a detailed analysis of the structural and luminescent properties of prepared glasses. In particular, the influence of the excitation wavelength and the ratio of the Eu^{3+}/Dy^{3+} ions on the emitted color was investigated. The borate-bismuth glasses described in the previous publication [I] with the composition (in mol%) $45B_2O_3$–$45Bi_2O_3$–$10AlF_3$ were used as matrices for selected RE^{3+} : Eu^{3+} and Dy^{3+}. The choice of Eu^{3+} and Dy^{3+} for simultaneous doping of materials resulted from the desire to obtain emission in a specific range of visible radiation. The RE^{3+} ions were introduced into the glasses in various proportions of Eu^{3+} to Dy^{3+}, but their total amount remained unchanged and was always 2% mol. Samples with the compositions shown in the table (Table 4) were selected for further testing.

Table 4. Detailed composition of prepared samples.

Name	B_2O_3	Bi_2O_3	AlF_3	Eu_2O_3	Dy_2O_3
BBO	50	50	-	-	-
BBO+2Eu	49	49	-	2	-
BBO+2Dy	49	49	-		2
BBO+10AlF_3	45	45	10	-	-
BBO+10AlF_3+2Eu	44	44	10	2	-
BBO+10AlF_3+2Dy	44	44	10	-	2
BBO+10AlF_3+Ln1	44	44	10	0.5	1.5
BBO+10AlF_3+Ln2	44	44	10	1	1
BBO+10AlF_3+Ln3	44	44	10	1.5	0.5

The obtained glasses were, as previously, transparent and slightly yellow. The XRD confirmed the amorphous nature of the samples, and DTA didn't differ from the previous results presented in publication (I). In this publication, significant effort has been made to carefully analyze the FTIR and Raman spectra to obtain information about the structural units of the studied samples. Spectra were deconvoluted, to analyze potential differences due to the addition of 10 mol% of AlF_3 in the spectra (Fig. 17). The peak parameters such as peak position (x_c), amplitude (A), and full width at half maximum (FWHM), were determined (Table 5). No significant differences can be seen in the spectra with and without AlF_3, except for a slight shift of peaks. The changes in peak positions

and parameters may be attributed to structural modifications that occurring in the glass matrix after the addition of AlF_3. Similar results were obtained in Raman measurements (Fig. 18). The parameters were collected in Table 6. No evidence of new bands connected to the presence of AlF_3 can be observed in the spectrum. Only slight changes in the peak positions due to addition of AlF_3, as seen in FTIR spectra, are noticeable. The detailed assignments of FTIR and Raman peaks are summarized in Table 7.

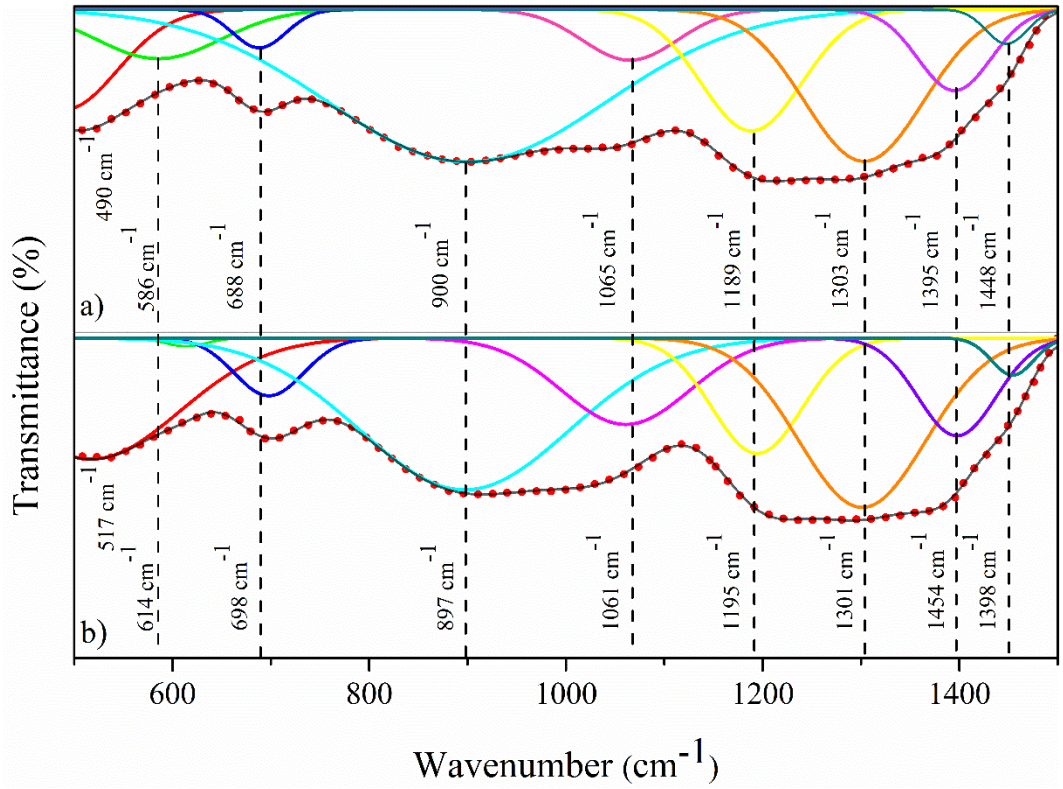

Figure 17 Deconvoluted FTIR spectra of BBO (a) and BBO+10AlF_3+Dy (b) glasses. Experimental data and gaussian components are shown by black and colored solid lines, respectively. The simulated spectrum is shown by red dots.

Table 5. Peak position x_c (cm^{-1}), amplitude A (a. u.) and full width at half maximum WFHM (cm^{-1}) of deconvoluted BBO and BBO+10AlF_3+ 2Dy FTIR spectra.

	BBO			BBO+10AlF_3 + 2Dy		
	x_c	A	FWHM	x_c	A	FWHM
1	490	7	128	517	15	212
2	586	4	150	614	1	50
3	688	3	64	698	7	83
4	900	11	334	897	19	251
5	1065	4	114	1061	11	153
6	1189	9	120	1195	15	108
7	1303	11	142	1301	21	152
8	1395	6	87	1398	12	93
9	1448	2	49	1454	5	50

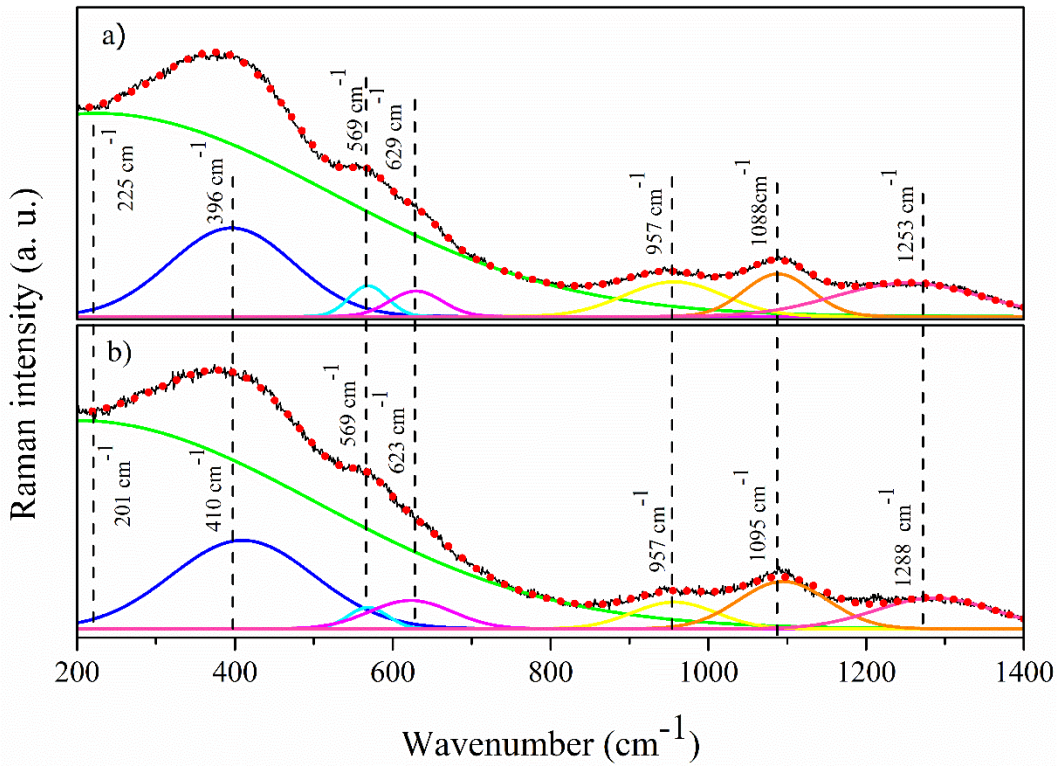

Figure 18 Raman spectra of BBO (a) and BBO+10AlF_3+Dy (b) glasses. Experimental data and gaussian components are shown by black and colored solid lines, respectively. The simulated spectrum is shown by red dots.

Table 6. Peak position x_c (cm^{-1}), amplitude A (a. u.) and full width at half maximum WFHM (cm^{-1}) of deconvolution BBO and BBO+10AlF_3+2Dy Raman spectra.

	BBO			BBO+10AlF_3 + 2Dy		
	x_c	**A**	**FWHM**	**x_c**	**A**	**FWHM**
1	225	7977	703	201	4207	712
2	396	3474	185	410	1787	212
3	569	1204	57	569	431	60
4	629	1002	78	623	573	124
5	957	1360	149	957	539	126
6	1088	1671	101	1095	956	133
7	1253	1317	218	1288	624	177

Table 7. Assignment of Raman and FTIR bands of the BBO and BBO + 10AlF_3+2Dy.

Raman peak position (cm-^{1})	**Raman assignments**	**FTIR peak position (cm^{-1})**	**FTIR assignments**
225, 201	Vibrations of Bi-O bonds in [BiO_3] and [BiO_6]	490, 517	Bi-O bending vibrations in [BiO_6] octahedral units
396, 410	Bi–O–Bi stretching vibrations in [BiO_6] octahedral units	586, 614	Bi – O and Bi-O-Bi stretching vibrations of [BiO_6] octahedral units
569	Bi–O stretching vibrations in [BiO_6] units	688, 698	Bending vibrations of B-O-B in [BO_3] triangles
629 ,623	Bending vibrations of B–O–B bridges in metaborate groups of [BO_3] triangular units	900 ,897	B-O stretching in BO4units from diborate groups Stretching B-O vibrations in [BO_4] units from diborate groups
957	Vibrational modes occurring in bonds like B-O-B and B—O in pyroborate groups of [BO3] units	1065, 1061	Stretching of B-O in [BO_4] units from tri, tetra and pentaborate groups
1088, 1095	existence of diborate groups	1189, 1195	B-O stretching vibrations of trigonal BO3units inboroxol rings
1253, 1288	stretching vibrations of B-O bands of/in non-bridging oxygens (NBO) in borate groups	1303, 1301	B-O stretching vibrations of trigonal [BO_3] units in the boroxol ring
		1395, 1398	B-O stretching vibrations of [BO_3] units in metaborate, pyroborate, and orthoborate groups
		1448, 1454	Antisymmetric stretching vibrations with non-bridging oxygens (NBOs) of B-O-B groups

An important aspect was the analysis of their luminescent properties, particularly the potential for generating white light with a specific color temperature through the simultaneous emission of RE^{3+} ions. Initially, optical characterization was performed using steady-state luminescence measurements to obtain detailed information about the luminescence properties of Eu^{3+}/Dy^{3+} doped glasses and the possibility of white-light generation through simultaneous excitation of rare-earth ions with a single wavelength. The excitations spectra for glasses doped with 2 mol% od Dy^{3+}, detecting at λ_{em} = 574 nm show peaks assigned to the transitions of Dy^{3+} ions from the ground energy level, $^6H_{15/2}$, to $^4F_{9/2}$, $^4I_{15/2}$, $^4G_{11/2}$ $^4I_{13/2}$, $^6P_{5/2}$, $^6P_{7/2}$, can be seen at 472, 453, 425, 388, 365, 351 nm (Fig. 19a). After excitation at λ_{ex} = 388 nm, emission spectra shows three bands corresponding to the transitions from the $^7F_{9/2}$ excited state to the $^6H_{15/2}$, $^6H_{13/2}$, and $^6H_{11/2}$

ground states at 481, 574, and 661 nm. When glasses are doped with 2 mol % of Eu^{3+} ions, excitation spectra observed after detection on the most intense peak at 612 nm consist of the several bands associated with the transition from the $^7F_{0,1}$ state to the $^5D_4$, $^5G_4$, $^5L_6$, $^5D_3$, $^5D_2$, and $^5D_1$ at 360, 374, 382, 394, 414, 465, 524, 529 nm, respectively (Fig.19b). After excitation at λ_{ex} = 394 nm, emission spectra shows five bands corresponding to the transitions from the $^5D_0$ excited state to the $^7F_0$, $^7F_1$, $^7F_2$, $^7F_3$, and $^7F_4$ at 578 nm, 591 nm, 615 nm, 652 nm, and 700 nm.

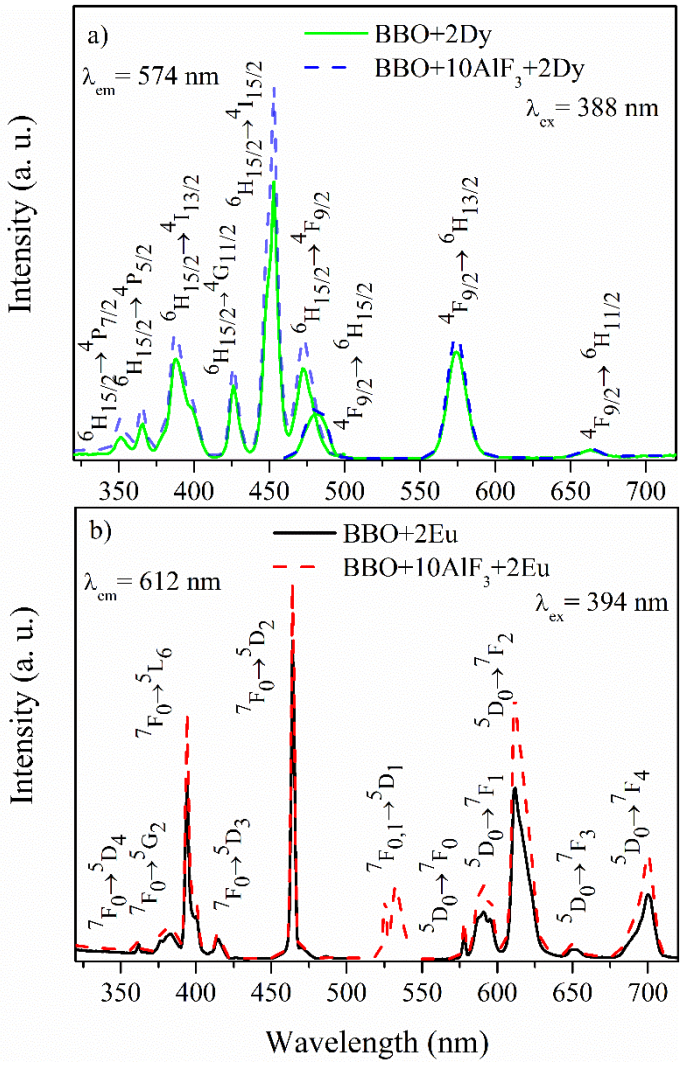

Figure 19 Excitation and emission spectra of BBO and BBO+10AlF_3 glasses doped with Dy^{3+}(a) and Eu^{3+} (b).

As examined in the previous publication (I), the luminescence intensity is higher for samples doped with 10 mol% of aluminum fluoride. To investigate the simultaneous

excitation of Eu^{3+}/Dy^{3+}, the four wavelengths were used: 365, 380, 388, and 394 nm (Fig.20 (a-d)), along with different molar ratios of Eu^{3+}/Dy^{3+}. In all samples, two characteristic peaks for Dy^{3+} ions can be observed at 483 nm (blue) and 574 nm (yellow), corresponding to the $^4F_{9/2}\rightarrow{}^6H_{15/2}$ and $^4F_{9/2}\rightarrow{}^6H_{13/2}$ transitions, respectively. The intensity ratio of the bands in the blue and yellow spectral regions can provide information about the local symmetry around RE^{3+} ions. In case of Dy^{3+}, the $^4F_{9/2}\rightarrow{}^6H_{13/2}$ transition is a magnetic dipole transition (MD) that is less sensitive to the crystal field around the optically active ion. The MD transition becomes prominent when the Dy^{3+} ions are surrounded by a highly symmetric environment with the inversion center. Conversely, the $^4F_{9/2}\rightarrow{}^6H_{13/2}$ emission represents a hypersensitive forced electric dipole transition (ED), which exhibit stronger emission when Dy^{3+} ions are in a low-symmetry site without an inversion center, corresponding to an amorphous glassy environment. In all samples, the band located at 574 nm exhibits stronger emission, indicating that in the proposed borate-bismuth glass matrix, Dy^{3+} ions are located at the low symmetry crystallographic sites, without an inversion center. Furthermore, the intensity of the ED and MD bands of Dy^{3+} ions varies with the concentration of Dy^{3+} ions and with the excitation wavelength.

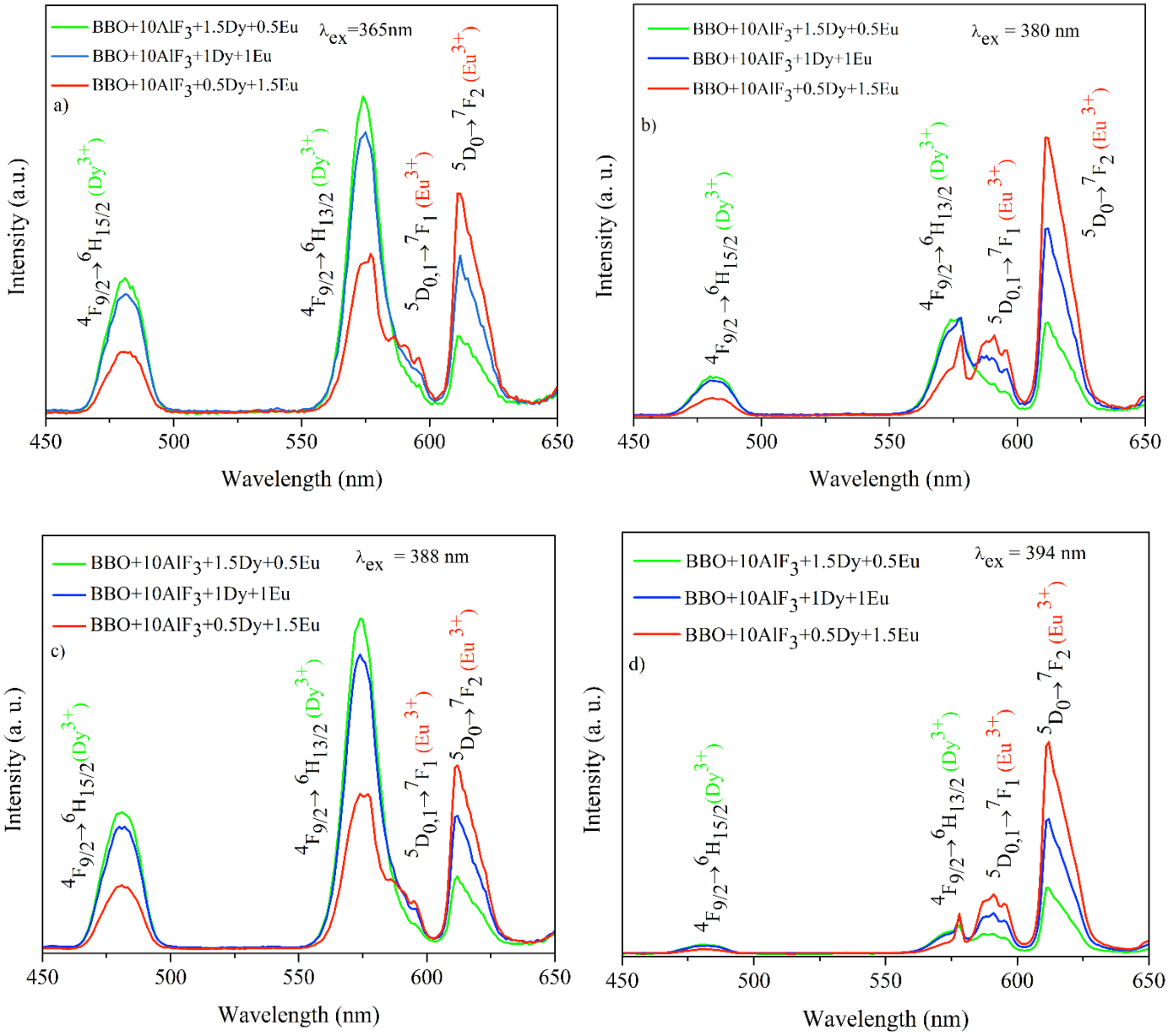

Figure 20 Excitation spectra of glass samples doubly doped with Eu^{3+}/Dy^{3+} under a) λ_{ex} = 365 nm, b) λ_{ex} = 380 nm, c) λ_{ex} = 388 nm, d) λ_{ex} = 394 nm.

After excitation at 394 nm, corresponding to the $^7F_0 \rightarrow {}^5L_6$ transition of Eu^{3+} ions, the emission of Dy^{3+} ions is very weak, and the luminescence of Eu^{3+} ions dominates the spectrum. This changes when the glasses are excited with one of the wavelengths associated with the Dy^{3+} ions transitions (365 nm, 388 nm). In these cases, the emission peaks associated with the Dy^{3+} ions dominate the spectrum. Nevertheless, the relation of band intensities at 483 nm and 574 nm is remains the same in all cases. A closer examination of the transitions associated with the Eu^{3+} ions suggests that they occupy low-symmetry sites. Similar to Dy^{3+} ions, Eu^{3+} ions exhibit two emission peaks at 590

nm and 612 nm , the ratio of which can provide information about the local symmetry around them. The first one, is related to the magnetic dipole (MD) transition from the $^5D_{0,1}$ excited levels to the $^7F_1$ ground state, while the band at 612 nm is an electric dipole (ED) transition. As in the case of Dy^{3+} ions, the ED transition has a stronger emission, indicating that the optically active ions are located in the non-inversion environment. The color emitted by the glasses was described by the x and y chromaticity coordinates and presented in the form of CIE diagrams (Fig. 21) when excited at λ_{ex} = 365 nm. The detailed corresponding chromaticity parameters (x,y) and color temperature CCT values calculated according to equation (12) are shown in Table 6 .

$$CCT = - 449n3 + 3525n2 - 6823n + 5520.33 \quad (12)$$

Where $n = (x-x_e)/(y-y_e)$ with $x_e = 0.332$ and $y_e = 0.186$.

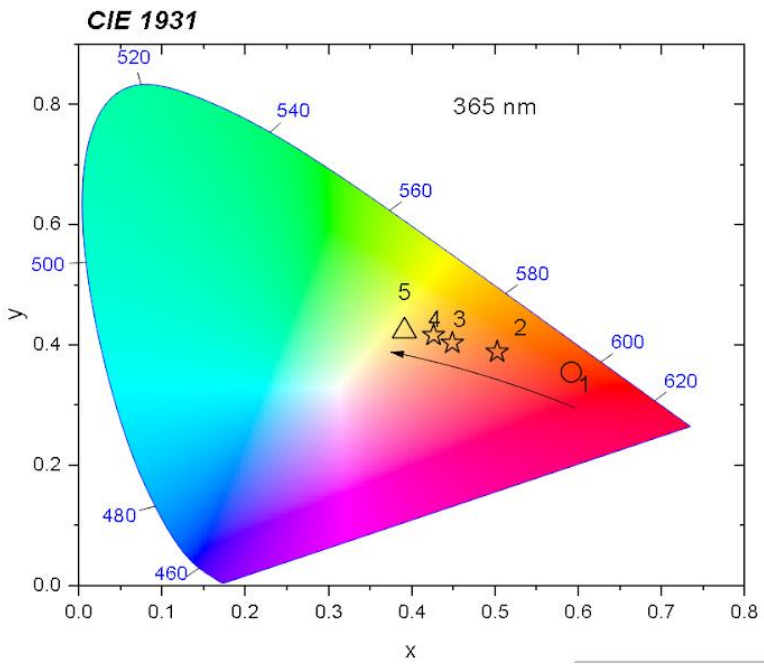

Figure 21 The 1931 CIE chromaticity diagram of single and triply doped with Eu^{3+}/Dy^{3+} glass samples.

For glass doped only with Eu^{3+} ions (black circle) excited at λ_{ex} = 394 nm, the emitted color is red. With the addition of Dy^{3+} ions, the emission shifts from reddish-orange to yellowish-orange for the BBO+10AlF_3+2Dy glass sample (black triangle). The corresponding color temperature varies from 1932K (BBO+10AlF3+2Eu) to 3352 K and 4032 K for BBO+10AlF_3+1.5Dy+0.5Eu and BBO+10AlF_3+2Dy, respectively. For BBO+10AlF_3+2Dy and BBO+10AlF_3+1.5Dy+0.5Eu samples, emission close to daylight was obtained. The emission color can be tuned by varying the molar ratios of the Eu^{3+}/ Dy^{3+}ions and by changing the excitation wavelength. The tendency to shift toward

yellowish–orange emission of samples doped with high values of Dy^{3+} ions is consistent with the luminescence analysis and can be explained by the fact that the Dy^{3+} ions mainly occupy the non-inversion symmetry sites. This promotes stronger emission at the 574 nm (yellow) band rather than the 488 (blue) nm band. As mentioned earlier, Eu^{3+} ions are also incorporated into non-inversion symmetry sites, which has a strong influence on the overall reddish-orange emission of the samples. Additionally, the color purity (CP) compared to the CIE1931 standard source C (x_i = 0.3101, y_i = 0.3162) coordinates was calculated using the weighted average of the sample emission color coordinates (x, y) relative to the illuminant coordinates (x_i, y_i) and the dominant wavelength coordinates (x_d, y_d) relative to (x_i, y_i) coordinates, according to the equation (13):

$$CP = \frac{\sqrt{(x-x_i)^2+(y-y_i)^2}}{\sqrt{(x_d-x_i)^2+(y_d-y_i)^2}} \times 100\% \quad (13)$$

with the dominant wavelength (λ_d) defined as a monochromatic wavelength of the spectrum, which coordinates are placed on the straight line connecting the phosphor with the C point. For BBO+10AlF_3+2Dy sample with the dominant wavelength at 573 nm and color purity of 50.25 %, BBO+10AlF_3:Ln1 glass exhibited a significant yellowish-orange emission with a color purity of 58.17 % at 580 nm. Next, in BBO+10AlF_3:Ln2 glass, considering a dominant emission wavelength of 585 nm close to orange light, the color purity was 62.25 %. In the BBO+10AlF_3:Ln3 glass sample, orange light was observed due to the 591 nm emission, with color purity of 71.05 %. The BBO+10AlF_3+2Eu sample exhibited high red light emission at 606 nm with color purity of 85.77 %. The CIE1931 color coordinates (x, y), correlated color temperature (CCT), dominant wavelength (λ_d), dominant wavelength coordinates (x_d, y_d) and color purity (CP) for λ_{ex} = 365 nm excitation of prepared samples and examples for other glasses doped with rare earth ions are presented in Table 8.

Table 8. Calculated x, y, and CCT for different excitation wavelengths of prepared samples and examples for other glasses doped with rare earth ions.

Sample	λ_{ex} = 365nm			
	x	y	CCT(K)	CP (%)
BBO+10AlF_3+2Dy	0.391	0.424	4050	50.25 %
BBO+10AlF_3:Ln1	0.426	0.417	3294	58.17 %
BBO+10AlF_3:Ln2	0.449	0.404	2806	60.25 %
BBO+10AlF_3:Ln3	0.502	0.389	2015	71.05 %
BBO+10AlF_3+2Eu	0.591	0.356	1875	85.77 %
Standard white	0.33	0.33	5455 [46]	
CdO-GeO_2-TeO_2: Dy^{3+}/Eu^{3+} glass	0.382	0.407	4153 [48]	
Y_2O_3-Al_2O_3-Bi_2O_3-B_2O_3-SiO_2: Dy^{3+}/Eu^{3+} glass	0.332	0.342	5520 [50]	

Additionally, the possibility of energy transfer between Eu^{3+}/Dy^{3+} doped glasses were investigated. The main condition under which this phenomenon can be present is the overlap of the absorption spectra of Eu^{3+} acting as acceptor and donor fluorescence (Dy^{3+}). In the case of the studied glasses, a partial overlap of the spectra in the range of 450–470 nm is observed (Fig. 22). The $^7F_0 \rightarrow {}^5D_2$ absorption band of Eu^{3+} ions at 464 nm overlaps with the $^4F_{9/2} \rightarrow {}^6H_{15/2}$ (484 nm) of Dy^{3+} ions. This suggests that energy transfer may occur from Dy^{3+} ions to Eu^{3+} ions in borate-bismuth glasses. Fig. 23 a shows the emission spectra of Eu^{3+}/Dy^{3+} codoped glass upon 351 nm and 388 nm excitation, corresponding to Dy^{3+} ions, where the Eu^{3+} ions should not be excited. However, the emission spectra, apart from the bands characteristic for Dy^{3+} ions, also reveal the europium $^5D_0 \rightarrow {}^7F_2$ and $^5D_0 \rightarrow {}^7F_4$ transitions. This indicates that Eu^{3+} ions are sensitized by Dy^{3+} ions. In Fig. 23 b, the excitation spectrum of the glass doped with Dy^{3+} ions, monitored at the $^4F_{9/2} \rightarrow {}^6H_{13/2}$ transition (Dy^{3+}), shows bands that can be assigned only to the transitions of Dy^{3+} ions. Similarly, the spectrum of the sample singly doped with Eu^{3+} ions monitored at 612 nm ($^5D_0 \rightarrow {}^7F_2$), contains only peaks originating from transitions of Eu^{3+} ions. However, the spectrum of the Eu^{3+} and Dy^{3+} codoped glass (BBO+10AlF_3+1Dy+1Eu), monitored at the $^5D_0 \rightarrow {}^7F_2$ Eu^{3+} transition, reveals additional bands observed in the Dy^{3+} single doped glass monitored at 574 nm. Therefore, the excitation upon 351 nm through Dy^{3+} ions (Fig. 23a) and the presence of Dy^{3+} bands in Dy^{3+}/Eu^{3+} excitation spectrum at 612 nm suggest that the energy transfer from Dy^{3+} to Eu^{3+} ions occurs. This can be supported by the spectral overlap of the Eu^{3+} absorption band and Dy^{3+} emission band seen in Fig.22.

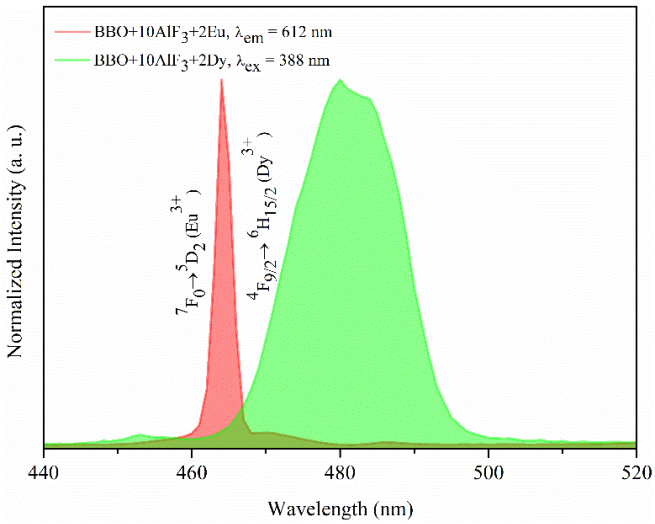

Figure 22. Partially overlap of the emission spectrum of BBO+10AlF_3+2Dy^{3+} at λ_{ex} = 388 nm and the excitation spectrum of BBO+10AlF_3+2Eu^{3+} λ_{em} = 612 nm.

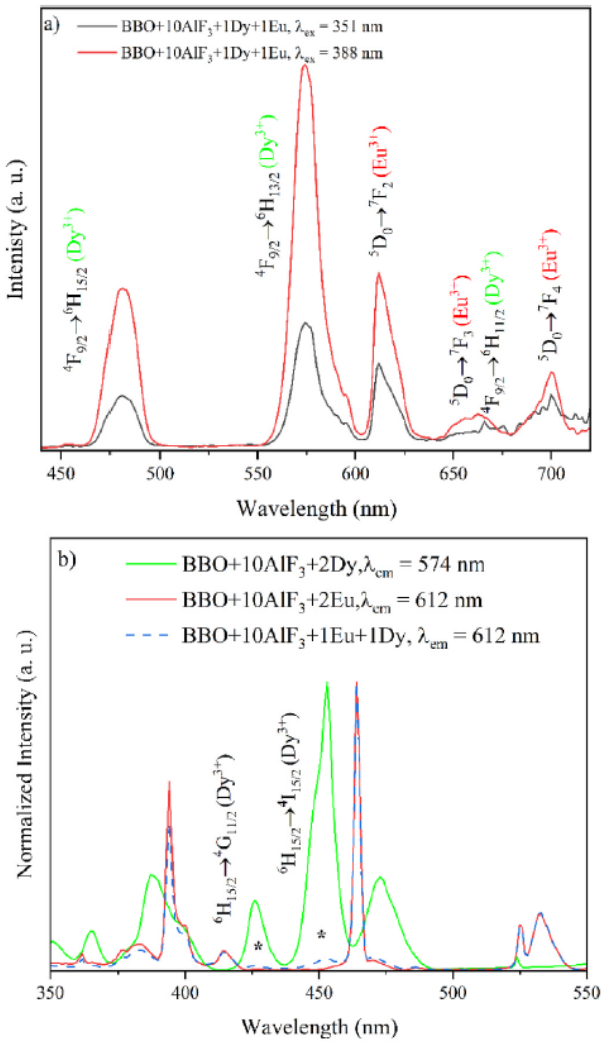

Figure 23. (a) Emission spectra of Eu^{3+}/Dy^{3+} codoped glass upon 351 nm and 388 nm excitation, (b) excitation spectra of BBO+10AlF_3+2Eu and BBO+10AlF_3+1Dy+1Eu glasses at λ_{em} = 612 nm and BBO+10AlF_3+2Dy at λ_{em} = 574 nm.

This behavior suggested that the energy transfer from Dy^{3+} to Eu^{3+} ions occurs, and the excitation of Dy^{3+} ions can contribute to the emission spectrum of the codoped glasses. Fig. 24 presents an energy level diagram of Eu^{3+} and Dy^{3+} ions and the possible energy transfer mechanism between both ions in the codoped glasses. This energy transfer mechanism can be described as follows:

$$^{7}F_{0}\ (Eu^{3+}) + {}^{4}F_{9/2}\ (Dy^{3+}) \rightarrow {}^{5}D_{2}\ (Eu^{3+}) + {}^{6}H_{15/2}\ (Dy^{3+})$$

Concretely, after excitation at 388 nm Dy^{3+} ions are excited from the $^{6}F_{15/2}$ ground state to the $^{4}I_{13/2}$ excited state and then relaxed non-radiatively to the $^{4}F_{9/2}$ level. From this level, the glass shows radiative emissions to the $^{6}H_{15/2}$ (480 nm), $^{6}H_{13/2}$ (574 nm), and $^{6}H_{11/2}$ (662 nm). Additionally, part of the energy can be transferred non-radiatively from the $^{4}F_{9/2}$ energy level of Dy^{3+} to the $^{5}D_{2}$ excited level of Eu^{3+}. Then the excited Eu^{3+} ions relaxed non-radiatively to the $^{5}D_{0}$ and next by radiative transitions to the $^{5}D0$, $^{7}F_{1}$, $^{7}F_{2}$, $^{7}F_{3}$, and $^{7}F_{4}$ occur.

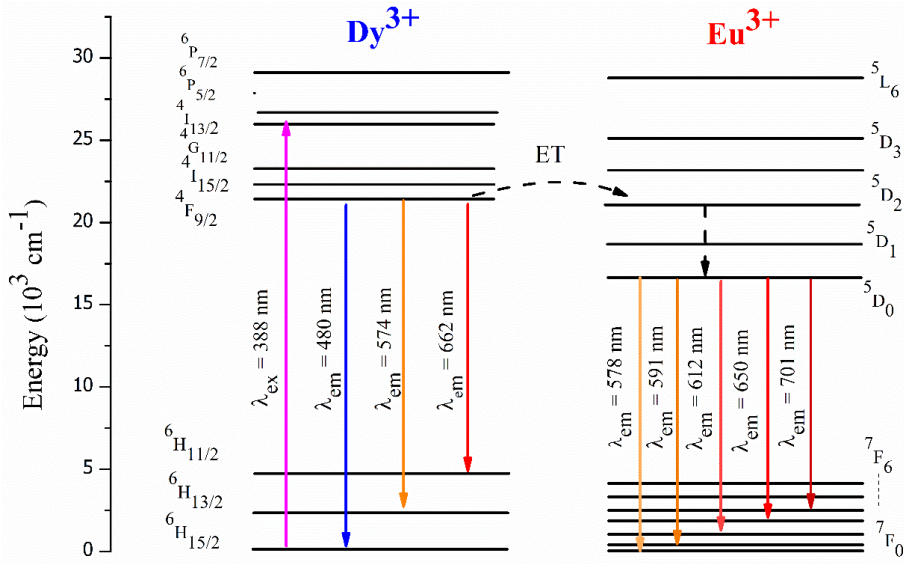

Figure 24 Energy levels of Eu^{3+} and Dy^{3+} ions.

To gain better insight into the luminescence properties of Eu^{3+} and Dy^{3+} doped glasses, luminescence decay curves were measured (Fig. 25). The obtained decay curves can be described as two-exponential decays by the following equation (14):

$$I(t) = A_1 \exp\left(\frac{-t}{\tau_1}\right) + A_2 \exp\left(\frac{-t}{\tau_2}\right) \quad (14)$$

Where A_1 and A_2 are the amplitudes of the two decay components, τ_1, and τ_2 are the short and long luminescence lifetimes, respectively. The τ_1 is attributed to the rare-earth ions placed in a low symmetry environment, while the τ_2 is a component related to the RE^{3+} in a higher symmetry crystal field. Both, τ_1 and τ_2 are components of the average lifetime $<\tau_{avg}>$, which was calculated using equation 15 [24]. The calculated values can be seen in Table 7.

$$\tau_{<avg>} = \frac{(A_1\,\tau_1^2 + A_2\,\tau_2^2)}{(A_1\,\tau_1 + A_2\,\tau_2)} \quad (15)$$

Table 9. Calculated parameters of luminescence decays of glasses doped with Eu^{3+}/Dy^{3+} at λ_{ex}=388 nm and observation at λ_{em}=574 nm.

Sample	τ_1(μs)	τ_2 (μs)	$<\tau_{avg}>$ (μs)
BBO+10AlF_3+1.5Eu+0.5 Dy	130	470	420
BBO+10AlF_3+1Eu+1Dy	180	450	350
BBO+10AlF_3+0.5Eu+1.5 Dy	150	410	320
BBO+10AlF_3+2Dy	60	330	300

The average lifetimes of the Dy^{3+}: $^4F_{9/2} \rightarrow {}^6H_{13/2}$ transition were found to be strongly related to the concentration of Eu^{3+} and Dy^{3+} ions. The lifetimes of dysprosium increase with decreasing Dy^{3+} content from 420 μs for BBO+10AlF_3+1.5Eu+0.5Dy sample to 320 μs for BBO+10AlF_3+0.5Eu+1.5 Dy. This agrees with other previous studies. The highest value is obtained for glass doped with 1.5 % of europium. This indicates that the lifetimes of Dy^{3+} increase with increasing europium content, which may be evidence of $Eu^{3+} \rightarrow Dy^{3+}$ energy transfer occurring in the borate-bismuth glass system. Additionally, to determine the influence of AlF_3 addition, lifetime measurements of single doped glasses were conducted. The BBO+2Eu and BBO+10AlF_3+2Eu glasses were excited at λ_{exc}=394 nm and observed around 612 nm (Fig. 23 b). The sample BBO+2Dy and BBO+10AlF_3+2Dy were monitored at 388 m excitation wavelength and observed at around 574 nm (Fig.23 b). A single exponential decay was observed in Eu^{3+} doped glasses, while a two exponential decay was observed in glasses doped with Dy^{3+} ions.

Similar behavior was observed by T. Lewandowski et al [51]. This behavior can be explained by the fact, that decay times of Dy^{3+} ions in glass matrix are strongly related to the Dy^{3+} ions concentration. It was found that in glasses with higher Dy^{3+} concentration, the double-exponential decay was observed. The calculated parameters are presented in Table 10. In the case of glasses doped with Eu^{3+}, the decay times did not differ much from each other. However, in Dy^{3+} doped samples, and increase of the 40 μs can be observed due to the addition of AlF_3.

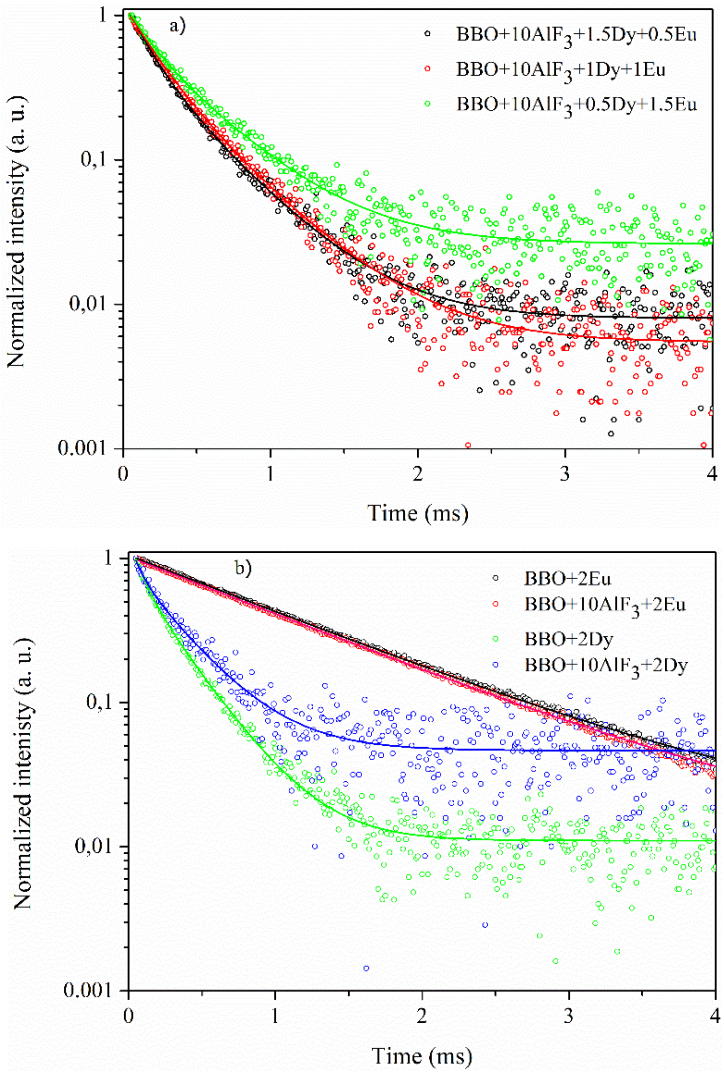

Figure 25 The luminescence decay times for (a) double and single (b) BBO glasses doped with Eu^{3+}/Dy^{3+} ions.

Table 10. Calculated parameters of luminescence decays of glasses doped with Eu^{3+}/Dy^{3+}.

	τ_1 (μs)	τ_2 (μs)	τ_{avg} (μs)
λ_{ex} = 394 nm, λ_{obs} = 612 nm,			
BBO+2Eu	1120	-	-
BBO+10AlF_3+2Eu	1110	-	-
λ_{ex} = 388 nm, λ_{obs} = 574 nm,			
BBO+2Dy	80	290	260
BBO+10AlF_3+2Dy	60	330	300

Presented in this publication, the B_2O_3-Bi_2O_3 glass system doped with AlF_3 and Eu^{3+}/Dy^{3+} ions in various molar ratios was successfully synthesized using a conventional melt quenching technique. RE^{3+} ions present in the studied glasses are placed mostly in low-symmetry crystallographic sites, without an inversion center. Color-tunable emission was achieved due to the different ratios of Eu^{3+}/Dy^{3+} addition. Glasses singly doped with Eu^{3+} emitted a reddish-orange color, when excited at 394 nm, while the addition of dysprosium ions, shifted the emitted color to a warm yellowish-orange close to daylight. The addition of AlF_3 significantly influenced the luminescence properties of Eu^{3+}/Dy^{3+} doped glasses. Samples doped with 10 mol% of aluminum fluoride exhibited enhanced luminescence compared to undoped ones. Additionally, all prepared samples were transparent, making them suitable for optical applications. Obtained borate-bismuth glasses doped with AlF_3 and Eu^{3+}/Dy^{3+} could thus serve as phosphors for solid-state lighting devices.

The above results confirm that the scientific and research theses presented in this doctoral dissertation have been fulfilled. Borate-bismuth glass matrices were synthesized, modified with the addition of AlF_3 and dopped with RE^{3+} ions. The obtained results indicated that, they are suitable for doping with RE^{3+} ions. It has been demonstrated that it is possible to vary the color of emitted light by changing the ratio of RE^{3+} ions, achieving the color close to warm white light in the proposed glasses doubly doped with Eu^{3+} and Dy^{3+} ions.

3.3. "From Structure to Luminescent Properties of B_2O_3-Bi_2O_3-SrF_2 Glass and Glass-Ceramics Doped with Eu^{3+} Ions"

In the publication entitled *" From Structure to Luminescent Properties of B_2O_3-Bi_2O_3-SrF_2 Glass and Glass-Ceramics Doped with Eu^{3+} Ions "* (III) results on new borate-bismuth glass ceramics doped with SrF_2 and Eu^{3+} ions were presented. The publication discusses the synthesis method of glass ceramics and explores the influence of annealing of glasses on the structure and luminescence properties of optically active Eu^{3+} ions. The matrix for glass ceramics was borate-bismuth glasses with a composition (in mol %) of $50B_2O_3$–$50Bi_2O_3$, as described in subsection 3.1 and marked as BBO. Strontium fluoride was introduced into the matrix in amounts of 10 mol% and 20 mol % as a precursor of the crystal phase, along with 2% mol Eu^{3+} ions. The glass ceramic synthesis took place in two stages. Firstly, the synthesis involved obtaining glasses using the traditional melt quenching method under conditions established in the previous scientific and research work. In the second step, the synthesized glasses underwent a crystallization process, with parameters selected to obtain SrF_2 crystals of nanometer size, dispersed in a borate-bismuth glassy matrix. In the case of borate-bismuth glasses, the issue of obtaining SrF_2 nanocrystals is more complicated because it is possible to obtain at least five crystalline phases of B_2O_3–Bi_2O_3 [52] and metastable bismuth orthoborate phases in this glasses [53]. The crystallization process therefore had to take into account many parameters, such as different times and temperatures of heat-treatment process, as well as the amount of SrF_2 addition. Therefore, the optimal parameters were obtained experimentally in order to obtain glass-ceramics with SrF_2 nanocrystals while maintaining the transparency of the materials.

Table 11. Compositions of the glass samples.

Name	B_2O_3	Bi_2O_3	SrF_2	Eu_2O_3
BBO	50	50	-	-
BBO+2Eu	49	49	-	2
BBO+10SrF_2	45	45	10	-
BBO+20SrF_2	40	40	20	-
BBO+10SrF_2+2Eu	44	44	10	2
BBO+20SrF_2+2Eu	44	44	10	-

Crystallization temperatures were selected based on the DSC measurements. The DSC curves make it possible to determine the characteristic temperatures of the glasses: the glass transition temperature (T_g), the onset of the crystallization process (T_x),

crystallization temperature (T_c), and melting temperature (T_m) (Fig. 26). Their knowledge allows to determining thermal parameters of glasses, such as the glass stability region (ΔT) and thermal stability (S) parameter, which describes the glass resistance against devitrification, calculated according to the equation (15).

$$S = \frac{(T_c - T_x)(T_c - T_g)}{T_g} \tag{15}$$

For BBO glass, ΔT is 110 ˚C, and S is 8.72. In other borate glasses S could be even about 1. The addition of SrF_2 to the base BBO composition led to the disappearance of the crystallization peak. Therefore, it can be said that it prevented the crystallization of the matrix. Unfortunately, no effect related to the crystallization of the SrF_2 phase in the BBO matrix was observed in these glasses.

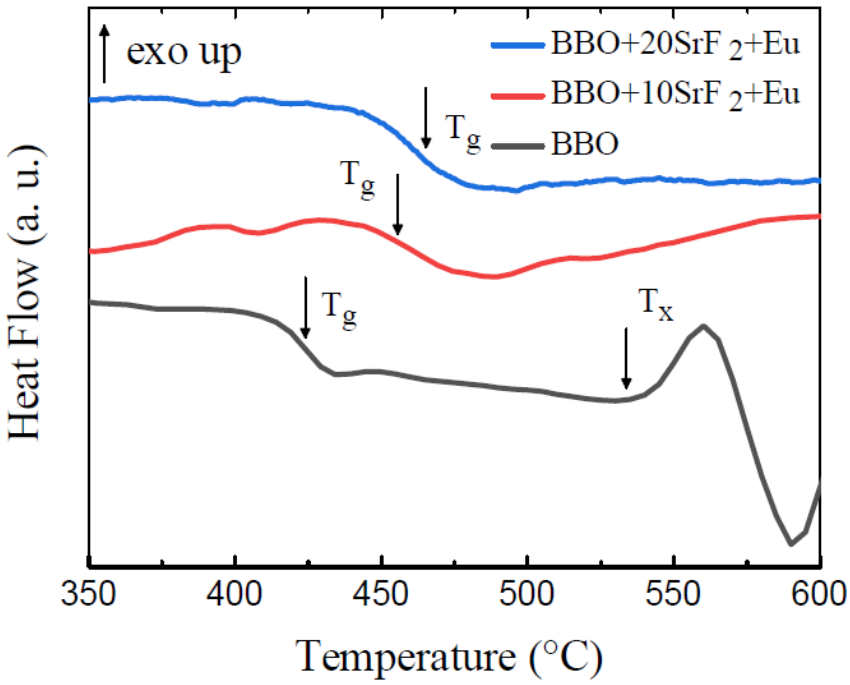

Figure 26 DSC curves of BBO, BBO+10SrF_2, and BBO+20SrF_2 glasses.

Before annealing, the amorphous nature of the as-prepared glasses was confirmed by XRD studies (Fig. 27). Since there have been no previous reports on the exact annealing parameters of these glasses that could results in SrF_2 nanocrystals, a temperature range from 560 to 590°C, increasing by 10 degrees, with durations of 1hour and 24 hours, was chosen (Fig. 28). The aim of the thermal treatment was the growth of SrF_2 nanocrystals within the glass matrix. Following each heat treatment, XRD measurements were conducted, to assess the presence of nanocrystals (Fig. 28, Fig. 29). The XRD patterns of

the samples annealed at 560 °C did not differ from the patterns of the unannealed samples, indicating a lack of long-range order. However, it should be noted that in the presented XRD results, a small amount of the nano-sized crystalline phase could have gone unnoticed. This is especially true since the amorphous phase in which the nanocrystals were dispersed gives a broad halo in the range of 25–35 (2θ), where major reflections from crystalline phases may exist. After annealing at 570 °C, differences between the BBO+10SrF_2 and BBO+20SrF_2 samples became evident. XRD patterns of the BBO+10SrF_2 sample revealed crystallization mainly in the $BiBO_3$ phase (Ref.Code 96-720-9482), with visible low-intensity reflections corresponding to the SrF_2 phase (Ref.Code 96-900-9044). There were also unidentified peaks observed in the diffractograms, which may be related to bismuth oxides. However, crystalline borates sometimes have highly unusual stoichiometries; therefore, it is difficult to fully characterize the presented diffraction pattern. On the other hand, BBO+20SrF_2 samples exhibited only the characteristic peaks of the SrF_2 crystalline phase (Ref.Code 96-900-9044). As can be seen, with the increase in annealing temperature, the amount of $BiBO_3$ crystalline phase in the BBO+10SrF_2 samples decreased, whereas a weak reflection of the SrF_2 phase was already present in the sample annealed at 580 °C. In the case of the annealed BBO+20SrF_2 glass, the SrF_2 phase crystallized regardless of the temperature increase. The obtained diffractograms confirm the conclusion drawn based on DSC studies that the presence of SrF_2 in the BBO matrix prevented its crystallization. Unfortunately, annealing the samples at temperatures of 570 °C and higher caused them to begin losing their transparency. Therefore, a temperature of 560 °C was chosen as a compromise between sample transparency and the presence of a crystalline phase within it. At this temperature, only samples heated for 24 h became opaque.

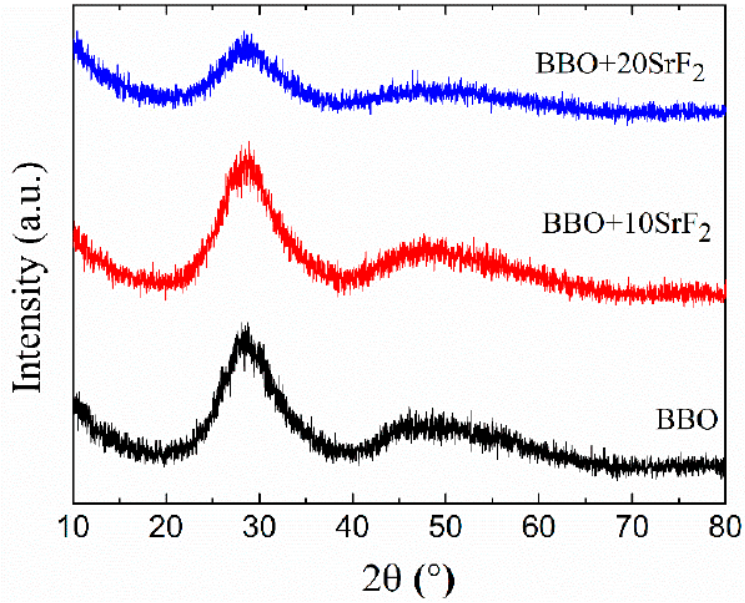

Figure 27 XRD patterns of BBO, BBO+10SrF_2, and BBO+20SrF_2 glasses.

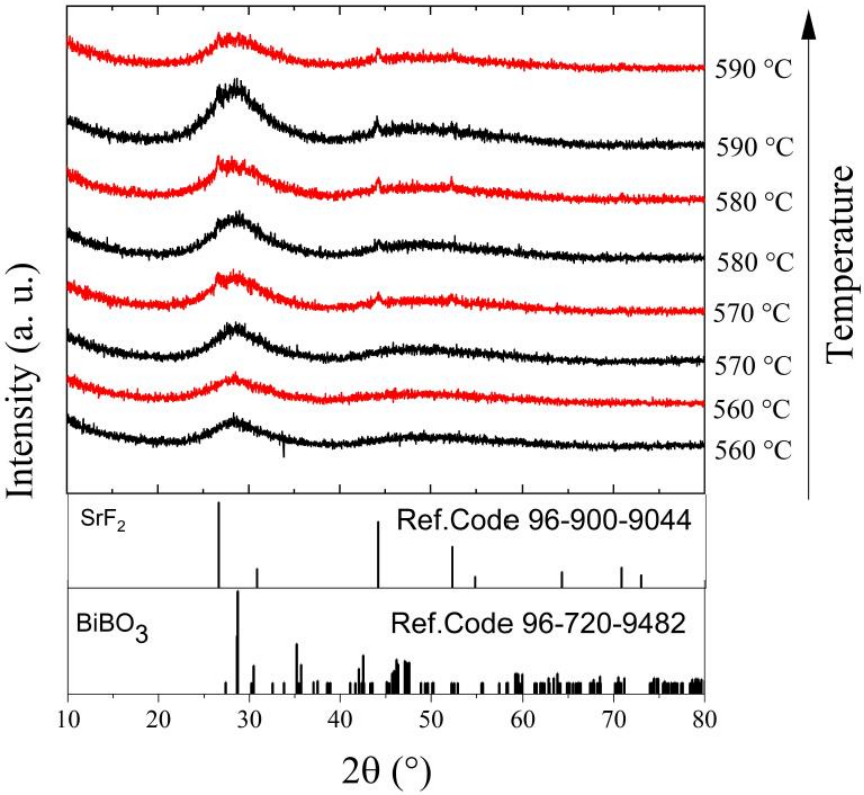

Figure 28 XRD patterns of BBO+10SrF_2 (black) and BBO+20SrF_2 (red) glasses after annealing in the temperature range of 560–590 ˚C for 1 h.

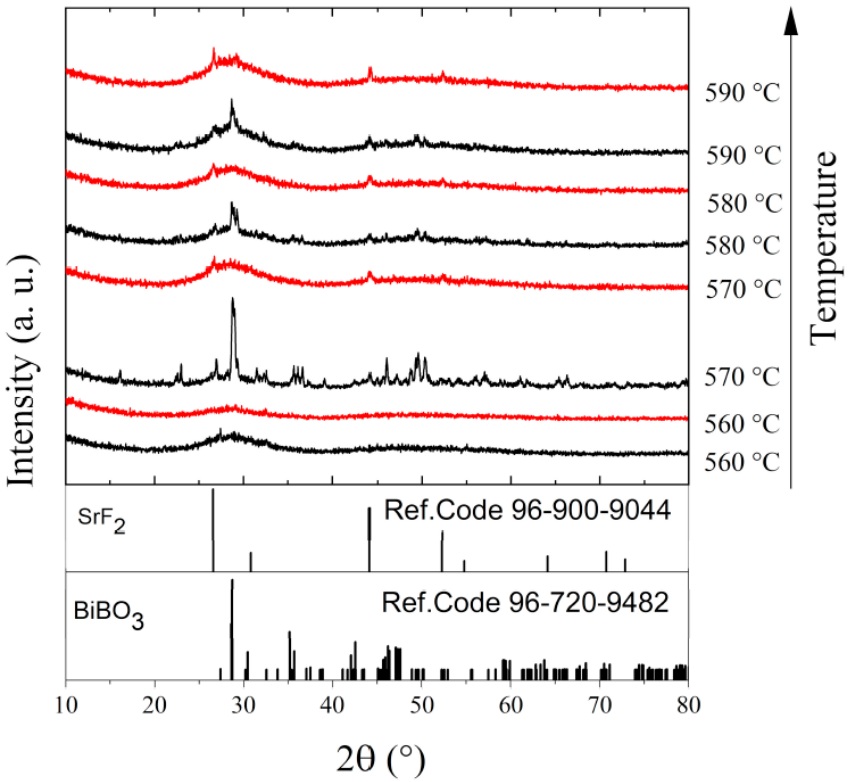

Figure 29 XRD patterns of BBO+10SrF_2 (black) and BBO+20SrF_2 (red) glasses after annealing in the temperature range of 560–590 ˚C for 24 h.

How annealing affects the structure of studied glasses was determined based on the results of FTIR spectroscopy (Fig. 30). Comparing the spectra of glass and glass ceramics, no significant differences were found.

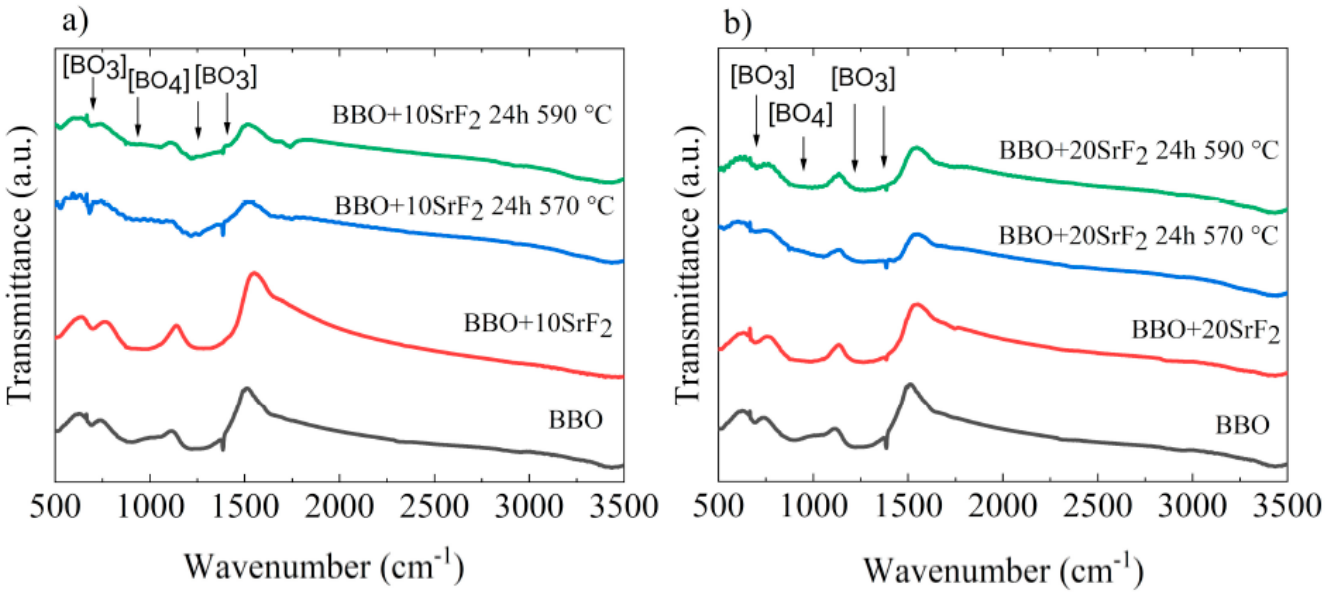

Figure 30 FTIR spectra of BBO+10SrF_2 (a) and BBO+20SrF_2 (b) as-prepared glasses and glasses after annealing at 570 °C and 590 °C. For comparison, the spectrum of as-prepared BBO glass was added to each figure.

Further information on the chemical states of elements in glasses and glass ceramics was provided by the results of XPS spectroscopy measurements. Particular emphasis was placed on the study of the valence states of Eu and Bi ions, as well as the chemical states of Sr that could indicate Sr chemical bonds with both fluorine and oxygen (Fig. 31). The research revealed that both Eu and Bi ions are in the 3+ valence state. Exemplary spectra of the Sr region of BBO+10SrF_2 and BBO+20SrF_2 glasses and glass ceramics after annealing at 560 °C for 24 h are shown in Figure 31. All spectra consisted of the Sr 3d spin-orbit doublet, but a detailed analysis of these peaks suggests the presence of more than one chemical state of Sr in all samples. Peaks at 133.5 and 135.5 eV could be assigned to the Sr $3d_{5/2}$ and Sr $3d_{3/2}$ in Sr-O, whereas peaks with energies equal to/of 134.0 and 136.0 eV could be attributed to Sr $3d_{5/2}$ and Sr $3d_{3/2}$ in Sr-F. The contribution of Sr-O and Sr-F doublets in the glasses was 59% and 41% (BBO+10SrF_2), and 67% and 33% (BBO+20SrF_2), respectively. The contribution of Sr-O and Sr-F doublets after annealing was, respectively, 80% and 20% (BBO+10SrF_2) and 52% and 48% (BBO+20SrF_2). Therefore, as can be seen, annealing did not change the ratio of the doublets in the same way in both samples. The increase in the contribution of the Sr-F doublet, which in turn indicated an increase in the amount of the SrF_2 crystal phase in the matrix, only took place in samples containing 20 mol % SrF_2. However, as the analysis of the X-ray diffractograms showed, SrF_2 as the only crystalline phase was also present only in the samples containing 20 mol % SrF_2. Therefore, it can be concluded from both of these methods that the formation of SrF_2 nanocrystals hindered the crystallization of the matrix.

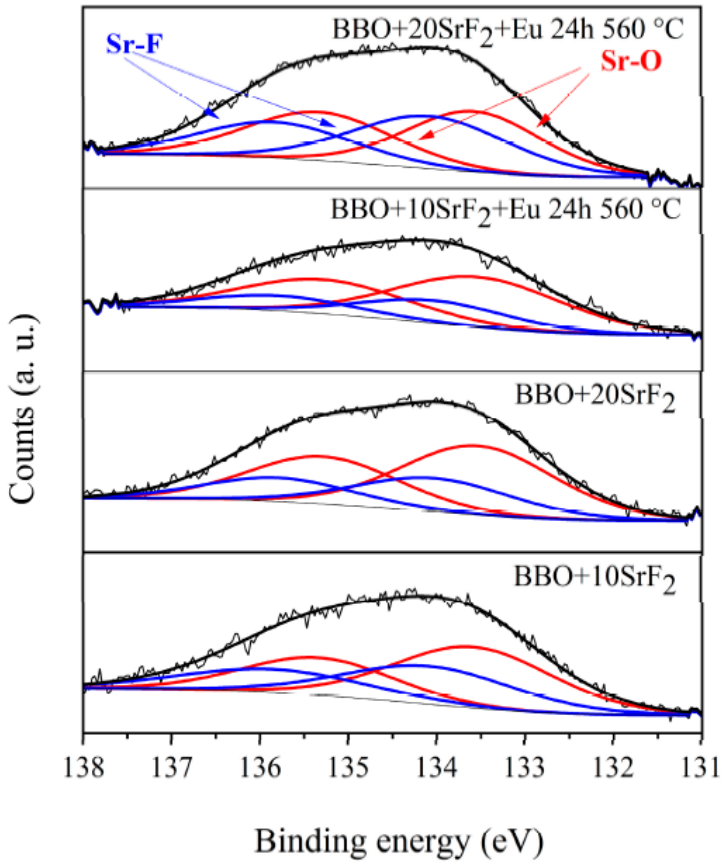

Figure 31 Sr 3d region of XPS spectra of BBO+10SrF_2 and BBO+20SrF_2 as-prepared glasses and glasses after annealing at 560 ˚C for 24 h.

One of the key aspects in the research on borate-bismuth glass ceramics was to determine the impact of crystallization on the luminescence of Eu^{3+} ions (Fig. 32). The BBO+10SrF_2+Eu and BBO+20SrF_2+Eu glasses monitored at the wavelength of λ_{em} = 615 nm, corresponding to the $^5D_0 \rightarrow {}^7F_2$ transition of Eu^{3+} ions, revealing several characteristics for 4f-4f transition peaks. Excitation bands at 382 and 465 nm may have been assigned to $^7F_0 \rightarrow {}^5G_4$ and $^5D_2$ transitions, whereas bands at 396, 415, and 533 nm originated from $^7F_0 \rightarrow {}^5L_6$, $^5D_3$, and $^5D_1$ transitions, respectively. A wavelength of 465 nm was selected for the observation of the emission spectra. This is the line with the highest intensity in the excitation spectrum. Emission spectra of BBO+10SrF_2+Eu glass and glass-ceramics crystallized at 560 °C (Figure 32b) consisted of several bands corresponding to Eu^{3+} radiative transitions at 581 nm ($^5D_0 \rightarrow {}^7F_0$), 594 nm ($^5D_0 \rightarrow {}^7F_1$), 615 nm ($^5D_0 \rightarrow {}^7F_2$), 655 nm ($^5D_0 \rightarrow {}^7F_3$), and 703 nm ($^5D_0 \rightarrow {}^7F_4$). As can be seen, there were no significant differences in the intensity of the bands between the BBO+Eu glass and the glass with the addition of 10 mol % of SrF_2. In addition, annealing of the

BBO+10SrF_2+Eu samples did not change the intensity of the spectral lines. However, if we look at the results concerning the structure of the annealed samples, the crystallization of the borane-bismuth matrix, apart from the SrF_2 crystal phase, cannot be ruled out. Assuming that this is the case, the emitted radiation could undergo scattering on defects. Looking at the emission spectra corresponding to the BBO+20SrF_2+Eu samples (Figure 33b), it can be noticed that the emission bands were at the same wavelengths as for the samples with 10 mol % of SrF_2. In addition, it is evident that annealing affected the intensity of Eu^{3+} ions emission. It is worth noticing that the SrF_2 crystalline phase was characterized by considerably lower phonon energy compared to the oxide materials. Therefore, if Eu^{3+} ions are located in the SrF_2 nanocrystals, this leads to a decrease in multi-phonon relaxation probability, and consequently to an increase in emission efficiency.

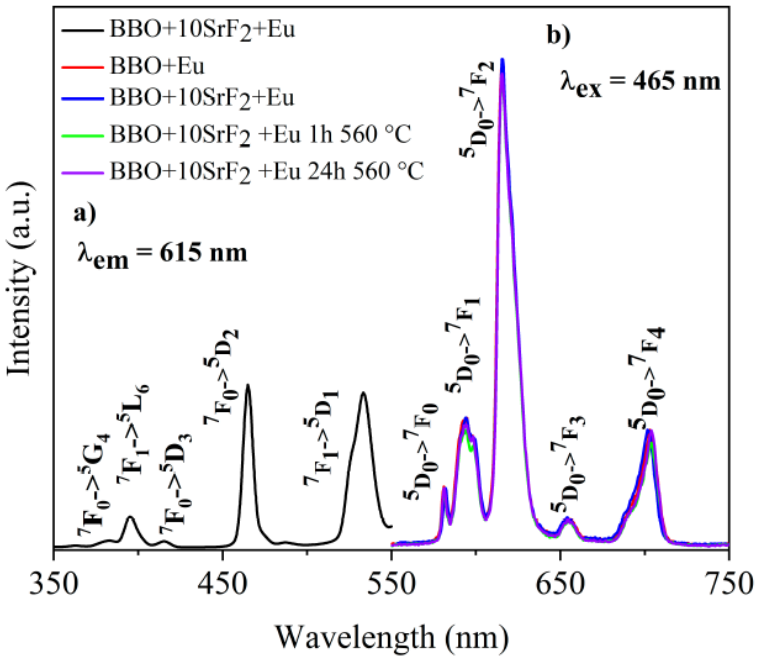

Figure 32 The excitation spectrum of BBO+10SrF_2+Eu glass (a), and the emission spectra of BBO+Eu glass, and BBO+10SrF_2+Eu glass and glass ceramics after annealing at 560 ˚C for 1 h and 24 h (b).

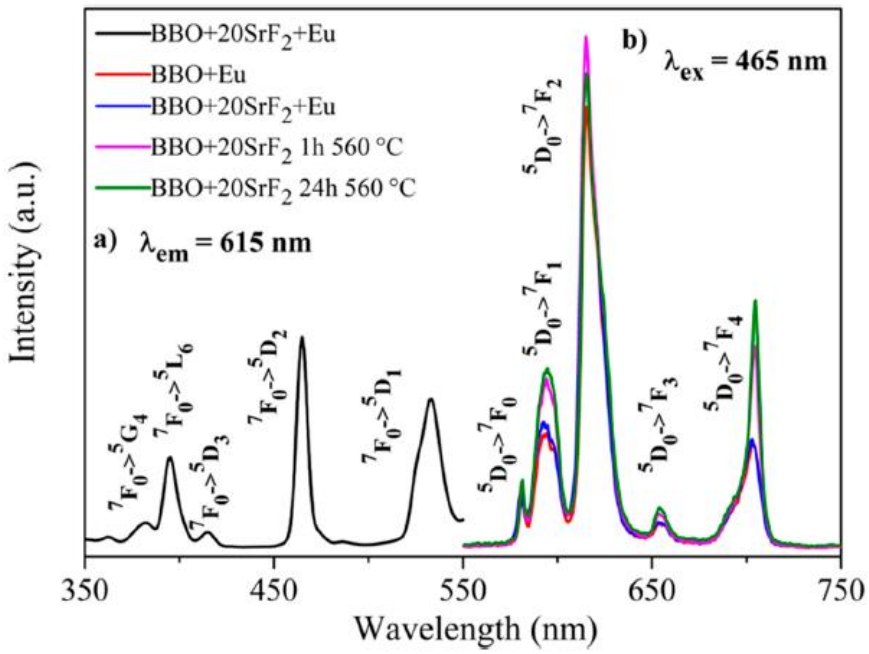

Figure 33 The excitation spectrum of BBO+20SrF_2+Eu glass (a), and the emission spectra of BBO+Eu glass, and BBO+20SrF_2 + Eu glass and glass ceramics after annealing at 560 ˚C for 1 h and 24 h (b).

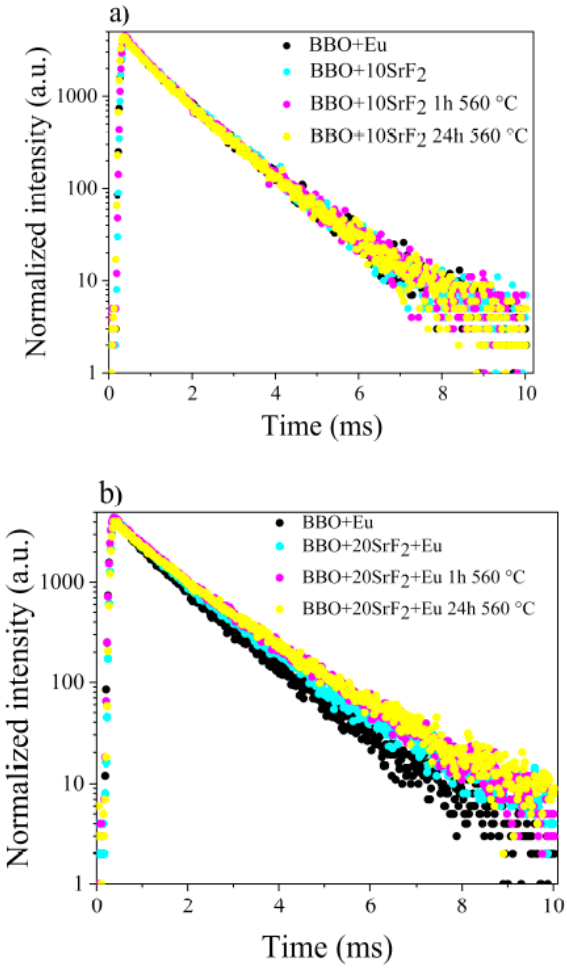

Figure 34 Luminescence decay curves of Eu-doped BBO and BBO+10SrF_2 samples (a), Eu-doped BBO and BBO+20SrF_2 samples (b).

Further studies on the influence of the environment on the luminescence of Eu^{3+} in the borate-bismuth glass and glass ceramics were conducted using time-resolved emission spectroscopy (TRES). Luminescence decay analysis was performed on as-prepared Eu^{3+} doped BBO, BBO+10SrF_2 and BBO+20SrF_2 samples. The decay curves were obtained by monitoring $^5D_0 \rightarrow {}^7F_2$ emission line (λ_{em} = 615 nm) upon excitation at λ_{exc} = 465 nm ($^7F_0 \rightarrow {}^5D_2$ transition) and are shown in Figure 34a,b. It was found that luminescence decays in both cases can be described as two-exponential decays according to the following equation (16):

$$\mathrm{I(t)} = A_1 \exp\left(\frac{-t}{\tau_1}\right) + A_2 \exp\left(\frac{-t}{\tau_2}\right) \tag{16}$$

where τ_1 and τ_2 are long and short luminescence lifetime components contributing to the average lifetime $< \tau_{avg} >$, and A_1 and A_2 are amplitudes of respective decay components. The lifetimes τ_1 and τ_2, amplitudes, and average lifetime calculated for the luminescence decay curves presented in Figure 34 are collected in Table 12.

Table 12. Fitting parameters of the luminescence decays and calculated Judd-Ofelt parameters.

	BBO +Eu	**BBO+10SrF_2 +Eu**	**BBO+20SrF_2 +Eu**	**BBO+10SrF_2 +Eu 1h 560˚C**	**BBO+10SrF_2 +Eu 24h 560˚C**	**BBO+20SrF_2 +Eu 1h 560˚C**	**BBO+20SrF_2 +Eu 24h 560˚C**
A_1	3913	4148	4267	3297	3431	3440	3338
A_2	3237	3115	2951	3893	3387	3046	2692
τ_1	1.2	1.18	1.28	1.24	1.22	1.45	1.48
τ_2	0.56	0.5	0.52	0.58	0.56	0.66	0.65
$< \tau_{avg} >$	1	1	1.1	1	1	1.2	1.2
Ω_2	5.64	5.15	5.54	6.06	5.86	4.48	5.11
Ω_4	3.89	3.74	3.59	3.78	3.85	3.86	4.07
R/O	3.76	3.45	3.69	4.04	3.90	3.06	2.73

This double-exponential nature of the decay curves indicates the presence of two different surroundings of Eu^{3+} ions. Long lifetime (τ_1) is correlated with higher symmetry of the crystal field, whereas short lifetime (τ_2) is associated with lower symmetry of the Eu^{3+} surroundings. Thus, in glasses containing SrF_2 or PbF_2 nanocrystals, a long lifetime is attributed to Eu^{3+} ions, which are located in the nanocrystals, and short lifetimes corresponds to the ions incorporated into the amorphous matrix. Concerning the tested samples, it can therefore be said that τ_1 represents the lifetime of Eu^{3+} ions incorporated into the SrF_2 nanocrystals, whereas τ_2 corresponded to ions surrounded by the glass matrix. However, in the case of the studied samples, the situation seems to be more

complicated. Two lifetimes were also observed in BBO+Eu glass, which did not contain strontium fluoride, and if to compare the results obtained for this glass with the values calculated for the BBO+10SrF_2 sample, the lifetimes are not much different. This means that the tested glass may have contained nanocrystalline areas that were formed during the glass preparation process, which are not visible in diffraction studies. Especially in borate glasses with various dopants, single exponential decay curves are usually observed. As can be seen, the longest τ_2 lifetime was observed for the BBO+20SrF_2 samples, especially those annealed for 24 h at 560 °C. It seems that in these samples the amount of Eu^{3+} ions incorporated into SrF_2 nanocrystals increased. This result is in line with the results obtained with the XRD. They show that SrF_2 as the only crystalline phase in the glass was present at 20 mol% of SrF_2, whereas at 10 mol% the matrix crystallization also took place. Changes in symmetry in the surroundings of the europium ions, as well as changes in the degree of covalence of bonds of these ions, can be observed based on Judd–Ofelt parameters. The Judd–Ofelt parameters Ω_2 and Ω_4 were calculated based on luminescence emission spectra using JOES application software and are presented in Table 12. Detailed information regarding software and calculations can be found in reference . The Ω_6 parameter was not determined in this study due to the unregistered emission band, located in the NIR range of wavelength, that corresponds to the $^5D_0 \rightarrow {}^7F_6$ transition band. The Ω_2 parameter is known to be structure sensitive and also depends on the covalence of Eu^{3+} bonds with the ligand. It is determined from $^5D_0 \rightarrow {}^7F_2$ hypersensitive transition. The high value of the Ω_2 parameter ($\Omega_2 > \Omega_4$) suggests that Eu^{3+} ions occupied mostly low-symmetry sites. This corresponds to the situation where Eu^{3+} ions were mainly located in the glassy matrix. On the other hand, the Eu-O bond in the glasses was highly covalent, which was also reflected in the high Ω_2 coefficients. In turn, the Ω_4 parameter is related to the rigidity of glasses and is often attributed to the emergence of long-range effects related to crystal lattice. Therefore, the processes of crystallization of glasses should consequently lead to an increase in this parameter. This behavior was observed, for example, in tellurite glass-ceramics containing SrF_2 nanocrystals. The parameters Ω_2 and Ω_4 calculated for the BBO+10SrF_2 and BBO+20SrF_2 glasses before and after annealing were different, but the change due to crystallization depended on the initial amount of SrF_2. In the BBO+10SrF_2 sample, both Ω_2 and Ω_4 were higher in the annealed samples.

Nevertheless, it is a sample where it was difficult to say that SrF_2 was the only crystalline phase in the glass matrix and it was, therefore, difficult to analyze the influence of the

appearance of SrF_2 nanocrystals on luminescence. On the other hand, in the case of the BBO+20SrF_2 sample, after crystallization the parameter Ω_2 was lower and Ω_4 was higher than in as-prepared glass. However, in the BBO glass containing 20 mol% of SrF_2, no additional crystallization of the matrix was observed after annealing; hence, it can be concluded that the observed change in the values of Ω_2 and Ω_4 parameters, as well as the increase in *t*1 time, are because Eu^{3+} ions were located in SrF_2 nanocrystals. These results follow the luminescence intensity ratio R (asymmetry ratio), which in the case of Eu^{3+} ions can be calculated from the expression (17):

$$R = I\,(^5D_0 \rightarrow {}^7F_2)/I(^5D_0 \rightarrow {}^7F_1) \tag{17}$$

The transition $^5D_0 \rightarrow {}^7F_1$ occurs via magnetic dipole and is independent of the host matrix, whereas $^5D_0 \rightarrow {}^7F_2$ has a pure electric dipole moment origin and is hypersensitive to changes in the crystal field around Eu^{3+} ions. In other words, a more intense $^5D_0 \rightarrow {}^7F_2$ transition indicates that the Eu^{3+} ions mainly occupy positions without an inversion center, whereas a more intense $^5D_0 \rightarrow {}^7F_1$ transition shows that the Eu^{3+} ions are located at sites with higher symmetry. Therefore, with the change in site symmetry of Eu^{3+} ions, when they take positions with higher symmetry, the asymmetry ratio coefficient should decrease. The intensity ratios calculated for the as-prepared BBO+20SrF_2 sample and the samples after annealing at 560 °C decreased with an increase in the annealing time (resulting in the growth of SrF_2 nanocrystals). This means that some of the Eu^{3+} ions were located in the structure of nanocrystals. Unfortunately, as shown earlier, BBO glass initially containing 10 mol % of SrF_2 may behave differently, which is most likely related to the not-completely-amorphous (after annealing) borate-bismuth matrix.

The obtained results presented in the publication are consistent with the theses of this doctoral dissertation. They confirm that it is possible to synthesizing borate-bismuth glass ceramics doped with SrF_2 nanocrystals and Eu^{3+} ions for luminescent applications. It has been proven that the structural modifications of parental glass, leading to SrF_2 nanostructure crystallization, depend strongly on the initial amount of strontium fluoride. The increase in luminescence intensity was observed after annealing in samples containing 20 mol% SrF_2. The luminescence lifetimes obtained for these glass-ceramics indicate that some of the Eu^{3+} ions were located in SrF_2 nanocrystals. This was also confirmed by the analysis of the Judd–Ofelt parameters Ω_2 and Ω_4, and luminescence intensity ratio R.

The above results affirm that the objectives and scope of this doctoral dissertation have been fulfilled. Borate-bismuth glasses and glass-ceramics with SrF_2 and Eu^{3+} ions were synthesized. The influence of SrF_2 on properties of glass matrices were investigated. It can therefore be concluded that the glasses and glass-ceramics described in this work could be considered as potential candidates for LED phosphors.

4.Conclusions

The aim of the scientific research discussed in this doctoral thesis was to synthesize and investigate the properties of new borate-bismuth glasses and glass ceramics containing metal fluorides for use as matrices for optically active RE^{3+} ions. Two-component borate-bismuth glasses were proposed as matrices in the B_2O_3-Bi_2O_3 system, modified by the addition of AlF_3 and SrF_2 and doped with rare earth ions: Eu^{3+}, Dy^{3+}, Tb^{3+} and Tm^{3+}. The use of various research techniques including X-ray diffraction, infrared spectroscopy, X-ray photoelectron spectroscopy, and thermal analysis enabled a comprehensive description of the structure and thermal properties of glasses.

The characterization of the optical and luminescent properties of the materials was based on the results of ultraviolet, visible, and luminescence emission and excitation spectra, time-resolved emission spectroscopy, and CIE chromaticity diagrams. The description of the luminescent properties of materials was complemented by calculations of theoretical Judd-Ofelt parameters and CCT values. The conducted research confirmed the possibility of synthesizing borate-bismuth glasses and glass ceramics in the B_2O_3-Bi_2O_3 system containing AlF_3 and SrF_2, which serve as suitable matrices for optically active RE^{3+} ions, using the traditional melt quenching method.

The conclusions drawn from the conducted research and their further analysis allow to assume that the proposed borate-bismuth glass and glass-ceramic matrices containing AlF_3 and SrF_2 are good matrices for doping with optically active RE^{3+} ions. According to the research thesis, these materials exhibit the desired properties of borate-bismuth glasses, such as chemical stability and transparency in the visible and IR range, and the addition of metal fluorides has a beneficial effect on the luminescence of RE^{3+} ions. It was also confirmed that it is possible to obtain light sources whose parameters can be modified by adjusting the amount of RE^{3+} ions and the wavelength of the excitation light. Based on the research conducted as part of this dissertation, a comprehensive description of a new group of glasses and glass-ceramics for applications in optoelectronics was developed, which can be considered as an alternative to currently used materials.

Summarizing, borate-bismuth glasses doped with RE^{3+} ions and fluorides (AlF_3 and SrF_2) were successfully synthesized. Investigation and discussion regarding the influence of the environment surrounding RE^{3+} ions on the properties of the synthesized materials have been conducted. It appears that borate-bismuth glass matrices modified with

fluorides exhibit the greatest potential, primarily due to the enhanced luminescence of RE^{3+} ions compared to the basic matrix. This confirms the hypothesis presented in this doctoral thesis: borate- bismuth glasses can serve as suitable matrices for dissolving RE^{3+} ions within them, and by changing their surroundings, their luminescent properties can be enhanced.

5.References

[I] **K. Milewska**, M. Maciejewski, M. Łapiński, A. Synak, M. Behrendt, W. Sadowski, B. Kościelska, Structural and luminescence properties of B_2O_3-Bi_2O_3-AlF_3 glass doped with Eu^{3+}, Tb^{3+} and Tm^{3+} ions, Journal of Non Crystalline Solids, Vol. 605, (2023), 122169. doi.org/10.1016/j.jnoncrysol.2023.122169.
[II] **K. Milewska**, M. Maciejewski, M. Žitňan, J. J. Velázquez, D. Galusek, W. Sadowski, B. Kościelska, Tunable emission and energy transfer of B_2O_3–Bi_2O_3–AlF_3 glass system doped with Eu^{3+}/Dy^{3+}, Journal of Luminescence, Vol. 269, (2024) 120440. Doi.org/10.1016/j.jlumin.2024.120440.

[III] **K. Milewska**, M. Maciejewski, A. Synak, M. Łapiński, A. Mielewczyk-Gryń, W. Sadowski, B. Kościelska, From Structure to Luminescent Properties of B_2O_3-Bi_2O_3-SrF_2 Glass and Glass-Ceramics Doped with Eu^{3+} Ions. Materials, 14, 4490. doi.org/10.3390/ma14164490.

[1] D. Chen, Z. Wang, Y. Zhou, P. Huang, and Z. Ji, “Tb3+/Eu3+: YF3 nanophase embedded glass ceramics: Structural characterization, tunable luminescence and temperature sensing behavior,” *J Alloys Compd*, vol. 646, pp. 339–344, Jun. 2015, doi: 10.1016/j.jallcom.2015.06.030.

[2] J. Cho, J. H. Park, J. K. Kim, and E. F. Schubert, “White light-emitting diodes: History, progress, and future,” *Laser and Photonics Reviews*, vol. 11, no. 2. Wiley-VCH Verlag, Mar. 01, 2017. doi: 10.1002/lpor.201600147.

[3] Y. Narukawa, I. Niki, K. Izuno, M. Yamada, Y. Murazaki, and T. Mukai, “Phosphor-conversion white light emitting diode using InGaN near-ultraviolet chip,” *Japanese Journal of Applied Physics, Part 2: Letters*, vol. 41, no. 4 A, Apr. 2002, doi: 10.1143/jjap.41.l371.

[4] Y. Wang *et al.*, “Recent development in rare earth doped phosphors for white light emitting diodes,” *Journal of Rare Earths*, vol. 33, no. 1, pp. 1–12, Jan. 2015, doi: 10.1016/S1002-0721(14)60375-6.

[5] Y. Shi *et al.*, “Energy transfer-based spectral properties of Tb-, Pr-, or Sm-codoped YAG:Ce nanocrystalline phosohors,” 2008.

[6] A. A. Setlur, W. J. Heward, M. E. Hannah, and U. Happek, “Incorporation of Si4+-N3- into Ce3+ -doped garnets for warm white LED phosphors,” *Chemistry of Materials*, vol. 20, no. 19, pp. 6277–6283, Oct. 2008, doi: 10.1021/cm801732d.

[7] Y. F. Cheung, Z. Ma, and H. W. Choi, “Color tunable LEDs,” in *Nitride Semiconductor Light-Emitting Diodes (LEDs): Materials, Technologies and Applications*, Elsevier Ltd., 2013, pp. 409–427. doi: 10.1533/9780857099303.2.409.

[8] C. Zhu, Y. Yang, X. Liang, S. Yuan, and G. Chen, “Rare earth ions doped full-color luminescence glasses for white LED,” *J Lumin*, vol. 126, no. 2, pp. 707–710, Oct. 2007, doi: 10.1016/j.jlumin.2006.10.028.

[9] N. M. Bobkova, “Characteristics of the Structural State of Bismuth Ions in Bismuth-Borate Glasses,” *Glass and Ceramics (English translation of Steklo i Keramika)*, vol. 75, no. 9–10, pp. 383–386, Jan. 2019, doi: 10.1007/s10717-019-00090-w.

[10] N. M. Bobkova, “Properties and Structure of Bismuth-Borate Glasses (Review),” *Glass and Ceramics (English translation of Steklo i Keramika)*, vol. 72, no. 9–10, pp. 360–365, Jan. 2016, doi: 10.1007/s10717-016-9790-2.

[11] A. V. Egorysheva, V. D. Volodin, and V. M. Skorikov, “Glass formation in the Bi 2O 3-B 2O 3-BaO system,” *Inorganic Materials*, vol. 44, no. 11, pp. 1261–1265, Nov. 2008, doi: 10.1134/S0020168508110228.

[12] L. Zur, J. Pisarska, and W. A. Pisarski, “Influence of heavy metal oxide and activator concentration on spectroscopic properties of Eu 3+, Dy 3+ and Tb 3+ ions in lead borate glasses,” *Optica Applicata*, vol. 42, no. 2, pp. 345–352, 2012, doi: 10.5277/oa120212.

[13] W. A. Pisarski, J. Pisarska, and W. Ryba-Romanowski, “Structural role of rare earth ions in lead borate glasses evidenced by infrared spectroscopy: BO3↔BO4 conversion,” in *Journal of Molecular Structure*, Jun. 2005, pp. 515–520. doi: 10.1016/j.molstruc.2005.01.022.

[14] J. Pisarska, A. Kos, and W. A. Pisarski, “Spectroscopy and energy transfer in lead borate glasses doubly doped with Dy3+-Tb3+ and Tb3+-Eu3+ ions,” *Spectrochim Acta A Mol Biomol Spectrosc*, vol. 129, pp. 649–653, Aug. 2014, doi: 10.1016/j.saa.2014.04.142.

[15] P. Pascuta, L. Pop, S. Rada, M. Bosca, and E. Culea, “The local structure of bismuth borate glasses doped with europium ions evidenced by FT-IR spectroscopy,” *Journal of Materials Science: Materials in Electronics*, vol. 19, no. 5, pp. 424–428, 2008, doi: 10.1007/s10854-007-9359-5.

[16] L. Zur, J. Pisarska, and W. A. Pisarski, “Influence of PbF2 concentration on spectroscopic properties of Eu3+ and Dy3+ ions in lead borate glasses,” *J Non Cryst Solids*, vol. 377, pp. 114–118, 2013, doi: 10.1016/j.jnoncrysol.2012.12.017.

[17] G. Krieke, A. Sarakovskis, and M. Springis, “Ordering of fluorite-type phases in erbium-doped oxyfluoride glass ceramics,” *J Eur Ceram Soc*, vol. 38, no. 1, pp. 235–243, Jan. 2018, doi: 10.1016/j.jeurceramsoc.2017.08.037.

[18] C. Ming, F. Song, X. Ren, L. An, and Y. Qin, “Tm3+/Er3+/Yb3+ tri-doped TeO 2-PbF2-AlF3 glass for white-light-emitting diode,” *Opt Commun*, vol. 304, no. 1, pp. 80–82, 2013, doi: 10.1016/j.optcom.2013.04.039.

[19] K. H. Kim, Y. G. Choi, W. Bin Im, and W. J. Chung, “Rare earth dependent formation of PbF2 nanocrystals and its effect on the emission properties in oxyfluoride glasses,” *Metals and Materials International*, vol. 19, no. 2, pp. 347–352, 2013, doi: 10.1007/s12540-013-2033-y.

[20] K. Bhargavi *et al.*, “Influence of Al3+ ions on self up-conversion in Ho3+ doped lead silicate glasses,” *Opt Mater (Amst)*, vol. 36, no. 7, pp. 1189–1196, 2014, doi: 10.1016/j.optmat.2014.02.027.

[21] M. Walas *et al.*, “Luminescent properties of Ln3+ doped tellurite glasses containing AlF3,” *Opt Mater (Amst)*, vol. 59, pp. 70–75, Sep. 2016, doi: 10.1016/j.optmat.2016.01.040.

[22] T. Kalpana *et al.*, “Influence of Al3 + ions on luminescence efficiency of Eu3 + ions in barium boro-phosphate glasses,” *J Non Cryst Solids*, vol. 419, pp. 75–81, Jul. 2015, doi: 10.1016/j.jnoncrysol.2015.03.033.

[23] C. Armellini, M. Ferrari, M. Montagna, G. Pucker, C. Bernard, and A. Monteil, “Terbium(III) doped silica-xerogels: e□ect of aluminium(III) co-doping.”

[24] A. J. Silversmith, A. P. Beyler, K. E. Arpino, D. M. Boye, and K. R. Hoffman, “Mechanisms of fluorescence enhancement in rare earth solgel glass containing Al3+,” in *Journal of Luminescence*, Mar. 2011, pp. 457–460. doi: 10.1016/j.jlumin.2010.11.018.

[25] P. P. Fedorov, A. A. Luginina, and A. I. Popov, “Transparent oxyfluoride glass ceramics,” *Journal of Fluorine Chemistry*, vol. 172. Elsevier, pp. 22–50, 2015. doi: 10.1016/j.jfluchem.2015.01.009.

[26] W. A. Pisarski, J. Pisarska, D. Dorosz, and J. Dorosz, “Rare earths in lead-free oxyfluoride germanate glasses,” *Spectrochim Acta A Mol Biomol Spectrosc*, vol. 134, pp. 587–591, Jan. 2015, doi: 10.1016/j.saa.2014.07.029.

[27] X. Qiao, X. Fan, and M. Wang, “Luminescence behavior of Er3+ in glass ceramics containing BaF2 nanocrystals,” *Scr Mater*, vol. 55, no. 3, pp. 211–214, Aug. 2006, doi: 10.1016/j.scriptamat.2006.04.023.

[28] S. R. Bae, Y. G. Choi, W. Bin Im, K. S. Lee, and W. J. Chung, “Rare earth doped silicate-oxyfluoride glass ceramics incorporating LaF 3 nano-crystals for UV-LED color conversion,” in *Optical Materials*, Elsevier B.V., 2013, pp. 2034–2038. doi: 10.1016/j.optmat.2012.09.025.

[29] X. Wang, J. Chen, J. Li, and H. Guo, “Preparation and luminescent properties of Eu-doped transparent glass-ceramics containing SrF2 nanocrystals,” in *Journal of Non-Crystalline Solids*, Jun. 2011, pp. 2290–2293. doi: 10.1016/j.jnoncrysol.2010.11.068.

[30] Y. Jiang *et al.*, “Er3+-doped transparent glass ceramics containing micron-sized SrF 2 crystals for 2.7 μm emissions,” *Sci Rep*, vol. 6, Jul. 2016, doi: 10.1038/srep29873.

[31] S. Li *et al.*, “Luminescence properties of Ba4Yb3F17:Er3+nanocrystals embedded in glass ceramics for optical thermometry,” *RSC Adv*, vol. 11, no. 37, pp. 22798–22804, Jun. 2021, doi: 10.1039/d1ra04038c.

[32] M. C. Gonçalves, L. F. Santos, and R. M. Almeida, “Rare-earth-doped transparent glass ceramics,” 2002.

[33] R. W. Hopper, “STOCHASTIC THEORY OF SCATI’ERING FROM IDEALIZED SPINODAL STRUCTURES II. Scattering in general and for the basic late stage model,” 1985.

[34] M. Reben, “The thermal study of oxyfluoride glass with strontium fluoride,” in *Journal of Non-Crystalline Solids*, Jul. 2011, pp. 2653–2657. doi: 10.1016/j.jnoncrysol.2010.12.055.

[35] B. M. Van Der Ende, L. Aarts, and A. Meijerink, “Near-infrared quantum cutting for photovoltaics,” *Advanced Materials*, vol. 21, no. 30, pp. 3073–3077, Aug. 2009, doi: 10.1002/adma.200802220.

[36] M. Walas, T. Lewandowski, A. Synak, M. Łapiński, W. Sadowski, and B. Kościelska, “Eu3+doped tellurite glass ceramics containing SrF2nanocrystals: Preparation, structure and luminescence properties,” *J Alloys Compd*, vol. 696, pp. 619–626, 2017, doi: 10.1016/j.jallcom.2016.11.301.

[37] C. Pr, S. Pr, R. J. Reeves, G. D. Jones, and R. % G. Syme, “Site-selective laser spectroscopy of Pr +C4"symmetry centers,” 1992.

[38] B. Kościelska *et al.*, “Structural and luminescence investigation of GeO2-PbO-Bi2O3-SrF2 glasses doped with Eu3 +, Tb3 + and Tm3 + ions,” *J Non Cryst Solids*, vol. 462, pp. 41–46, Apr. 2017, doi: 10.1016/j.jnoncrysol.2017.02.007.

[39] M. H. Imanieh, I. R. Martín, A. Nadarajah, J. G. Lawrence, V. Lavín, and J. González-Platas, “Upconversion emission of a novel glass ceramic containing Er3+, Yb3+:Sr1-xYxF2+x nano-crystals,” *J Lumin*, vol. 172, pp. 201–207, Apr. 2016, doi: 10.1016/j.jlumin.2015.12.026.

[40] Q. Luo, X. Qiao, X. Fan, S. Liu, H. Yang, and X. Zhang, “Reduction and luminescence of europium ions in glass ceramics containing SrF2 nanocrystals,” *J Non Cryst Solids*, vol. 354, no. 40–41, pp. 4691–4694, Oct. 2008, doi: 10.1016/j.jnoncrysol.2008.07.019.

[41] Z. X. Hou, Z. L. Xue, and S. H. Wang, “Synthesis and spectroscopic properties of Er 3+-doped CaF 2 nanocrystals in transparent oxyfluoride tellurite glass-ceramics,” *J Alloys Compd*, vol. 514, pp. 109–112, Feb. 2012, doi: 10.1016/j.jallcom.2011.11.013.

[42] N. Kaur, A. Khanna, M. Gónzález-Barriuso, F. González, and B. Chen, “Effects of Al3 +, W6 +, Nb5 + and Pb2 + on the structure and properties of borotellurite glasses,” *J Non Cryst Solids*, vol. 429, pp. 153–163, Dec. 2015, doi: 10.1016/j.jnoncrysol.2015.09.005.

[43] M. Poulain, M. Saad, and M. Foulâin, “Glass forming ability criterion GLASS FORMING ABILITY CRITERIOT{,” 1987. [Online]. Available: https://www.researchgate.net/publication/310746926

[44] U. Gross *et al.*, “Vibrational analysis study of aluminum trifluoride phases,” in *Journal of Physical Chemistry A*, Jul. 2007, pp. 5813–5819. doi: 10.1021/jp072388r.

[45] A. Va´zquezva´zquez, T. Lo´pezlo´pez, R. R. Go´mezgo´mez, R. Bokhimi, A. Morales, and O. Novaros, “X-Ray Diffraction, FTIR, and NMR Characterization of Sol-Gel Alumina Doped with Lanthanum and Cerium,” 1997.

[46] L. Mishra *et al.*, “White light emission and color tunability of dysprosium doped barium silicate glasses,” *J Lumin*, vol. 169, pp. 121–127, Jan. 2016, doi: 10.1016/j.jlumin.2015.08.063.

[47] Z. Ci *et al.*, “Warm white light generation from a single phase Dy3+ doped Mg2Al4Si5O18 phosphor for white UV-LEDs,” *Physical Chemistry Chemical Physics*, vol. 16, no. 23, pp. 11597–11602, Jun. 2014, doi: 10.1039/c4cp00357h.

[48] D. A. Rodríguez-Carvajal, A. N. Meza-Rocha, U. Caldiño, R. Lozada-Morales, E. Álvarez, and M. E. Zayas, “Reddish-orange, neutral and warm white emissions in Eu3+, Dy3+ and Dy3+/Eu3+ doped CdO-GeO2-TeO2 glasses,” *Solid State Sci*, vol. 61, pp. 70–76, 2016, doi: 10.1016/j.solidstatesciences.2016.09.009.

[49] G. Lakshminarayana *et al.*, “Er3+/Dy3+ codoped B2O3-TeO2-PbO-ZnO-Li2O-Na2O glasses: Optical absorption and fluorescence features study for visible and near-infrared fiber laser applications,” *J Non Cryst Solids*, vol. 503–504, pp. 366–381, Jan. 2019, doi: 10.1016/j.jnoncrysol.2018.10.025.

[50] D. V. K. Reddy *et al.*, “Tunable white light by varying excitations in yttrium alumino bismuth borosilicate glasses co-doped with Dy 3+ -Eu 3+ for cool WLED applications,” *J Non Cryst Solids*, vol. 513, pp. 167–182, Jun. 2019, doi: 10.1016/j.jnoncrysol.2019.03.011.

[51] T. Lewandowski *et al.*, “Structural and luminescent study of TeO2-BaO-Bi2O3-Ag glass system doped with Eu3+ and Dy3+ for possible color-tunable phosphor application,” *Opt Mater (Amst)*, vol. 79, pp. 390–396, May 2018, doi: 10.1016/j.optmat.2018.03.031.

[52] A. Bajaj and A. Khanna, “Crystallization of bismuth borate glasses,” *Journal of Physics Condensed Matter*, vol. 21, no. 3, 2009, doi: 10.1088/0953-8984/21/3/035112.

[53] P. Becker, R. Fröhlich, and correctly Bi, “Crystal Growth and Crystal Structure of the Metastable Bismuth Orthoborate BiBO 3 The phase diagram Bi 2 O 3-B 2 O 3 determined by Levin and McDaniel in 1962 [1] shows the occurrence of five different crystalline compounds,” 2004. [Online]. Available: http://znaturforsch.com

List of Figures

List of Tables

Copies of the publications used in the doctoral dissertation

[I] **Karolina Milewska**, Michał Maciejewski, Marcin Łapiński, Anna Synak, Mirosław Behrendt, Wojciech Sadowski, Barbara Kościelska, *Structural and luminescence properties of B_2O_3-Bi_2O_3-AlF_3 glass doped with Eu^{3+}, Tb^{3+} and Tm^{3+} ions*, Journal of Non Crystalline Solids, Vol. 605, (2023), 122169

Journal of Non-Crystalline Solids 605 (2023) 122169

Contents lists available at ScienceDirect

Journal of Non-Crystalline Solids

journal homepage: www.elsevier.com/locate/jnoncrysol

Structural and luminescence properties of B_2O_3-Bi_2O_3-AlF_3 glass doped with Eu^{3+}, Tb^{3+} and Tm^{3+} ions

Karolina Milewska [a,*], Michał Maciejewski [a], Marcin Łapiński [a], Anna Synak [b], Mirosław Behrendt [b], Wojciech Sadowski [a], Barbara Kościelska [a]

[a] Faculty of Applied Physics and Mathematics, Institute of Nanotechnology and Materials Engineering, Gdańsk University of Technology, ul. Gabriela Narutowicza 11/12, 80-233 Gdańsk, Poland

[b] Institute of Experimental Physics, Faculty of Mathematics, Physics and Informatics, University of Gdańsk, ul. Wita Stwosza 57/246, 80-952 Gdańsk, Poland

ARTICLE INFO

Keywords:
Borate bismuth glasses
Luminescence
Rare-earth ions
Aluminum fluoride
CIE diagram

ABSTRACT

The B_2O_3-Bi_2O_3-AlF_3 glass system doped with Eu^{3+}, Tb^{3+}, Tm^{3+} and triply doped with $Eu^{3+}/Tm^{3+}/Tb^{3+}$ ions in different molar ratios were successfully synthesized. Glass transition and crystallization temperatures were examined by Differential Scanning Calorimetry (DSC) measurements. X-ray Diffraction (XRD) confirmed the amorphous character of the samples. Fourier Transform Infrared Spectroscopy (FTIR) revealed that the glass matrix consists of $[BO_3]$ and $[BO_4]$ structural units, while X-ray Photoelectron Spectroscopy (XPS) confirmed the presence of AlF_3. An increase in luminescence spectra intensity was detected by Photoluminescence Spectroscopy (PL), due to the presence of 10 mol% of AlF_3. The RE^{3+} ions embedded in the glass matrix can be simultaneously excited by a single UV light. According to the CIE results the emitted color can be tunable by varying the excitation wavelength and sample composition. The presented results confirm that the proposed glass system could be a candidate for color-tunable phosphors in LEDs.

1. Introduction

In recent years a lot of research has been focused on new materials for optoelectronic applications [1,2]. Especially, there is a great demand for efficient, durable, and environmentally friendly white light sources [3]. This trend is mainly related to the fact that traditional incandescent and fluorescent lamps are gradually being replaced by light-emitting diodes (LEDs) [4,5].

The common white LED consists of a UV- emitting chip and a YAG: Ce^{3+} phosphor encapsulated in epoxy resin [6,7]. Such a solution is nowadays commercially used with success. Unfortunately, there are still some disadvantages that need to be overcome [8]. The main problems are the lack of a red color emitter, leading to the emission of cold white light, the poor thermal stability of the epoxy material, and the occurrence of the "halo effect" [4,6,9,10].

An alternative way to generate white light is the simultaneous emission of rare-earth ions embedded in a single host material in the blue, red, and green spectral regions under UV excitation [11,12]. Therefore, the research on new matrices for rare-earth ions are highly needed.

For optically active dopants, a suitable host material is crucial because the local environment around the RE^{3+} ions can significantly affect their emission spectra [13]. Numerous studies have shown that glass materials seem to be a good choice for such a matrix [11,14-16]. Over the years, many different glass compositions have been investigated as potential candidates for such an application [17]. For example, white light was generated from a single host, by combining the red, blue, and green emission from aluminoborate glass triply co-doped with Eu^{3+}, Tb^{3+}, and Tm^{3+} under UV excitation [18]. Also, Mungra et al. synthesized glass containing Eu^{3+}, Tb^{3+}, and Tm^{3+} that emits in the white range of spectrum upon 358 nm excitation [19]. Tunable emission and white light were obtained in phosphate glass co-doped with Eu^{3+} and Dy^{3+} by changing the concentrations of rare earth ions in the glass matrix [20]. The photoluminescence spectra of Dy^{3+}, Tb^{3+}, and Eu^{3+} doped $Mg_{21}Ca_4(PO_4)_{18}$ glass showed emission in blue, green, yellow, and orange spectral regions, which together resulted in an overall white light emission [21].

Borate-bismuth glasses appear to be very attractive candidates as host matrices for optically active RE^{3+} ions [22–25]. The B_2O_3-Bi_2O_3 glass system is widely known [26]. Beginning with the publication of

* Corresponding author.
E-mail address: karolina.milewska@pg.edu.pl (K. Milewska).

https://doi.org/10.1016/j.jnoncrysol.2023.122169
Received 28 October 2022; Received in revised form 16 January 2023; Accepted 23 January 2023
Available online 28 January 2023

Levin and McDaniel, numerous studies have been performed on its optical and structural properties as well as fabrication conditions [27,28,29].

The combination of boron and bismuth oxides leads to very good optical properties, which are important when glass is considered to be used as a matrix in luminescence applications. [30,31]. Borate-bismuth glasses are characterized by a high refractive index and good transmittance in the wide range of the light spectrum. They have good chemical and thermal resistance and relatively low phonon energy. They can be easily fabricated at low temperatures, which makes them eco-friendly and easy to manufacture [30]. All these properties make them a suitable host matrix for the addition of RE^{3+} ions.

The emission spectra of optically active ions strongly depend on the local environment around them [32,33]. Even a small change in the matrix composition can affect the luminescence properties of the material. The method of introducing various dopants to change the RE^{3+} surrounding is well known [34,35]. Aluminum fluoride acts as such a modifier. It was found that the addition of AlF_3 increases the emission intensity in the TeO_2-BaO-Bi_2O_3-AlF_3 glass system doped with Eu^{3+}, Tb^{3+}, and Tm^{3+} [36]. In the presence of Al_2O_3 in Nd^{3+} doped TeO_2ZnO and GeO_2PbO glasses, the photoluminescence intensity was up to 30% higher compared to undoped glasses [37]. In Eu^{3+} doped SiO_2-B_2O_3-Gd_2O_3–Na_2O-Al_2O_3 glasses, the luminescence intensity reached the maximum value at 3 mol% Al_2O_3 addition [38]. Fanai et al. reported an increase in luminescence in glasses co-doped with Al^{3+}ions, which was attributed to a reduction in cross-relaxation [39].

The mechanism of luminescence enhancement is not entirely clear and its under debate for a long time [40]. Lochhead et al. proposed the idea that higher intensity of the emission spectrum of RE^{3+} ions can be caused by the fact that Al^{3+} ions prevent rare-earths ions from clustering in the glass matrix, which results in their more uniform distribution [41]. This was for a long time generally accepted explanation, supported by more works [42,41].

After a few years, later studies conducted by Silversmith et al. suggested the theory, that RE^{3+} ions are preferably located in the glass matrix in positions rich in Al^{3+} ions, affecting their local symmetry and leading to the enhancement of luminescence [43]. This was consistent with molecular dynamics simulations performed on the SiO_2-Al_2O_3 system by Monteil et al. [44,45].

The research on new materials that could be applied in modern lighting technology are still very important. In this work, the structural, physical, and luminescent properties of B_2O_3-Bi_2O_3-AlF_3 and B_2O_3-Bi_2O_3-AlF_3: Ln^{3+} (Ln^{3+} = Tm^{3+}, Tb^{3+}, and Eu^{3+}) glasses were investigated. To the best of our knowledge, no similar study has ever been performed before on such a glass composition. Especially, the attention was focused on luminescence properties and CIE chromatic coordinates diagrams. The influence of 10 and 20 mol% of AlF_3 addition on the intensity of the photoluminescence (Pl) spectra was also investigated. Additionally, the possibility of energy transfer processes from Tb^{3+} to Eu^{3+} ions was studied.

2. Materials and methods

Borate-bismuth glasses with the nominal composition (in mol%): $50B_2O_3$–$50Bi_2O_3$ (BBO), $45B_2O_3$–$45Bi_2O_3$–$10AlF_3$ (BBO+$10AlF_3$) and $40B_2O_3$–$40Bi_2O_3$–$20AlF_3$ (BBO+$20AlF_3$) were synthesized using conventional melt quenching technique in air atmosphere. Next, to study the influence of AlF_3 addition on luminescent properties, samples singly doped with Ln^{3+} ions (BBO+Eu, BBO+$10AlF_3$+Eu, BBO+$10AlF_3$+Tb, BBO+$10AlF_3$+Tm) were prepared. Based on the obtained results, the BBO+$10AlF_3$ sample has been chosen, to be modified by the addition of Ln^{3+} ions, where $Ln^{3+} = 0.5Eu^{3+} + 0.5Tb^{3+} + 1Tm^{3+}$ (BBO+$10AlF_3$:Ln1), $Ln^{3+} = 0.7Eu^{3+} + 0.5Tb^{3+} + 0.8Tm^{3+}$ (BBO+$10AlF_3$:Ln2), $Ln^{3+} = 0.05Eu^{3+} + 0.95Tb^{3+} + 1Tm^{3+}$ (BBO+$10AlF_3$:Ln3). Moreover, to examine the possibility of energy transfer between Tb^{3+} and Eu^{3+} ions glass of BBO+$10AlF_3$+1Eu+1 Tb glass was prepared. The compositions of the samples are presented in Table 1. Mixed raw materials (H_3BO_3, $Bi_5OH(OH)_9(NO_3)_4$, AlF_3, Eu_2O_3, Tm_2O_3, $Tb(NO_3)_3$ were melted in porcelain crucibles at 950 °C for 20 min. Next, melts were poured onto a hot steel plate at a temperature of 250 °C, pressed by another plate immediately, and then cooled down to room temperature.

To determine the amorphous character of as-prepared glasses X-ray diffraction technique (XRD) was used. Measurements were carried out on a Bruker D2 Phaser diffractometer with Cu Kα radiation (λ=1.5406 Å) on powder samples. To investigate the thermal properties of glass samples, differential thermal analysis (DTA) was performed on Netzsch Simultaneous TGA-DSC, STA 449 F1 using aluminum crucible and air atmosphere, with a 10 K/min heating rate. DTA results allowed for the determination of characteristic temperatures of glass samples, such as glass transition (T_g) and crystallization (T_c) temperatures. To know the structural units, present in the glass matrices, Fourier transform infrared spectroscopy (FTIR) measurements were obtained using a Perkin-Elmer Frontier MIR/FIR spectrometer with a TGS detector. Data were collected on pellet samples with potassium bromide (KBr) in a weight ratio (Sample: KBr) 1:100. X-ray photoelectron spectroscopy (XPS) analysis was used to determine the valence states of ions present in the samples. Measurements were carried out using an Omnicron NanoTechnology spectrometer with a 128-channel collector. XPS measurements were conducted in ultra-high vacuum conditions, below 1.1×10^{-8} mBar. The Mg-Kα X-ray source with an X-ray anode set to 15 keV and 300 W was used to excite the photoelectrons. The SCINCO FluoroMate FS-2 fluorescence spectrometer collected the luminescence emission and excitation spectra on pellet samples mixed with KBr in a weight ratio of 1:1. The results were collected in form of a quasi-three-dimensional, colorful image, with the wavelength in the horizontal axis, the time in the vertical axis, and the intensity expressed by a range of colors. Time-resolved emission spectra (TRES) were obtained using a pulsed spectrofluorometer described in detail [46]. The excitation source was the laser system PL 2143A/SS with Nd: YAG laser and the PG 401/SH optical parametric generator emitting pulses of FWHMz30 ps from EXSPLA. The Bruker Optics 2501S spectrometer and the Hammamatsu streak camera (C4334–01 model) were used to analyze the emission signal. All performed operations were automated and controlled by the Hamamatsu HPDTA software. Time decays were acquired, by slicing the steak camera image at a specified time interval.

3. Results and discussion

3.1. DTA analysis

The DTA technique was used to determine the glass transition (T_g) and glass crystallization (T_c) temperatures of the as-prepared glasses. Fig. 1 presents DTA curves of the BBO, BBO+$10AlF_3$, and BBO+$20AlF_3$ samples. In all samples both, T_g and T_c are present.

It is well known that thermal characterization of a material, can

Table 1
Compositions of synthesized samples.

Name	Sample composition (molar ratio)					
	B_2O_3	Bi_2O_3	AlF_3	Eu_2O_3	Tb_2O_3	Tm_2O_3
BBO	50	50	–	–	–	–
BBO+Eu	49	49	–	2	–	–
BBO+$10AlF_3$	45	45	10	–	–	–
BBO+$20AlF_3$	40	40	20	–	–	–
BBO+$20AlF_3$: Eu	39	39	20	2	–	–
BBO+$10AlF_3$: Eu	44	44	10	2	–	–
BBO+$10AlF_3$: Tb	44	44	10	–	2	–
BBO+$10AlF_3$: Tm	44	44	10	–	–	2
BBO+$10AlF_3$: Eu/Tb	44	44	10	1	1	–
BBO+$10AlF_3$: Ln1	44	44	10	0.5	0.5	1
BBO+$10AlF_3$: Ln2	44	44	10	0.5	0.7	0.8
BBO+$10AlF_3$: Ln3	44	44	10	0.05	0,95	1

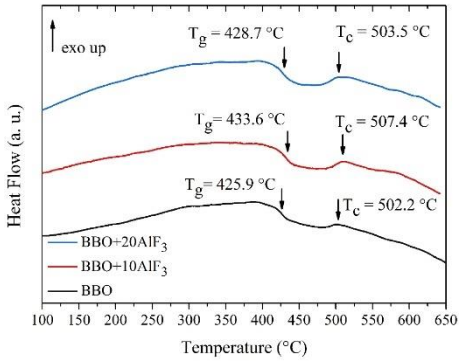

Fig. 1. DTA curves of BBO, BBO+10AlF_3 and BBO+20AlF_3.

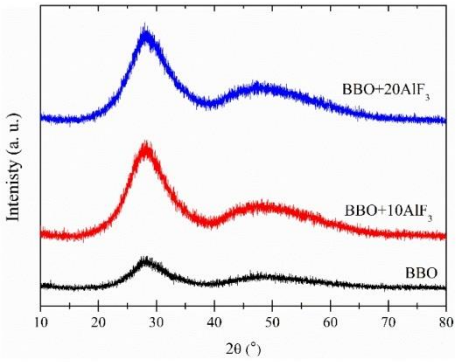

Fig. 2. XRD patterns of as-prepared BBO, BBO+10AlF_3 and BBO+20AlF_3 glasses.

provide important information about the structural changes in the glass matrix, caused by the addition of a glass modifier [47]. Glass transition temperatures of the samples doped with AlF_3 were found to be higher than T_g of the undoped one. This can be explained by the correlation between the glass transition temperature and the enthalpy of bonds in the glass matrix [48]. Due to the addition of aluminum fluoride, new linkages between glass components could form, resulting in a higher energy barrier for molecule motion to overcome and increase the thermal stability of the glass matrix [48]. This phenomenon could also be an explanation for higher crystallization temperatures. The presence of strong bonds could lead to an increase in the stability of glass matrix, resulting in a higher value of crystallization temperatures. However, in the case of the studied samples, despite the shift of T_g and T_c temperatures to higher values, the stability of the glasses decreases after the introduction of AlF_3. It can be concluded based on the calculated Δ T and S parameters presented in Table 2.

The ΔT parameter determines the stability properties of glass, which is the difference between the onset of the crystallization peak (T_x) and T_g, specifying the range of glass stability. It can be noticed that with the addition of aluminum fluoride, the range of glass stability decreases. The S parameter describing the glass resistance against devitrification was calculated based on [49]:

$$S = \frac{(Tc - Tx)(Tc - Tg)}{Tg} \tag{1.1}$$

In the studied glasses, the values of S are 3.62, 3.45, and 3,14 for BBO, BBO + 10AF_3, and BBO + 20AlF_3, respectively. These results are similar to those obtained for other borate glasses [50,51]. The decreasing trend of the S parameter connected with the amount of AlF_3 doping is clearly seen. This indicates that AlF_3 addition to the basic glass matrix (BBO) results in the lower stability of the borate-bismuth glass matrix and a higher tendency to crystallization.

3.2. XRD analysis

The XRD results confirm the amorphous nature of the as-prepared glass samples. Fig. 2 presents the diffraction patterns of BBO, BBO+10AlF_3, and BBO+20AlF_3 glasses. No difference due to the addition of AlF_3, can be seen. Only two board humps in the range of 20- 40 (2θ) and 40–65 (2θ) indicate the lack of long-range order in the glass matrices are present.

Table 2
Thermal parameters of BBO, BBO+10AlF_3, and BBO+20AlF_3 glass samples.

Sample	T_g (°C)	T_x (°C)	T_c (°C)	Δ T (°C)	S (°C)
BBO	425,9	482	503,5	56,1	3.62
BBO+10AlF_3	433,6	487,1	507,4	53,5	3.45
BBO+20AlF_3	428,7	484,5	503,2	55,8	3.14

3.3. FTIR analysis

The FTIR spectra of the BBO, BBO+10AlF_3, and BBO+20AlF_3 glasses are presented in Fig. 3. The broad absorption bands in the range 645–760 cm^{-1} and 1182–1356 cm^{-1} can be assigned to the deformation vibration of [BO_3] groups [26,52,53]. Additionally, also band around 1356–1478 cm^{-1} is associated with the stretching vibrations of [BO_3] units. The tetrahedral units [BO_4] are visible in the spectrum at 790–1110 cm^{-1} [53].

The bands that could be assigned to the presence of AlF_3 should be visible at 642 and 646 cm^{-1}, corresponding to the stretching vibrations of Al-F bonds [54,55]. Also, the presence of aluminum fluoride could be confirmed by vibrations of Al-O bonds in AlO_4 units at around 1124 cm^{-1} [54,55]. Unfortunately, these regions are dominated by broad bands from [BO_3] and [BO_4] units. Due to this fact, the existence of AlF_3 can be overlapped by them, resulting in no significant changes in spectra of glass samples doped with 10 and 20 mol% of AlF_3.

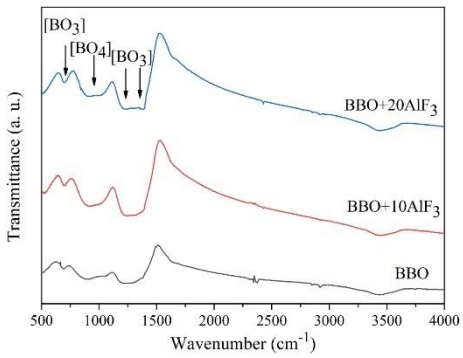

Fig. 3. FTIR spectra of as-prepared BBO, BBO+10AlF_3, and BBO+20AlF_3 glasses.

3.4. XPS analysis

To confirm the presence of AlF_3 in the glass matrix, the XPS measurements were performed. Due to the similar compositions of all samples, the XPS spectrum for one composition: BBO+10AlF_3 is presented in Fig. 4. Two signals connected with the presence of Al^{3+} ions can be distinguished in the band observed in the 72–77 eV range. First, at 75,5 eV can be assigned to the presence of Al-F bonds in AlF_3 [56,57]. Second, at 74,5 may be associated with the Al-O bonds in Al_2O_3. The contribution of Al-F and Al-O bonds was established at 15% and 85%, respectively. The XPS analysis confirms the presence of AlF_3 in prepared glass samples. To get a better insight into the structure of glass matrix, the investigation of Bi ions was performed. Fig. 4 (right) shows the Bi 4f spin-orbit doublet in the region 155–167 eV [58,59]. After deconvolution four separate bands can be seen. Peaks at 159.0 and 165.0 eV can be attributed to Bi 4f $_{7/2}$ and Bi 4f $_{5/2}$ peaks of Bi^{3+}, whereas two peaks at 157 and 163 eV can be described to Bi f $_{7/2}$ and Bi f $_{5/2}$ of Bi^0, respectively.

3.5. Luminescence analysis

To study the luminescence properties and determine the influence of AlF_3 on luminescence intensity, the samples: BBO, BBO+10ALF$_3$, and BBO+20AlF_3 doped with 2 mol% of Eu^{3+} ions were used. It is known that the luminescence spectra of Eu^{3+} ions are suitable probes for the study of local symmetry in glass matrices [60]. The intensity of their 4f-4f transitions strongly depends on the local surrounding around the optically active ions. Therefore, the variation of the glass composition can affect their emission spectrum [60,61]. Europium ions show two characteristic bands in the emission spectrum, corresponding to the $^5D_0 \rightarrow {}^7F_1$ and $^5D_0 \rightarrow {}^7F_2$ transitions [62,63]. The $^5D_0 \rightarrow {}^7F_1$ transition is called a magnetic dipole transition (~ 590 nm), and its intensity is independent of the local environment around Eu^{3+} ions. The $^5D_0 \rightarrow {}^7F_2$ (~ 612 nm), is a forced electric dipole transition [62]. This transition is hypersensitive to the surrounding of europium ions, which is why it can be used to analyze the local symmetry of glass matrices. Fig. 5a shows the excitation spectra of BBO+Eu, BBO+10AlF_3+Eu, and BBO+20AlF_3 + Eu glasses observed at λ_{em} = 615 nm, which corresponds to the $^5D_0 \rightarrow {}^7F_2$ transition of Eu^{3+} ions [19,64]. Several characteristic for 4f-4f transitions peaks can be seen in the spectrum. Excitation bands at: 363, 382, 395, 416, 465 and 533 nm can be assigned to the $^7F_0 \rightarrow {}^5D_4$, $^5G_2$, $^5L_6$, $^5D_3$, $^5D_2$, $^5D_1$ transitions, respectively [19,64]. It can be seen that the intensities of the excitation spectra change with the composition of the samples. The highest intensity is observed for glass doped with 10% mol of AlF_3 addition. For glass with 20% mol AlF_3, the intensity is even lower than for the undoped matrix. The band at λ_{ex}= 465 nm is characterized by the highest intensity in the excitation spectrum and was selected as adequate to observe the emission spectra of the glasses. Fig. 5b shows the emission spectra of the BBO+Eu, BBO+10AlF_2+Eu, and BBO+20AlF_3+Eu glasses, which consist of several bands corresponding to Eu^{3+} radiative transitions at 578 nm ($^5D_0 \rightarrow {}^7F_0$), 591 nm ($^5D_0 \rightarrow {}^7F_1$), 615 nm ($^5D_0 \rightarrow {}^7F_2$), 652 nm ($^5D_0 \rightarrow {}^7F_3$) and 700 nm ($^5D_0 \rightarrow {}^7F_4$) [19,64]. It was found that the electric dipole transition intensity ($^5D_0 \rightarrow {}^7F_2$) is higher than the magnetic dipole transition in all glass samples. This suggests that Eu^{3+} ions are placed in the site without an inversion center [65].

The local field symmetry around RE^{3+} ions can be also determined from the ratio between the luminescence intensities of an electric dipole and a magnetic dipole transitions ($^5D_0$–$^7F_2$/$^5D_0$–$^7F_1$), which is called the red to orange (R/O) ratio [65]. In the studied glasses, the R/O ratios are 3.26 and 3.17 for BBO+10AlF_3+2Eu and BBO+20AlF_3+2Eu, respectively. The variation of this parameter confirms that the surrounding of RE^{3+} ions is affected, by the addition of AlF_3. Moreover, the dominance of the electric dipole transition in all samples leads to the dominance of the red color emission. When the intensity of the electric dipole is higher than the intensity of the magnetic dipole transition, Eu^{3+} ions occupy sites without inversion symmetry [66].

It can be clearly seen that the addition of AlF_3 has a strong effect on the luminescence properties of bismuth-borate glass doped with Eu^{3+} ions. The emission intensity varies with AlF_3 concentration, reaching a maximum at 10 mol% of AlF_3 addition and then decreasing with a higher AlF_3 content.

The reason for the higher intensity of Eu^{3+} ions at lower AlF_3 concentration may be explained by the fact, that the local symmetry of Eu^{3+}

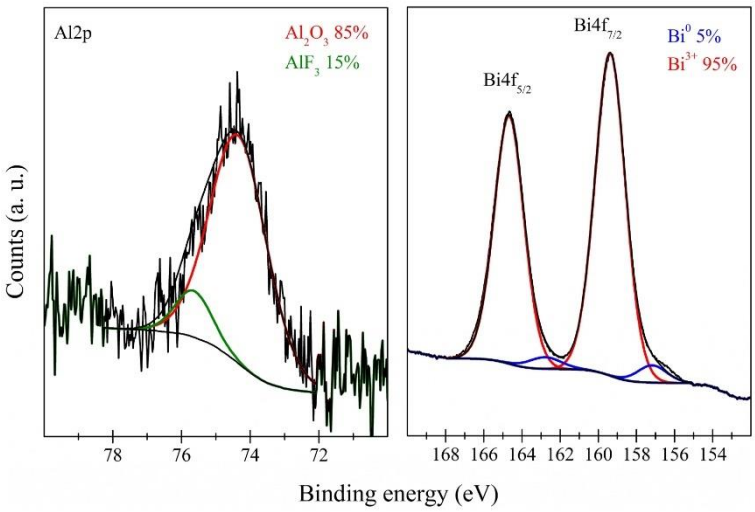

Fig. 4. XPS spectra of BBO+10AlF_3 sample.

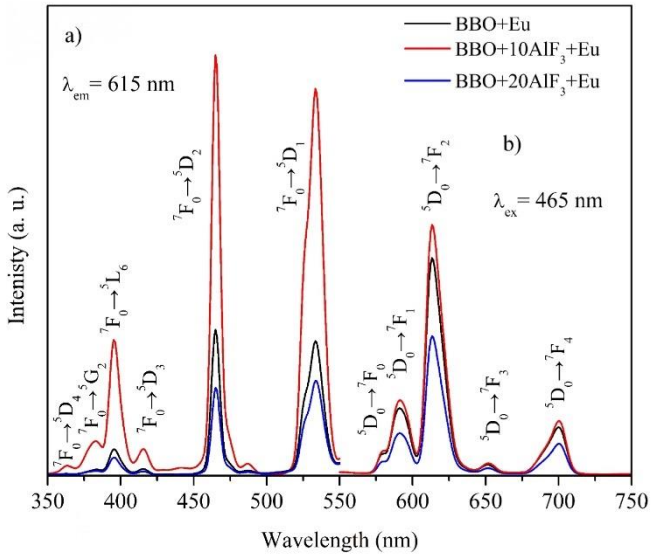

Fig. 5. Excitation (a) and emission (b) spectra of samples doped with Eu^{3+} ions.

ions could be reduced, due to the presence of Al^{3+} ions. While the decrease of Eu^{3+}intensity in higher Al^{3+} concentration could indicate the higher symmetry around Re^{3+} ions. Similar results were obtained in sol-gel glass doped with Al^{3+} [43]. This is consistent with the trend observed in the excitation spectra. Due to the highest intensity in the excitation spectra, the BBO+10AlF$_3$ composition was selected for further singly and triply co-doping with Eu^{3+}, Tb^{3+}, and Tm^{3+} ions.

Fig. 6. shows the excitation (a) and emission (b) spectra of the BBO+10AlF3+Tb^{3+} glass sample. Under 544 nm observation, the excitation spectrum consists of three peaks at 354, 378 and 486 nm corresponding to $^7F_6 \rightarrow {}^5D_2, {}^5D_3, {}^5D_4$, of Tb^{3+} respectively [67]. The emission spectrum for the 378 nm excitation shows peaks at 496 nm ($^5D_4 \rightarrow {}^7F_6$), 549 ($^5D_4 \rightarrow {}^7F_5$), 594 nm ($^5D_4 \rightarrow {}^7F_4$) and 628 nm ($^5D_4 \rightarrow {}^7F_3$), which can be assigned to the 4f-4f transitions of Tb^{3+} ions.

The excitation and emission spectra of the BBO+10AlF$_3$+Tm glass sample are presented in Fig. 7a and b respectively. The excitation spectra monitored at 455 nm wavelength consist of one peak at 358 nm due to $^3H_6 \rightarrow {}^1D_2$ transition of Tm^{3+} [18,68]. Under 358 nm excitation, the emission spectrum shows peak at 455 nm, corresponding to the $^1D_2 \rightarrow {}^3F_4$ transition of Tm^{3+} ions. The luminescence decays for Eu^{3+}, Tb^{3+} and Tm^{3+} ions exhibit one-exponential character, with lifetimes of about 1 ms for $Eu^{3+}$and Tb^{3+} ions (Fig. 8). However, the decay time for

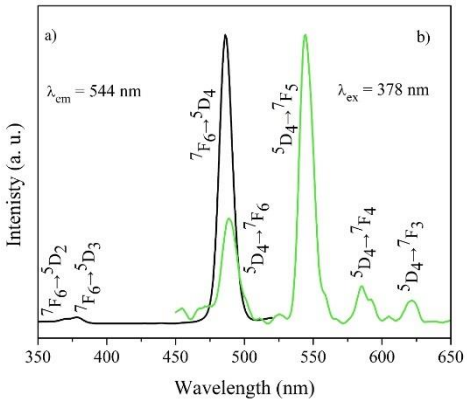

Fig. 6. The excitation spectra monitored at 544 nm (a) and emission spectra monitored at 378 nm excitation (b) of the BBO+10AlF$_3$+Tb sample.

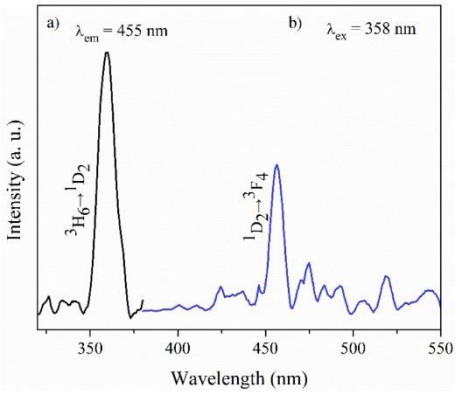

Fig. 7. The excitation spectra monitored at 455 nm (a) and emission spectra monitored at 358 nm excitation (b) of the BBO+10AlF$_3$+Tm sample.

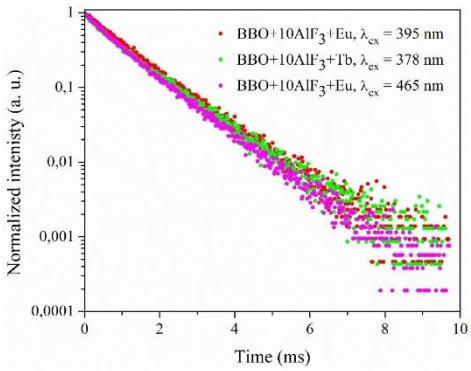

Fig. 8. Luminescence decay curves of BBO+10AlF$_3$+2Eu obtained for λ_{ex} = 395 nm, λ_{ex} = 465 nm (observation at around λ_{em} = 620 nm) and BBO+10AlF$_3$+2 Tb at λ_{ex} = 378 nm (observation at around λ_{em} = 544 nm), respectively.

Tm^{3+}ions was on the order of microseconds.

The excitation spectra of glass samples singly doped with Eu^{3+}, Tb^{3+} and Tm^{3+} ions measured at 454,544 and 615 nm are shown in Fig. 9. The key objective was to investigate the possibility of sample excitation with one wavelength characteristic for Eu^{3+}, Tb^{3+}, and Tm^{3+} ions in order to achieve simultaneous emission from all added rare-earth ions.

Based on Fig. 9. Three excitation wavelengths (355 nm, 378 nm, and 395 nm) have been chosen as adequate for excitation Eu^{3+}, Tb^{3+}, and Tm^{3+}, respectively. They were used to excite the triply doped samples to investigate, whether it is possible to use these lines to excite also other Ln^{3+} ions, for which the excitation line is not characteristic (Figs. 10–12).

When the samples were excited at a wavelength of 378 nm (Fig. 10), only bands originating from Eu^{3+} and Tb^{3+} ions can be seen in the emission spectrum. No peaks assigned to the Tm^{3+} ions were recognized. The bands at 494 nm, 551 nm, 584 nm and 620 nm may be described to the Tb^{3+} ions, $^5D_4 \rightarrow {}^7F_6$ and $^5D_4 \rightarrow {}^7F_5$, $^5D_4 \rightarrow {}^7F_4$, $^5D_4 \rightarrow {}^7F_3$ transitions, respectively [18,69]. The presence of Eu^{3+} ions is represented by several

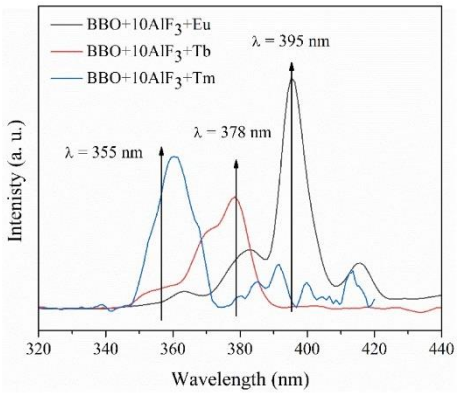

Fig. 9. Excitation spectra of BBO+10AlF$_3$+Re^{3+} (*Re*=Eu, Tm, Tb) glass samples monitored at 455, 545, and 615 nm wavelengths.

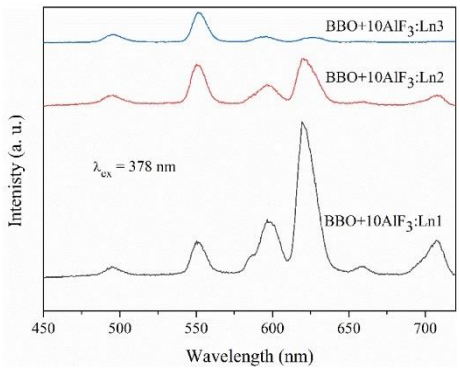

Fig. 10. The emission spectra of BBO+10AlF$_3$:Ln1, Ln2, and Ln3 samples under 378 nm excitation.

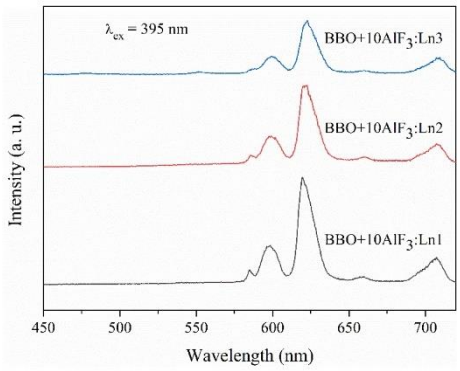

Fig. 11. The emission spectra of BBO+10AlF$_3$:Ln1, BBO+10AlF$_3$:Ln2, BBO+10AlF$_3$:Ln3 samples under 395 nm excitation.

peaks: 584 nm ($^5D_0 \rightarrow {}^7F_0$), 597 nm ($^5D_0 \rightarrow {}^7F_1$), 619 nm ($^5D_0 \rightarrow {}^7F_2$), 658 nm ($^5D_0 \rightarrow {}^7F_3$), 710 nm ($^5D_0 \rightarrow {}^7F_4$) [18,61].

The emission spectra under 395 nm excitation (Fig. 11), consist of several bands at 584 nm ($^5D_0 \rightarrow {}^7F_0$), 597 nm ($^5D_0 \rightarrow {}^7F_1$), 619 nm ($^5D_0 \rightarrow {}^7F_2$), 658 nm ($^5D_0 \rightarrow {}^7F_3$) and 706 ($^5D_0 \rightarrow {}^7F_4$), which can be assigned to Eu^{3+} ions [18,70]. In the emission spectra of the samples excited with λ_{ex}=355 nm also lines corresponding to Eu^{3+} and Tb^{3+} ions (apart of the lines characteristic for Tm^{3+}) can be seen (Fig. 12).

Under 355 nm excitation, the emission spectrum (Fig. 12) shows bands at 459 nm, that can be assigned to the $^1D_2 \rightarrow {}^3F_4$ blue transition of Tm^{3+} ions [18]. Peaks at 494 nm, 551 nm, 584 nm and 622 nm may be described to the Tb^{3+} ions, $^5D_4 \rightarrow {}^7F_6$, $^5D_4 \rightarrow {}^7F_5$, $^5D_4 \rightarrow {}^7F_4$, $^5D_4 \rightarrow {}^7F_3$ transitions, respectively [18,70]. The presence of Eu^{3+} ions is represented by several peaks: 584 nm ($^5D_0 \rightarrow {}^7F_0$), 597 nm ($^5D_0 \rightarrow {}^7F_1$), 619 nm ($^5D_0 \rightarrow {}^7F_2$), 658 nm ($^5D_0 \rightarrow {}^7F_3$), 710 nm ($^5D_0 \rightarrow {}^7F_4$) [18,64]. Therefore, this excitation wavelength was chosen to significantly affect the color of the emission.

The obtained results indicate the possibility of emission in the red, green, and blue spectral range. In particular, the sample BBO+10AlF$_3$:Ln3 shows simultaneous emission from all added rare-earth ions at λ_{ex} =

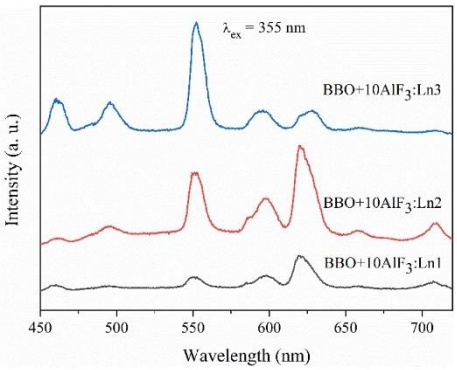

Fig. 12. The emission spectra of BBO+10AlF$_3$:Ln1, Ln2, Ln3 samples under 355 nm excitation.

355 nm. However, further studies are needed to determine the appropriate Ln^{3+} ratio and excitation wavelength to obtain white light emission from borate-bismuth glass matrix triply co-doped with $Eu^{3+}/Tb^{3+}/Tm^{3+}$.The luminescence decay times of excited Eu^{3+}, Tb^{3+}, and Tm^{3+} ions in triply co-doped glass samples aren't significantly different from the results for singly doped glasses.

3.6. Energy transfer between Tb^{3+} and Eu^{3+} in co-doped glasses

In glasses where Tb^{3+} and Eu^{3+} ions are present, energy transfer can occur. According to the Forster-Dexter theory, energy transfer from Tb^{3+} to Eu^{3+} ions can be expected, when the emission band of Tb^{3+} partially overlaps with the absorption band of the Eu^{3+} ions [71].

Firstly, the examination of this phenomenon can be done by comparing the luminescence spectra of glasses singly doped with Eu^{3+} and Tb^{3+}ions. Fig. 13 presents the excitation spectrum of the BBO+10AlF$_3$+Eu sample observed at λ_{em} = 615 nm wavelength, which corresponds to the $^5D_0 \rightarrow {}^7F_2$ transition of europium ions, and the emission spectrum of the BBO+10AlF$_3$+Tb glass at λ_{ex} = 378 nm assigned to the $^7F_6 \rightarrow {}^5D_3$ transition of Tb^{3+} ions. In the 500–550 nm region, the partially overlapping of both spectra can be seen, which suggests that energy transfer between Tb^{3+} and Eu^{3+} in the proposed glass system is present [72].

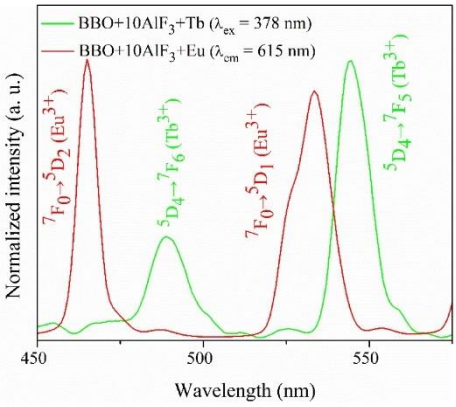

Fig. 13. The excitation spectrum of BBO+10AlF$_3$+Eu glass at λ_{em} = 615 nm (Eu^{3+}), and the emission spectrum of the BBO+10AlF$_3$+Tb glass under λ_{ex} =378 nm (Tb^{3+}).

Next, to gain insight into the energy transfer process, the luminescence spectra of double co-doped glasses were depicted. Fig. 14a shows the excitation spectra of the BBO+10AlF$_3$+1Eu+1 Tb sample under λ_{em} = 615 nm and λ_{em} = 544 nm. When glass is monitored at 544 nm ($^5D_4 \rightarrow {}^7F_5$: Tb^{3+}), only transitions of Tb^{3+} ions are present. However, under 615 nm ($^5D_0 \rightarrow {}^7F_2$: Eu^{3+}) characteristic bands for both $Eu^{3+}$and Tb^{3+} ions are present in the spectrum.

This means, that there is a possibility of obtaining the emission lines from europium using wavelength characteristics for both, Eu^{3+} (395 nm) and Tb^{3+} (378 nm) ions. This can be seen in Fig. 14b, which presents the double co-doped glass excited at λ_{ex} = 395 nm (Eu^{3+}), the emission spectrum consists of four bands assigned to the $^5D_0 \rightarrow {}^7F_{1-4}$ transitions of Eu^{3+} ions. Upon this excitation, bands corresponding to Tb^{3+} ions were not detected. However, when the glass is excited at λ_{ex} = 378 nm, connected to the $^7F_6 \rightarrow {}^5D_3$ transition of Tb^{3+}, both emission lines corresponding to Tb^{3+} and Eu^{3+} ions are present in the emission spectrum. This behavior confirms that the energy transfer process from Tb^{3+} ions to Eu^{3+} ions occurs in the borate-bismuth glass system [71,72,73]. Based on the obtained results, the energy transfer (ET) mechanism in double doped glasses can be proposed as follows:

$$^5D_4(Tb^{3+}) + {}^7F_0(Eu^{3+}) \rightarrow {}^7F_5(Tb^{3+}) + {}^5D_1(Eu^{3+}) \quad (1.2)$$

Upon λ_{ex} = 378 nm, Tb^{3+} ions are excited from $^7F_6$ ground state to the $^5D_3$ excited state. Subsequently, the non-radiative relaxation process to the $^5D_4$ state occurs. From $^5D_4$ state the radiative transitions directly to the ground states at 496 nm ($^5D_4 \rightarrow {}^7F_6$), 549 ($^5D_4 \rightarrow {}^7F_5$), 594 nm ($^5D_4 \rightarrow {}^7F_4$) and 628 nm ($^5D_4 \rightarrow {}^7F_3$) occurs. Part of the energy from $^5D_4$ energy level of Tb^{3+} can be transferred to the $^5D_1$ level of Eu^{3+} due to the existing overlap of the $^5D_4 \rightarrow {}^7F_5$ emission band of Tb^{3+} and $^7F_0 \rightarrow {}^5D_1$ excitation band of Eu^{3+} ions. Then, relaxed non-radiatively to the $^5D_0$ and next by radiative transitions to the $^7F_0$ (578 nm), $^7F_1$ (591 nm), $^7F_2$ (615 nm), $^7F_3$ (652 nm) and $^7F_4$ (700 nm) levels. Fig. 15 presents the schematically illustrated energy levels of Eu^{3+}, and Tb^{3+} ions, which are involved in the energy transfer process and additionally the energy levels for Tm^{3+} ion. In triply doped samples energy transfer could be also present [18].

3.7. CIE chromaticity diagrams

The CIE chromatic coordinates for BBO+10AlF$_3$ glasses singly doped with Eu^{3+}, Tb^{3+}, Tm^{3+} and triply doped with $Eu^{3+}/Tb^{3+}/Tm^{3+}$ ions (BBO+10AlF$_3$:Ln1, BBO+10AlF$_3$:Ln2, BBO+10AlF$_3$:Ln3) upon different excitations wavelengths are shown in Fig. 16. At λ_{ex} = 395 nm, the BBO+10AlF$_3$+Eu^{3+} glass sample emits red light (white triangle) while the BBO+10AlF$_3$+Tb^{3+} sample at λ_{ex} = 378 nm emits green light (white square), which is a typical color of terbium ions emission. The BBO+10AlF$_3$+Tm^{3+} excited with λ_{ex} = 355 nm, emits in blue spectral range (white circle). In the case of samples triply co-doped with $Eu^{3+}/Tb^{3+}/Tm^{3+}$ions, λ_{exc} = 355 nm wavelength was selected to investigate the CIE chromatic coordinates. The colors of the obtained light depend on the composition of the samples. The emission of orange-yellowish light was achieved for BBO+10AlF$_3$:Ln1 (a) and BBO+10AlF$_3$:Ln2 (b). The color closest to white light was obtained at 355 nm excitation of the BBO+10AlF$_3$:Ln3 (c) glass sample, where the addition of europium ions responsible for the reddish-orange color component was the lowest. The reason for such a difference in color change can be attributed to the presence of a new band in the emission spectrum. This sample reveals the peaks of all three added rare earth ions. It can be seen, that emitted color can be tuned by varying the rare-earth ions ratios. However, in order to achieve the generation of white light in the proposed bismuth-

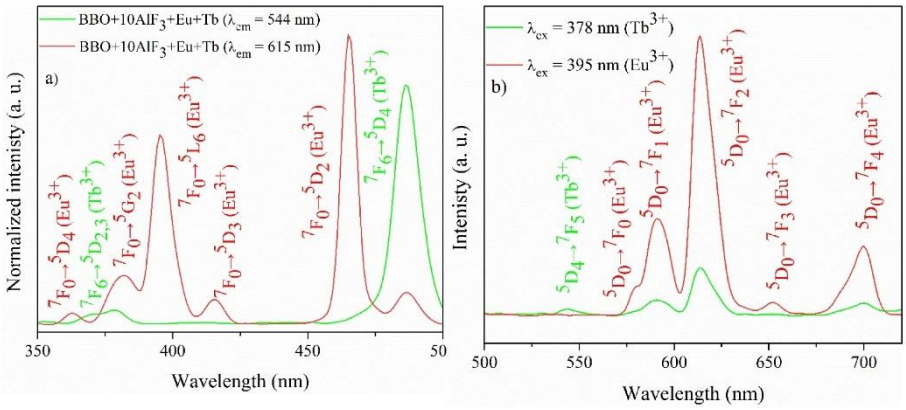

Fig. 14. a) excitation spectra for BBO+10AlF$_3$+1Eu+1 Tb sample under λ_{em} = 544 nm, and λ_{em} = 615 nm; b) emission spectra for BBO+10AlF$_3$+1Eu+1 Tb at λ_{ex}= 395 nm, and λ_{ex} = 387 nm.

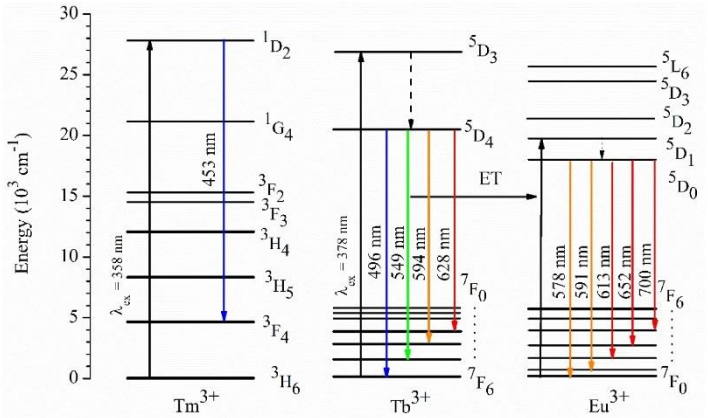

Fig. 15. Partial energy level diagram of Tm^{3+}, Tb^{3+} and Eu^{3+}.

borate glass system, further studies are required, to consider an appropriate ratio of rare-earth ions and excitation wavelength. The detailed corresponding chromaticity parameters (x, y) and correlated color temperature CCT values calculated according to Eq. (1.3) are shown in Table 3 [74].

$$CCT = -449n^3 + 3525n^2 - -6823n + 5520.33 \quad (1.3)$$

Where $n = (x\text{-}x_e)/(y\text{-}y_e)$ with $x_e = 0.332$ and $y_e = 0.186$.

4. Conclusions

The B_2O_3-Bi_2O_3–10AlF_3 glass system singly doped with Eu^{3+}, Tb^{3+}, Tm^{3+}, and triply doped with $Eu^{3+}/Tb^{3+}/Tm^{3+}$ ions in different molar ratios was successfully synthesized using the conventional melt quenching technique. The prepared samples were amorphous and consisted of [BO_3] triangular and [BO_4] tetrahedral structural units. The XPS studies confirmed the presence of Al^{3+}ions in the form of AlF_3 and Al_2O_3 in the glass matrix. The influence of aluminum fluoride on the luminescence properties of glasses was examined. It was found that the addition of 10 mol% of AlF_3 to the basic borate-bismuth matrix resulted in the enhancement of excitation and emission spectra. The simultaneous emission of $Eu^{3+}/Tb^{3+}/Tm^{3+}$ doped glasses was achieved at λ_{exe}=355 nm. The emitted color can be tuned by modifying the rare-earth ions ratio and the excitation wavelength. Due to the overlaps of the emission band of Tb^{3+} and the absorption band of Eu^{3+} ions, energy transfer mechanism was proposed. To achieve the generation of white light in the presented glass system, further studies on the composition and molar ratio of the optically active dopants are required. Based on the obtained results borate-bismuth glasses seem to be an adequate host matrix for the addition of rare-earth ions. Moreover, they can be considered as candidates for luminescence applications, especially for color-tunable light sources.

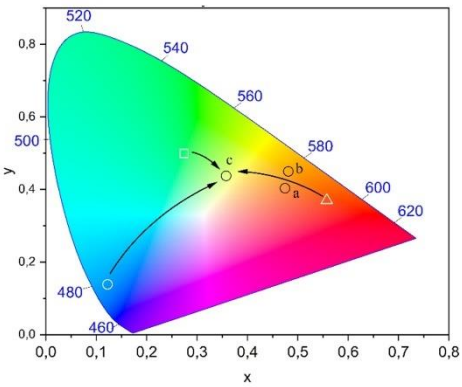

Fig. 16. CIE chromaticity diagram of BBO+10AlF$_3$ glasses singly doped with Eu^{3+} at λ_{exc} = 395 nm (white triangle), Tb^{3+} at λ_{ex} = 378 nm (white square), Tm^{3+} at λ_{ex} = 355 nm (white circle) and triply doped with $Eu^{3+}/Tb^{3+}/Tm^{3+}$ samples at λ_{ex} = 355 nm: BBO+10AlF$_3$:Ln1 (a), BBO+10AlF$_3$:Ln2 (b), BBO+10AlF$_3$:Ln3 (c).

Table 3
Calculated x, y and CCT parameters.

Sample	λ_{ex} [nm]	x	y	CCT (K)	Reference
BBO+10AlF$_3$:Ln1	355	0.47	0.40	2475	Present work
BBO+10AlF$_3$:Ln2	355	0.48	0.45	2727	Present work
BBO+10AlF$_3$:Ln3	355	0.36	0.44	4804	Present work
Standard white	–	0.33	0.33	5455	[75]
YAG+blue chips (II)	–	0.29	0.30	5610	[76]
CdO-GeO2-TeO$_2$: Dy^{3+}/Eu^{3+} glass	382	0.41	0.40	3435	[66]
B_2O_3-TeO$_2$-PbO-ZnO-Li$_2$O—Na$_2$O-Er^{3+}/Dy^{3+} glass	–	0.36	0.43	4753	[77]

Funding

This research did not receive any specific grant from funding agencies in the public, commercial, or not-for-profit sectors.

Data availability

The data that support the findings of this study are available from the corresponding author upon reasonable request.

CRediT authorship contribution statement

Karolina Milewska: Conceptualization, Methodology, Investigation, Validation, Writing – original draft, Data curation, Formal analysis, Visualization, Project administration. **Michał Maciejewski:** Investigation, Data curation. **Marcin Łapiński:** Investigation, Data curation. **Anna Synak:** Investigation, Data curation. **Mirosław Behrendt:** Investigation, Data curation. **Wojciech Sadowski:** Supervision, Resources. **Barbara Kościelska:** Supervision, Validation, Conceptualization, Writing – review & editing.

Declaration of Competing Interest

The authors declare that they have no known competing financial interests or personal relationships that could have appeared to influence the work reported in this paper.

Data availability

Data will be made available on request.

References

[1] K. Siva Rama Krishna Reddy, K. Swapna, Sk. Mahamuda, M. Venkateswarlu, A. S. Rao, G. Vijaya Prakash, Investigation on structural and luminescence features of Dy^{3+} ions doped alkaline earth boro tellurite glasses for optoelectronic devices, Opt. Mater. 85 (2018) 200–210, https://doi.org/10.1016/j.optmat.2018.08.057.
[2] D. Chen, Z. Wang, Y. Zhou, P. Huang, Z. Ji, Tb^{3+}/Eu^{3+}: YF$_3$ nanophase embedded glass ceramics: structural characterization, tunable luminescence and temperature sensing behavior, J. Alloys Compd. 464 (2015) 339–344, https://doi.org/10.1016/j.jallcom.2015.06.030.
[3] I.H. Cho, G. Anoop, D.W. Suh, S.J. Lee, J.S. Yoo, On the stability and reliability of $Sr_{1-x}Ba_xSi_2O_2N_2:Eu^{2+}$ phosphors for white LED applications, Opt. Mater. Express 2 (2012) 1292–1305, https://doi.org/10.1364/OME.2.001292.
[4] Y.N. Ahn, K.D. Kim, G. Anoop, G G.S. Kim, J.S. Yoo, Design of highly efficient phosphor-converted white light-emitting diodes with color rendering indices (R_1-R_9) ≥ 95 for artificial lighting, Sci. Rep. 9 (2019) 16848, https://doi.org/10.1038/s41598-019-53269-0.
[5] J. Cho, J.H. Park, J.K. Kim, E.F. Schubert, White light-emitting diodes: history, progress, and future, Laser Photonics Rev 11 (2017), 1600147, https://doi.org/10.1002/lpor.201600147.
[6] Y. Wang, G. Zhu, S. Xin, Q. Wang, Y. Li, Q. Wu, Ch. Wang, X. Wang, X. Ding, W. Geng, Recent development in rare earth doped phosphors for white light emitting diodes, J. Rare Earths 33 (2015) 1–12, https://doi.org/10.1016/S1002-0721(14)60375-6.
[7] Y. Shi, Y. Wang, Y. Wen, Z. Zhao, B. Liu, Z. Yang, Tunable luminescence Y3Al5O12: $0.06Ce^{3+}$, xMn^{2+} phosphors with different charge compensators for warm white light emitting diodes, Opt. Express. 20 (2012) 21656, https://doi.org/10.1364/OE.20.021656.
[8] P.J. Yadav, N.D. Meshram, C.P. Joshi, S.V. Moharil, Improved yellow phosphors for solid state white lighting, in: AIP Conference Proceedings 1728, 2016, 020199, https://doi.org/10.1063/1.4946250.
[9] Y. Narukawa, I. Niki, K. Izuno, M. Yamada, Y. Murazki, T. Mukai, Phosphor-conversion white light emitting diode using InGaN near ultraviolet chip, J.Appl. Phys. 41 (2002) L371, https://doi.org/10.1143/JJAP.41.L371.
[10] Y.F. Cheung, Z. Ma, H.W. Choi, Color Tunable LEDs, Nitride Semiconductor Light Emitting Diodes (LEDs): Materials, Technologies and Applications, Woodhead Publishing Limited, 2014, pp. 409–427, https://doi.org/10.1533/9780857099303.2.409.
[11] A. Jose, T. Krishnapriya, G. Anns, T.A. Jose, J. Cyriac, N.V. Unnikrishnan, P.R. Biju, Cool/warm white light luminescent traits and energy transfer studies of $Dy^{3+}/Er^{3+}/Sm^{3+}$ triply doped multicomponent borosilicate glasses for lighting applications, J. Non Cryst. Solid. 562 (2021), 120775, https://doi.org/10.1016/j.jnoncrysol.2021.120775.
[12] V.D.S.D. Souza, F.J.F. Caixeta, K.D.O. Lima, R.R. Gonçalves, Modulating white light emission temperature in $Ho^{3+}/Yb^{3+}/Tm^{3+}$ triply doped nanostructured GeO$_2$-Nb$_2$O$_5$ materials for WLEDs applications, J.Lumin 248 (2022), 118978, https://doi.org/10.1016/j.jlumin.2022.118978.
[13] K. Milewska, M. Maciejewski, A. Synak, M. Łapiński, A. Mielewczyk-Gryń, W. Sadowski, B. Kościelska, From structure to luminescent properties of B_2O_3-Bi_2O_3-SrF_2 glass and glass-ceramics doped with Eu^{3+} ions, Materials (Basel) 14 (2021) 4490, https://doi.org/10.3390/ma14164490. -.
[14] C. Zhu, Y. Yang, X. Liang, S. Yuan, G. Chen, Rare earth ions doped full-color luminescence glasses for white LED, J.Lumin 126 (2007) 707–710, https://doi.org/10.1016/j.jlumin.2006.10.028.
[15] C.A.T. Laia, A. Ruivo, Photoluminescent Glasses and Their Applications, in: B. Pedras (Ed.), Fluorescence in Industry. Springer Series On Fluorescence (Methods and Applications), Springer, Cham, 2019, pp. 365–388, https://doi.org/10.1007/4243_2019_12.
[16] B. Kościelska, M. Walas, T. Lewandowski, M. Łapiński, M. Dębowski, A. Synak, A. Klonkowski, W. Sadowski, I. Byliński, W. Wiczk, Structural and luminescence investigation of GeO2-PbO-Bi2O3-SrF2 glasses doped with Eu^{3+}, Tb^{3+} and Tm^{3+} ions, J. Non Cryst. 462 (2017) 41–46, https://doi.org/10.1016/j.jnoncrysol.2017.02.007.
[17] W.J. Chung, Y.H. Nam, A review on phosphor in glass as a high power LED color converter, ECS J. Solid State Sci. Technol. 9 (2020), 016010, https://doi.org/10.1149/2.0142001JSS.
[18] C. Zhao, J. Cai, R. Li, S. Tie, X. Wan, J. Shen, White light emission from $Eu^{3+}/Tb^{3+}/Tm^{3+}$ triply doped aluminoborate glass excited by UV light, J. Non Cryst. 358 (2012) 604–608, https://doi.org/10.1016/j.jnoncrysol.2011.11.011.

[19] M. Mungra, F. Steudel, B. Ahrens, S. Schweizer, Tm/Tb/Eu triple-doped lithium aluminoborate glass for white light generation, J. Lumin. 192 (2017) 71–76, https://doi.org/10.1016/j.jlumin.2017.06.028.

[20] T.A. Lodi, M. Sandrini, A.N. Medina, M.J. Barboza, F. Pedrochi, A. Steimacher, Dy: eu doped CaBAl glasses for white light applications, Opt Mater (Amst) 76 (2018) 231–236, https://doi.org/10.1016/j.optmat.2017.12.043.

[21] T.S. Dhapodkar, A.R. Kadam, N. Brahme, S.J. Dhoble, Efficient white light-emitting $Mg_{21}Ca_4Na_4(PO_4)_{18}$: Dy^{3+}, Tb^{3+}, Eu^{3+} triple doped glasses: a multipurpose glasses for WLEDs, solar cell efficiency enhancement, and smart windows applications, Mater. Today Chem. Today 24 (2022), 100938, https://doi.org/10.1016/j.mtchem.2022.100938.

[22] J.A. Jiménez, B. Darley, Optical spectroscopy and excited-state dynamics of Eu^{3+}-doped bismuth borate glasses containingCuO, ChemPhysChem 21 (2020) 1688–1694, https://doi.org/10.1002/cphc.202000396.

[23] I. ArulRayappan, K. Selvaraju, K. Marimuthu, Structural and luminescence investigations on Sm^{3+} doped sodium fluoroborate glasses containing alkali/alkaline earth metal oxide, Phys. B: Condenss. Matter 406 (2011) 548–555, https://doi.org/10.1016/j.physb.2010.11.037.

[24] M.B. Saisudha, J. Ramakrishna, Optical absorption of Nd^{3+}, Sm^{3+} and Dy^{3+} in bismuth borate glasses with large radiative transition probabilities, Opt. Mater. 18 (2002) 403–417, https://doi.org/10.1016/S0925-3467(01)00181-1.

[25] M. Mariyappan, S. Arunkumar, K. Marimuthu, Effect of Bi_2O_3 on the structural and spectroscopic properties of Sm^{3+} ions doped sodiumfluoroborate glasses, J. Mol. Struct. 1105 (2016) 214–224, https://doi.org/10.1016/j.molstruc.2015.10.043.

[26] N.M. Bobkova, Properties and structure of bismuth-borate glasses (review), Glass Ceram. 72 (2016) 360–365, https://doi.org/10.1007/s10717-016-9790-2.

[27] Mc Daniel, E.M. Levin, C. McDaniel, J. Am. Ceram. Soc. 45 (1962) 355–360.

[28] P. Becker, Thermal and optical properties of glasses of the system Bi_2O_3– B_2O_3, Cryst. Res. Technol. 38 (2003) 74–82, https://doi.org/10.1002/crat.200310009.

[29 A.C. Wright, S.A. Feller, A.C. Hannon, in: Society of Glass Technology, International Conference on Borates Glasses, Crystals and Melt, Sheffield, Society of Glass Technology, 1997.

[30] N.M. Bobkova, Characteristics of the structural state of bismuth ions in bismuth-borate glasses, Glass Ceram 75 (2019) 383–386, https://doi.org/10.1007/s10717-019-00090-w.

[31] I.I. Oprea, H. Hesse, K. Betzler, Optical properties of bismuth borate glasses, Opt. Mater. (Amst.) 26 (2004) 235–237, https://doi.org/10.1016/j.optmat.2003.10.006.

[32] C. Armellini, M. Ferrari, M. Montagna, G. Pucker, C. Bernard, A. Monteil, Terbium (III) doped silica-xerogels: effect of aluminium(III) co-doping, J. Non-Cryst. Solids 245 (1999) 115–121, https://doi.org/10.1016/S0022-3093(98)00856-4.

[33] V. Lavín, U.R. Rodríguez-Mendoza, I.R. Martín, V.D. Rodríguez, Optical spectroscopy analysis of the Eu^{3+} ions local structure in calcium diborate glasse, J. Non Cryst. Solid. 319 (2003) 200–216, https://doi.org/10.1016/S0022-3093(02)01914-2.

[34] Yiting Tao, Sasa Yan, Ying Du, Panting Wang, Danping Chen, Effect of Al^{3+} on the spectroscopic properties of Eu^{2+} and Tb^{3+} Doped high silica glass, Ceram. Int. 47 (2021) 18030–18036, https://doi.org/10.1016/j.ceramint.2021.03.118.

[35] M. Ennouri, B. Gelloz, H. Elhouichet, Impact of Ag species on luminescence and spectroscopic properties of Eu^{3+} doped fluoro-phosphate glasses, J. Non Cryst. Solid. 570 (2021), 120938, https://doi.org/10.1016/j.jnoncrysol.2021.120938.

[36] M. Walas, A. Pastwa, T. Lewandowski, A. Synak, I. Gryczyński, W. Sadowski, B. Kościelska, Luminescent properties of Ln^{3+} doped tellurite glasses containing AlF_3, Opt.Mater 59 (2016) 70–75, https://doi.org/10.1016/j.optmat.2016.01.040.

[37] C.D.S. Bordon, E.S. Magalhaes, D.M. da Silva, L.R.P. Kassab, C.B. de Araújo, Influence of Al_2O_3 on the photoluminescence and optical gain performance of Nd^{3+} doped germanate and tellurite glasses, Opt. Mater. 109 (2020), 110342, https://doi.org/10.1016/j.optmat.2020.110342.

[38] G. Hu, Y. Zhou, R. Liua, Ch. Li, Lina Liua, H. Lina, F. Zenga, Z. Su, Regulation of luminescence properties of SBGNA: Eu^{3+} glass by the content of B_2O_3 and Al_2O_3, Opt. Mater. 106 (2020), 110025, https://doi.org/10.1016/j.optmat.2020.110025.

[39] A.L. Fanai, U. Khan, S. Rai, Luminescence enhancement of Pr^{3+} doped sol-gel silica glass as a result of Al^{3+} co doping, J. Non Crystal. Solid. 503 (2019) 89–93, https://doi.org/10.1016/j.jnoncrysol.2018.09.027.

[40] S. Rai, A.L. Fanai, Optical properties of Ho^{3+} in sol-gel silica glass co-dopedwith Aluminium, J. Non Cryst. Solid. 449 (2016) 113–118, https://doi.org/10.1016/j.jnoncrysol.2016.07.023.

[41] M.J. Lochhead, K.L. Bray, Rare-earth clustering and aluminum codoping in Sol—Gel silica: investigation using europium (III) fluorescence spectroscopy, Chem. Mater. 7 (1995) 572, https://doi.org/10.1021/cm00051a019.

[42] L. Bokatial, S. Rai, Optical properties of Sm^{3+} ions in sol-gel derived alumino-silicate glasses, J. Opt. 41 (2012) 94, https://doi.org/10.1007/s12596-012-0069-x.

[43] A.J. Silversmith, A.P. Beyler, K.E. Arpino, D.M. Boye, K.R. Hoffman, Mechanisms of fluorescence enhancement in rare earth sol–gel glass containing Al^{3+}, J. Lumin. 131 (2011) 457–460, https://doi.org/10.1016/j.jlumin.2010.11.018.

[44] A. Monteil, S. Chaussedent, G. Alombert-Goget, N. Gaumer, J. Obriot, S.J. L. Ribeiro, Y. Messaddeq, A. Chiasera, M. Ferrari, Clustering of rare earth in glasses, aluminum effect: experiments and modeling, J. Non-Cryst. Solid. 348 (2004) 44–50, https://doi.org/10.1016/j.jnoncrysol.2004.08.124.

[45] J. Silversmith, N.T.T. Nguyen, B.W. Sullivan, D.M. Boye, C. Ortiz, K.R. Hoffman, Rare-earth ion distribution in sol–gel glasses co-doped with Al^{3+}, J. Lumin. 128 (2008) 931–933, https://doi.org/10.1016/j.jlumin.2007.

[46] B. Grobelna, P. Bojarski, B. Kuklinski, A. Kubicki, A. Synak, Optical properties and luminescence kinetics of $Ln_{1.9}Pr_{0.1}(WO_4)_3$, Opt. Mater. 34 (2011) 103–108, https://doi.org/10.1016/j.optmat.2011.07.011.

[47] Y. Yang, Y. Liu, P. Cai, R. Maalej, H.J. Seo, Thermal stability and spectroscopic properties of Ho^{3+} doped tellurite-borate glasses, J. Rare Earths 33 (2015) 939–945, https://doi.org/10.1016/S1002-0721(14)60509-3.

[48] N. Kaur, A. Khanna, M. González-barriuso, F. González, B. Chen, Effects of Al^{3+}, W^{6+}, Nb^{5+} and Pb^{2+} on the structure and properties of borotellurite glasses, J. Non Cryst. Solid. 429 (2015) 153–163, https://doi.org/10.1016/j.jnoncrysol.2015.09.005.

[49] M. Saad, M. Poulain, Glass forming ability criterion, Mater. Sci. Forum 19 20 (1987) 11–18, https://doi.org/10.4028/www.scientific.net/MSF.19-20.11.

[50] E.R. Shaaban, M. Shapaan, Y.B. Saddeek, Structural and thermal stability criteria of Bi_2O_3-B_2O_3 glasses, J. Phys.: Condens. Matter 20 (2008), 155108, https://doi.org/10.1088/0953-8984/20/15/155108.

[51] N. Mary, M. Rebours, E. Castel, S. Vaishnav, W. Deng, A.M.T. Bell, F. Clegg, B. L. Allsopp, A. Scrimshire, P.A. Bingham, Enhanced thermal stability of high bismuth borate glasses by addition of iron, J. Non-Cryst. Solids 500 (2018) 149–157, https://doi.org/10.1016/j.jnoncrysol.2018.07.061.

[52] P. Pascuta, L. Pop, Lidia, S. Rada, M. Bosca, Maria, E. Culea, The local structure of bismuth borate glasses doped with europium ions evidenced by FTIR spectroscopy, J. Mater. Sci. Mater. Electron. 19 (2008) (2008) 424–428, https://doi.org/10.1007/s10854-007-9359-5.

[53] A.A. Ali, Y.S. Rammah, R. El-Mallawany, D. Souri, FTIR and UV spectra of pentaternary borate glasses, Measurement 105 (2017) 72–77, https://doi.org/10.1016/j.measurement.2017.04.010.

[54] U. Gross, S. Rüdiger, E. Kemnitz, K. Brzezinka, S. Mukhopadhyay, C. Bailey, A. Wander, N. Harrison, Vibrational analysis study of aluminum trifluoride phases vibrational analysis study of aluminum trifluoride phases, J. Phys. Chem. A (2007) 5813–5819, https://doi.org/10.1021/jp072388r.

[55] A. Vazquez, T. Lopez, R. Gomez, Bokhimi, A. Morales, O. Novaro, X-ray diffraction, FTIR, and NMR characterization of sol-gel alumina doped with lanthanum and cerium, J. Solid State Chem. 128 (1997) 161–168, https://doi.org/10.1006/jssc.1996.7135.

[56] R. Ramos, G. Cunge, B. Pelissier, O. Joubert, Cleaning aluminum fluoride coatings from plasma reactor walls in $SiCl_4$/Cl_2 plasmas, Plasma Source. Sci.Technol 16 (2007) 711–715, https://doi.org/10.1088/0963-0252/16/4/004.

[57] C. Song, B. Yu, M. Wang, L. Qian, Rapid and maskless nanopatterning of aluminosilicate glass surface via friction-induced selective etching in HF solution, RSC Adv. 5 (2015) 79964–79968, https://doi.org/10.1039/C5RA13049B.

[58] B. Oprea, T. Radu, S. Simon, XPS investigation of atomic environment changes on surface of B_2O_3–Bi_2O_3 glasses, J. Non Cryst. 379 (2013) 35–39, https://doi.org/10.1016/j.jnoncrysol.2013.07.024.

[59] Y. Li, P. Xiong, G. Liu, M. Peng, Z. Ma, Visible and near-infrared emission in $Ba_3Sc_4O_9$: Bi Phosphor: an Investigation on Bismuth valence modification, Inorg. Chem. 60 (2021) 13510–13516, https://doi.org/10.1021/acs.inorgchem.1c01835.

[60] T.N. Lam Tran, A. Chiasera, A. Lukowiak, M. Ferrari, Eu^{3+} as a powerful structural and spectroscopic tool for glass photonics, Materials (Basel) 15 (2022) 1847, https://doi.org/10.3390/ma15051847.

[61] S. Fazal, F. Zaman, S. Ali, Y. Iqbal, N. Chanithima, S. Tuscharoen, M. Ali, K. Hayat, S. Zulfiqar, M. Arshad, A. El-Denglawey, J. Kaewkhao, Investigation of europium-doped aluminium phosphate glass for red light generation, Ceram. Int. 48 (2022) 24751–24757, https://doi.org/10.1016/j.ceramint.2022.05.124.

[62] J. Dahiya, A. Hooda, A. Agarwal, S. Khasa, Tuneable colour flexibility in Dy^{3+}&Eu^{3+}co-doped lithium fluoride bismuth borate glass system for solid state lighting applications, J. Non Cryst. Solids. 576 (2022), 121237, https://doi.org/10.1016/j.jnoncrysol.2021.121237.

[63] M.A. Cherbib, S. Kapoor, M. Bockowski, M.M. Smedskjaer, L. Wondraczek, Luminescence behaviour of Eu^{3+} in hot-compressed silicate glasses, J. Non-Cryst. Solids: X. 4 (2019), 100041, https://doi.org/10.1016/j.nocx.2019.100041.

[64] O. Malta, P. Santa-Cruz, G. Sá, F Gilberto, Auzel, françois, fluorescence enhancement induced by the presence of small silver particles in Eu^{3+} doped materials, J. Lumin. 33 (1985) 261–272, https://doi.org/10.1016/0022-2313(85)90003-1.

[65] S.H. Nandyala, G. Hungerford, J.D. Santos, B.M. Walsh, L. Di Silvio, A. Stamboulis, Time resolved and excitation emission matrix luminescence behaviour of boro silicate glasses doped with Eu^{3+} ions for red luminescent application, Mater. Res. Bull. 140 (2021), 111340, https://doi.org/10.1016/j.materresbull.2021.

[66] D.A. Rodríguez-Carvajal, A.N. Meza-Rocha, U. Caldino, R. Lozada-Morales, E. Alvarez, Ma.E. Zayas, Reddish-orange, neutral and warm white emissions in Eu^{3+}, Dy^{3+} and Dy^{3+} /Eu^{3+} doped CdO-GeO_2-TeO_2 glasses, Solid State Sci. 61 (2016) 70–76, https://doi.org/10.1016/j.solidstatesciences.2016.09.009.

[67] K. Tao, Y. Ye, H. Bai, S. Wang, Synthesis and luminescence characteristics of Tb^{3+}-doped fluorophosphate glass for UV detection, J. Non-Cryst. Solids. 572 (2021), 121012, https://doi.org/10.1016/j.jnoncrysol.2021.121012.

[68] K. Linganna, S. Ju, Ch. Basavapoornima, V. Venkatramu, C.K. Jayasankar, Luminescence and decay characteristics of Tb^{3+}-doped fluorophosphate glasses, J. Asian Ceram. Soc. 6 (2018) 82–87, https://doi.org/10.1080/21870764.2018.1442674.

[69] Y. Qiao, Luminescence, energy transfer and tunable white emitting of borosilicate glass doubly doped with Tb/Sm or triply doped with Ce/Tb/Sm for white LEDs, Mater. Sci. Eng.: B. 276 (2022), 115565, https://doi.org/10.1016/j.mseb.2021.115565.

[70] S. Gopi, S.K. Jose, E. Sreeja, P. Manasa, N.V. Unnikrishnan, C. Joseph, P.R. Biju, Tunable green to red emission via Tb sensitized energy transfer in Tb/Eu co-doped alkali fluoroborate glass, J. Lumin. 192 (2017) 1288–1294, https://doi.org/10.1016/j.jlumin.2017.09.009.

[71] Y. Ma, M. Feia, W. Zhanga, L. Tenga, R.Weia F.Hua, H. Guo, Energy transfer and tunable luminescent properties in Eu^{2+} /Tb^{3+} /Eu^{3+} co-doped oxyfluoride

aluminosilicate glass, J. Lumin. 219 (2020), https://doi.org/10.1016/j.jlumin.2019.116966.

[72] J. Pisarska, A. Kos, M. Soltys, L. Żur, W.A. Pisarski, Energy transfer from Tb^{3+} to Eu^{3+} in lead borate glass, J. Non-Cryst. 388 (2014) 1–5, https://doi.org/10.1016/j.jnoncrysol.2014.01.019.

[73] S. Jiang, L. Li, Ch. Duan, X. Zhou, M. Yin, Energy transfer from Tb^{3+} to Eu^{3+} in zinc lead borate glass, J. Rare Earth. 28 (2010) 312–315, https://doi.org/10.1016/S1002-0721(10)60284-0.

[74] Y. Yan, H. Zhang, H. Huo, T. Wang, X. Zou, Ch. Su, W. Hu, Luminescence and energy transfer of Dy3+–Eu3+ co-doped glass-ceramics containing ZnMoO4, J. Alloy. Compd. 897 (2022) 163–164, https://doi.org/10.1016/j.jallcom.2021.163164.

[75] L. Mishra, A. Sharma, A.K. Vishwakarma, K. Jha, M. Jayasimhadri, B.V. Ratnam, K. Jang, A.S. Rao, R.K. Sinha, White light emission and color tunability of dysprosium doped barium silicate glasses, J. Lumin. 169 (2016) 121–127, https://doi.org/10.1016/j.jlumin.2015.08.063.

[76] Z. Ci, Q. Sun, S. Qin, M. Sun, X. Jiang, X. Zhang, Y. Wang, Warm white light generation from a single phase Dy^{3+} doped $Mg_2Al_4Si_5O_{18}$ phosphor for white UV LEDs, Phys. Chem. Chem. Phys. 16 (2014) 11597–11602, https://doi.org/10.1039/C4CP00357H.

[77] G. Lakshminarayana, K.A. Bashar, S.O. Baki, A. Lira, U. Caldino, A.N. Meza-rocha, C. Falcony, E. Camarillo, I.V. Kityk, M.A. Mahdi, absorption and fluorescence features study for visible and near-infrared fiber laser applications, J. Non-Cryst. Solid. 503 (2018) 366–381, https://doi.org/10.1016/j.jnoncrysol.2018.10.025.

[II] Karolina Milewska, Michał Maciejewski, Michal Žitňan, José J. Velázquez, Dušan Galusek, Wojciech Sadowski, Barbara Kościelska, Tunable emission and energy transfer of B_2O_3–Bi_2O_3–AlF_3 glass system doped with Eu^{3+}/Dy^{3+}, Journal of Luminescence, Vol. 269, (2024) 120440

Journal of Luminescence 269 (2024) 120440

Contents lists available at ScienceDirect

Journal of Luminescence

journal homepage: www.elsevier.com/locate/jlumin

Full Length Article

Tunable emission and energy transfer of B_2O_3–Bi_2O_3–AlF_3 glass system doped with Eu^{3+}/Dy^{3+}

Karolina Milewska [a,*], Michał Maciejewski [a], Michal Žitňan [b], José J. Velázquez [b], Dušan Galusek [b,c], Wojciech Sadowski [a], Barbara Kościelska [a]

[a] Institute of Nanotechnology and Materials Engineering, Faculty of Applied Physics and Mathematics, Gdańsk University of Technology, ul. Gabriela Narutowicza 11/12, 80-233 Gdańsk, Poland

[b] FunGlass-Centre for Functional and Surface Functionalized Glass, Alexander Dubček University of Trenčín, Študentská 2, Trenčín 911 50, Slovakia

[c] Joint Glass Centre of the IIC SAS, TnUAD, and FChPT STU, Trenčín, Slovakia

ARTICLE INFO

Keywords:
Glass
Luminescence
Rare-earth ions
Light-emitting diodes

ABSTRACT

The structure and luminescent properties of the B_2O_3–Bi_2O–AlF_3 glass system doped with Eu^{3+}/Dy^{3+} ions in different molar ratios were studied. A series of glasses were synthesized by the conventional melt quenching technique. Glass transition and crystallization temperatures were examined by Differential Thermal Analysis (DTA) measurements. The amorphous character of the prepared samples was confirmed by the X-ray diffraction (XRD) method. Raman and FTIR spectra were collected and deconvoluted to investigate the glass microstructure. Luminescence spectra revealed that the added rare-earth ions can be excited by a single wavelength. The emitted color can be tuned by changing the ratios of the Eu^{3+}/Dy^{3+} ions and the excitation wavelength. Furthermore, the influence of the addition of AlF_3 on the luminescence and decay times was investigated. In the glasses with 10 mol% AlF_3 an enhancement of the emission and excitation spectra was detected. The energy transfer analysis confirms the energy transfer between Eu^{3+} and Dy^{3+} ions in the glass matrix. Additionally, the results of this study indicate that the B_2O_3–Bi_2O–AlF_3 glasses doped with Eu^{3+} and Dy^{3+} can be used as a color tunable phosphor.

1. Introduction

Rare-earth (RE) doped luminescent materials have enjoyed great interest for many years due to their wide range of applications [1,2]. Light-emitting materials can be used in optoelectronic devices, biomarkers, displays, optical fibers, lasers, and so on [3–7]. A significant part of the research in this field is focused on rare-earth-ion-doped phosphors for solid-state lighting (SSL) based devices, such as light-emitting diodes (LEDs) [8,9]. They are characterized by several advantages over conventional incandescent or fluorescent lamps, such as high efficiency, brightness, long lifetime, good reliability, and low energy consumption [10]. This is crucial since the electrical lighting sector is responsible for almost 19 % of the world's total electricity consumption [11]. Therefore, development of novel and environmentally safe materials that are efficient and durable are extremely important [2,12–14].

In this sense, the use of RE ions plays an important role. These ions have the unique ability to emit light due to their 4f-4f or 4d-4f transitions when excited at an appropriate wavelength [15]. Neutral white-light emission can be achieved by single Dy^{3+} doped materials. Trivalent dysprosium ions emit several characteristic lines in the luminescence spectrum, with two main bands in the blue (470 nm–500 nm) and yellow (570 nm–600 nm) regions due to the $^4F_{9/2}\rightarrow{}^6H_{15/2}$ and $^4F_{9/2}\rightarrow{}^6H_{13/2}$ transitions, respectively [16,17].

Appropriate adjustment of the blue and yellow luminescence intensity ratio can lead to white light emission [15,18,19]. However, there is a tendency to achieve warm light instead of cold, unnatural white color [20]. To obtain that warm light, Eu^{3+} ions can be used as red emitters because their most intense band corresponding to the $^5D_0\rightarrow{}^7F_2$ transition of Eu^{3+} is at ~615 nm, which is in the red region of the visible light spectrum [21,22].

Moreover, an appropriate proportion of Eu^{3+}/Dy^{3+} in the host matrix can lead to color-adjustment resulting in a warm white light emission. This effect was obtained in several Dy^{3+}/Eu^{3+} doped matrices, e.g. in yttrium alumino bismuth borosilicate and CdO-GeO_2-TeO_2 glasses [4,23] and oxyfluoride glass-ceramics (GCs) [24]. Also, white color was

* Corresponding author.
E-mail address: karolina.milewska@pg.edu.pl (K. Milewska).

https://doi.org/10.1016/j.jlumin.2024.120440
Received 19 August 2023; Received in revised form 5 December 2023; Accepted 4 January 2024
Available online 9 January 2024

obtained in Dy^{3+} and Eu^{3+} co-doped lithium fluoride bismuth borate glass [25]. Investigation of $Zn(PO_3)_2$ glass doped with Eu^{3+} and Dy^{3+} ions reveal white light emission shifted from neutral white at 348 nm excitation to warm white upon 445 nm [26].

The aim of this work was to synthesize B_2O_3–Bi_2O_3–AlF_3 glasses doped with Eu^{3+}/Dy^{3+} ions, that could be used as a phosphor in LEDs. This study provides a detailed analysis of the structural and luminescent properties of these prepared glasses, in particular, the influence of the excitation wavelength and the ratio of the Eu^{3+}/Dy^{3+} ions on the resulting emitted color was investigated. Additionally, the influence of AlF_3 addition on the luminescence intensity was analyzed. The obtained results confirm that the B_2O_3–Bi_2O_3–AlF_3 glasses can be used as a suitable matrix for optically active RE ions and can be considered as a new phosphor material.

2. Materials and methods

The B_2O_3–Bi_2O_3 glasses samples with composition (in mol %) $50B_2O_3$–$50Bi_2O_3$, $45B_2O_3$–$45Bi_2O_3$-10 AlF_3, $44B_2O_3$–$44Bi_2O_3$–$10AlF_3$-$xEu^{3+}/(2\text{-}x)\ Dy^{3+}$ (where x = 2.0; 1.5; 1.0; 0.5 or 0.0) were prepared using the conventional melt quenching technique. Appropriate amounts of raw materials, (H_3BO_3 (99.0 %, Chempur), $Bi_5O(OH)_9(NO_3)_4$ (98.0 %, Chempur), AlF_3 (99+%, Alfa Aesar), Eu_2O_3 (99,9 %, Onyxmet), and Dy_2O_3 (99,9 %, Onyxmet), were mixed in an agate mortar. Batches of 10 g were put in porcelain crucibles, placed into a furnace, and heated to 950 °C for 0.5 h in air. The melts were poured on a pre-heated steel plate

Table 1
Sample names, corresponding nominal compositions of the studied glasses in mol% and their photographs.

Sample	B_2O_3	Bi_2O_3	AlF_3	Eu_2O_3	Dy_2O_3	
BBO	50	50	–	–	–	
BBO+2Eu	49	49	–	2	–	
BBO+2Dy	49	49	–	2	–	
BBO+10AlF_3	45	45	10	–	–	
BBO+10ALF_3+2Eu	44	44	10	2	–	
BBO+10AlF_3+2Dy	44	44	10	–	2	
BBO+10AlF_3:Ln1	44	44	10	0.5	1.5	
BBO+10AlF_3:Ln2	44	44	10	1	1	
BBO+10AlF_3:Ln3	44	44	10	1.5	0.5	

(250 °C) and pressed with another steel plate. Detailed descriptions of the compositions and photographs of prepared glasses are presented in Table 1. All obtained samples were transparent and slightly yellow.

To determine the thermal properties of prepared glass samples, differential thermal analysis (DTA) was conducted on Netzsch Simultaneous TGA-DSC, STA 449 F1. The measurements were performed in air atmosphere, using aluminum crucible, with a 10 K/min heating rate. The obtained results were used for determination the glass transition (T_g) and crystallization (T_c) temperatures. The amorphous structure of the glasses was confirmed by XRD measurements on powdered samples using a diffractometer with Cu Kα radiation (λ = 1.5406 Å) (D2 Phaser, Bruker). Raman spectroscopy was applied on polished samples using a Renishaw inVia Reflex instrument with a 532 nm excitation wavelength. FTIR measurements were performed on a spectrometer with a TGS detector (PerkinElmer Frontier MIR/FIR) using pellet samples mixed with potassium bromide (KBr) in a weight ratio (Sample:KBr) of 2:100. The emission and excitation spectra were collected on a spectrofluorometer (Horiba Yvon Fluorolog 3). The emission lifetimes were calculated from the luminescence decay curves recorded at the same equipment using a pulsed lamp.

3. Results and discussion

3.1. Structural characterization

The DTA technique was used to determine the glass transition (T_g) and glass crystallization (T_c) temperatures of BBO and BBO+10AlF_3 samples. The obtained DTA curves are shown in Fig. 1. For glass doped with AlF_3, T_g and T_c were found to be higher in comparison to undoped one. Such changes in these parameters could result from the fact, that the addition of a glass modifier, such as AlF_3, may affects the structure of the borate-bismuth glass matrix [27]. New connections are created between glass components, which may increase the energy barrier for molecule motion to overcome and increase the thermal stability of the glass matrix [27]. Additionally, the determination of the T_g and T_c allows to calculate the Saad-Poulain parameter (S) corresponding to the thermal stability of the glasses [28]:

$$S = \frac{(T_c - T_x)(T_c - T_g)}{T_g} \quad (1)$$

Also, the Δ T parameters, which is the difference between the onset of the crystallization peak (T_x) and T_g were calculated. This parameter determines the glass stability region. All the thermal parameters of the examined samples are presented in Table 2.

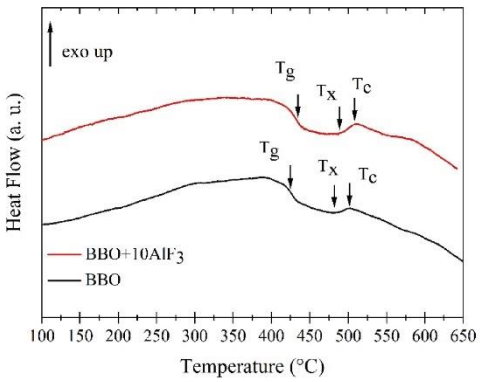

Fig. 1. Differential thermal analysis (DTA) curves of the BBO and BBO+10AlF_3 glass samples.

Based on the calculated S and Δ T parameters the stability of the glass decreases after AlF_3 addition. The values of S are 3.62 and 3.45 for BBO and BBO+10AF_3, respectively. The obtained results are similar to results for other borate glasses [29,30]. It can be concluded that 10 mol % of AlF_3 addition to the basic glass (BBO) results in the lower stability of glass and its higher tendency of crystallization [31].

The amorphous character of the glass samples was confirmed by the XRD method. Fig. 2 shows the diffractograms of the BBO glass matrix and the sample modified by the addition of 10 mol % AlF_3. The obtained results show only the broad amorphous halos, which are due to the presence of short-range order at 20–35° and 40–70°.

Fig. 3 presents the deconvoluted FTIR spectra of the BBO and BBO+10AlF_3+2Dy glasses and the peaks parameters such as peak position (x_c), amplitude (A), and full width at half maximum (FWHM) are listed in Table 3. The peak at around 500 cm^{-1} can be assigned to the Bi–O bending vibrations in [BiO_6] octahedral units [32,33]. The peak in the rage 586-614 cm^{-1} may be attributed to the Bi–O and Bi–O–Bi stretching vibrations of [BiO_6] octahedral units [32,33]. The peak in the range of 688–698 cm^{-1} may be present due to the bending vibrations of B–O–B in [BO_3] triangles [32,33]. The band near 900 cm^{-1} can be ascribed to the B–O stretching in [BO_4] units from diborate groups [33]. The peak at around 1060 cm^{-1} may be assigned to the B–O stretching vibrations in [BO_4] units from tri, tetra, and pentaborate groups [34]. The broad band observed in the 1100-1500 cm^{-1} region consists of four peaks at around 1190, 1300,1450 cm^{-1}. Peaks at 1190 cm^{-1} and 1300 cm^{-1} may be attributed to the B–O stretching vibrations of trigonal [BO_3] units in boroxol rings [34]. At around 1390 cm^{-1} B–O stretching vibrations of [BO_3] units in metaborate, pyroborate, and orthoborate groups [33,34]. The peak at around 1450 cm^{-1} can be assigned to the presence of antisymmetric stretching vibrations with non-bridging oxygens (NBOs) of the B–O–B groups [33,34]. No significant differences can be seen in the spectra with and without AlF_3. Only a slight shift of peaks can be seen. The change in peaks positions and parameters may be due to structural modifications that occur in glass matrix after AlF_3 addition. Similar behavior was observed in other glasses, due to the presence of glass modifier [33]. The detailed assignments of FTIR peaks are summarized in Table 5.

Raman spectra of the BBO and the BBO+10AlF_3+2Dy glasses are shown in Fig. 4. The obtained spectra consist of broad bands, which could have hidden peaks. Due to this fact, to conduct detailed analysis, spectra were deconvoluted. The peak positions (x_c), amplitude (A), and full width at half maximum (FWHM) are presented in Table 4. The peak observed around 220 cm^{-1} can be assigned to the vibrations of Bi–O bond in [BiO_3] and [BiO_6] structural units [32,33]. Bi–O–Bi stretching vibrations can be seen around 400 cm^{-1} [32,33]. Band at 569 cm^{-1} may be attributed to the stretching vibrations between Bi–O bonds in [BiO_6] units [35]. The peak near 620 cm^{-1} may be due to the bending vibrations of B–O–B in metaborate groups of [BO_3] units [33,36]. The peak at 957 cm^{-1} can be assigned to the vibrational modes in B–O–B and B–O bonds in pyroborate [BO_3] groups [37,38]. At about 1090 cm^{-1} vibrations of diborate groups may be present [39]. The broad band in the range 1253 cm^{-1} corresponds to the stretching vibrations of B–O bands of non-bridging oxygens (NBOs) in borate groups [14]. The detailed information's on bands assignments are listed in Table 5. No evidence of new bands connected to the presence of AlF_3 can be seen in the spectrum. Only slight changes in the peak's positions due to addition of AlF_3 can be seen, like in FTIR spectra.

Table 2
Thermal parameters of BBO and BBO+10AlF_3 glass samples.

Sample	T_g (° C)	T_x (° C)	T_c (° C)	Δ T (° C)	S (° C)
BBO	425.9	482	503.5	56.1	3.62
BBO+10AlF_3	433.6	487.1	507.4	53.5	3.45

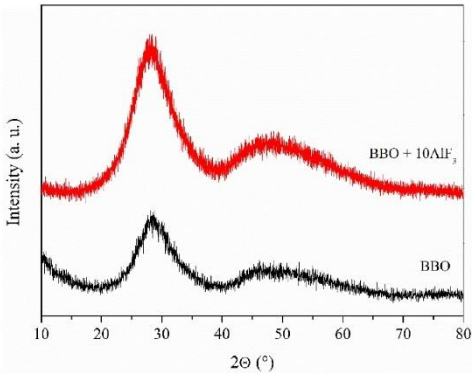

Fig. 2. X-ray diffraction patterns of the BBO and BBO+10AlF$_3$ glass samples.

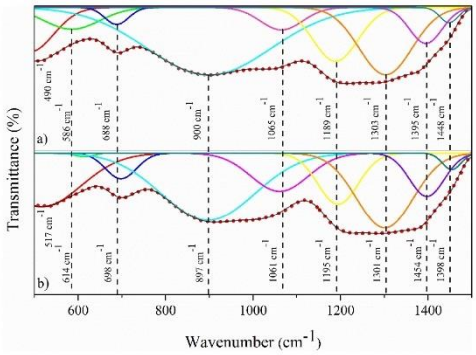

Fig. 3. Deconvoluted FTIR spectra of BBO (a) and BBO+10AlF$_3$+2Dy (b) glasses. Experimental data and gaussian components are shown by black and colored solid lines, respectively. The simulated spectrum is shown by red dots.

Table 3
Peak position x_c (cm^{-1}), amplitude A (a. u.) and full width at half maximum FWHM (cm^{-1}) of deconvoluted BBO and BBO+10AlF$_3$+2Dy FTIR spectra.

	BBO			BBO+10AlF$_3$+2Dy		
	x_c	A	FWHM	x_c	A	FWHM
1	490	7	128	517	15	212
2	586	4	150	614	1	50
3	688	3	64	698	7	83
4	900	11	334	897	19	251
5	1065	4	114	1061	11	153
6	1189	9	120	1195	15	108
7	1303	11	142	1301	21	152
8	1395	6	87	1398	12	93
9	1448	2	49	1454	5	50

3.2. Optical characterization

3.2.1. Steady state luminescence

First, the optical characterization was performed by using steady-state luminescence measurements that have been carried out to obtain detailed information about the luminescence properties of Eu^{3+}/Dy^{3+} doped glasses and the possibility of white-light generation by simultaneous excitation of rare-earth ions with one wavelength.

Table 4
Peak position x_c (cm^{-1}), amplitude A (a. u.) and full width at half maximum FWHM (cm^{-1}) of deconvolution BBO and BBO+10AlF$_3$+2Dy Raman spectra.

	BBO			BBO+10AlF$_3$+2Dy		
	x_c	A	FWHM	x_c	A	FWHM
1	225	7977	703	201	4207	712
2	396	3474	185	410	1787	212
3	569	1204	57	569	431	60
4	629	1002	78	623	573	124
5	957	1360	149	957	539	126
6	1088	1671	101	1095	956	133
7	1253	1317	218	1288	624	177

Table 5
Assignment of Raman and FTIR bands of the BBO and BBO+10AlF$_3$+2Dy.

Raman peak position (cm-1)	Raman assignments	FTIR peak position (cm^{-1})	FTIR assignments
225, 201	Vibrations of Bi–O bonds in [BiO_3] and [BiO_6]	490, 517	Bi–O bending vibrations in [BiO_6] octahedral units
396, 410	Bi–O–Bi stretching vibrations in [BiO_6] octahedral units	586, 614	Bi–O and Bi–O–Bi stretching vibrations of [BiO_6] octahedral units
569	Bi–O stretching vibrations in [BiO_6] units	688, 698	Bending vibrations of B–O–B in [BO_3] triangles
629, 623	Bending vibrations of B–O–B bridges in metaborate groups of [BO_3] triangular units	900, 897	B–O stretching in BO4units from diborate groups Stretching B–O vibrations in [BO_4] units from diborate groups
957	Vibrational modes occurring in bonds like B–O–B and B–O in pyroborate groups of [BO_3] units	1065, 1061	Stretching of B–O in [BO_4] units from tri, tetra and pentaborate groups
1088, 1095	existence of diborate groups	1189, 1195	BeO stretching vibrations of trigonal [BO_3] units in boroxol rings
1253, 1288	stretching vibrations of B–O bands of non-bridging oxygens (NBO) in borate groups	1303, 1301	B–O stretching vibrations of trigonal [BO_3] units in the boroxol ring
		1395, 1398	B–O stretching vibrations of [BO_3] units in metaborate, pyroborate, and orthoborate groups
		1448, 1454	Antisymmetric stretching vibrations with non-bridging oxygens (NBO) of B–O–B groups

Fig. 5 shows the emission and excitation spectra of the single-doped samples with Eu^{3+} and Dy^{3+}. Moreover, to determine the influence of AlF$_3$ on luminescence intensity, Fig. 5 also shows the spectra of glasses without aluminum fluoride. Particularly, Fig. 5 (a) shows the emission and excitation spectra for samples doped with 2 mol % of Dy^{3+} ions. By detecting at $\lambda_{em} = 574$ nm the excitation spectra show peaks assigned to the transitions of Dy^{3+} ions from the ground energy level, $^6H_{15/2}$, to $^4F_{9/2}$, $^4I_{15/2}$, $^4G_{11/2}$ $^4I_{13/2}$, $^6P_{5/2}$, $^6P_{7/2}$, can be seen at 472, 453, 425, 388, 365, 351 nm [14,40]. After excitation at $\lambda_{ex} = 388$ nm emission spectra shows three bands corresponding to the transitions from the $^7F_{9/2}$ excited state to the $^6H_{15/2}$, $^6H_{13/2}$, and $^6H_{11/2}$ ground states at 481, 574, and 661 nm. On the other hand, Fig. 5 (b) shows the excitation and emission spectra of glass doped with 2 mol % of Eu^{3+} ions. Excitation spectra observed after detection on the most intense emission peak at

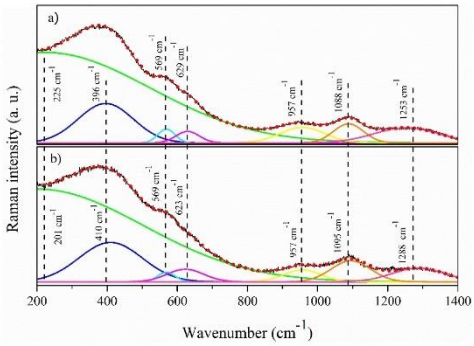

Fig. 4. Raman spectra of BBO (a) and BBO + 10AlF_3 + 2Dy (b) glasses. Experimental data and gaussian components are shown by black and colored solid lines, respectively. The simulated spectrum is shown by red dots.

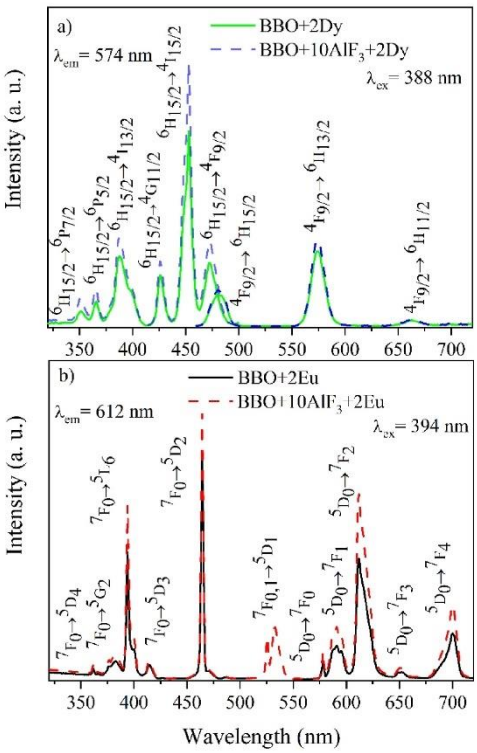

Fig. 5. Excitation and emission spectra of BBO and BBO+10AlF_3 glasses doped with Dy^{3+}(a) and Eu^{3+} (b).

612 nm consist of the several bands associated with the transition from the $^7F_{0,1}$ state to the $^5D_4$, $^5G_4$, $^5L_6$, $^5D_3$, $^5D_2$, and $^5D_1$ at 360, 374, 382, 394, 414, 465, 524, 529 nm, respectively [41,42]. In all glasses, the luminescence intensity is higher for samples doped with 10 mol % aluminum fluoride. These results agree with other studies on AlF_3 doped glasses [43–45]. According to them, the enhancement in the luminescence of rare-earth ions present in glass matrix can be provided by lowering of the non-radiative transitions and promoting the probabilities of radiative transitions [43]. However, it should be remembered that other explanations can be found in the literature, such as thesis, that presence of Al^{3+} ions in glass matrix provides more uniform distribution of RE^{3+} ions [44,46]. Additionally, the excitation and emission spectra of other samples doped with Dy^{3+} ions upon λ_{ex} = 388 nm and λ_{em} = 574 nm, and Eu^{3+} ions at λ_{ex} = 394 nm and λ_{em} = 612 nm are presented in Fig. 6 (a) and 6 (b).

Simultaneous excitation of Eu^{3+}/Dy^{3+} ions was performing using four different wavelengths corresponding to the transitions of Eu^{3+} and Dy^{3+} ions, see Fig. 7(a–d). These figures present the emission spectra for different excitation wavelengths (365, 380, 388, and 394 nm, respectively) of Eu^{3+}/Dy^{3+} codoped samples with different molar ratios. All these wavelengths are placed in the range that InGaN-based LED chips can be excited, so they could be used for SSL technology [26]. In all samples, two characteristic peaks for Dy^{3+} ions can be seen at 483 nm (blue) and 574 nm (yellow), assigned to the $^4F_{9/2}\rightarrow{}^6H_{15/2}$ and $^4F_{9/2}\rightarrow{}^6H_{13/2}$ transitions, respectively [47]. It is already known that the emission properties of RE ions embedded in a glass matrix can be affected by the structure of the host material [9,48]. In this sense, the intensity ratio of the bands in the blue and yellow spectral regions can be used to obtain information about the local symmetry around these RE^{3+} ions. In case of Dy^{3+}, the $^4F_{9/2}\rightarrow{}^6H_{13/2}$ transition is a magnetic dipole transition (MD) that is less sensitive to the crystal field around the optically active ion. The MD transition is prominent when the Dy^{3+} ions are surrounded by a highly symmetric environment with the inversion center. In contrast, the $^4F_{9/2}\rightarrow{}^6H_{13/2}$ emission is hypersensitive forced electric dipole transition (ED) [5]. This transition has a stronger emission when Dy^{3+} ions are in a low-symmetry site without an inversion center [18,22], corresponding to an amorphous glassy environment. In all samples, the band located at 574 nm has stronger emission, indicating that in the proposed borate-bismuth glass matrix, Dy^{3+} ions are located at the low symmetry crystallographic sites, without an inversion center. Furthermore, the intensity of the ED and MD bands of Dy^{3+} ions changes with the concentration of Dy^{3+} ions and with the excitation wavelength.

After excitation at 394 nm, corresponding to the $^7F_0\rightarrow{}^5L_6$ transition of Eu^{3+} ions, the emission of Dy^{3+} ions is very weak, and the luminescence of Eu^{3+} ions dominates the spectrum. This changes when the glasses are excited with one of the wavelengths associated with the Dy^{3+} ions transitions (365 nm, 388 nm). In these cases, the emission peaks associated with the Dy^{3+} ions dominate the spectrum. Nevertheless, the relation of bands intensity at 483 nm and 574 nm is still the same in all cases. A closer look at the behavior of the transitions connected with the Eu^{3+} ions suggests that the Eu^{3+} ions are in a low-symmetry sites. Similarly, to Dy^{3+} ions, Eu^{3+} ions have two emission peaks at 590 nm and 612 nm which ratio can bring information about the local symmetry around them. The first one, is related to the magnetic dipole (MD) transition from the $^5D_{0,1}$ excited levels to the $^7F_1$ ground state, while the band at 612 nm is an electric dipole (ED) transition [49]. As in the case of Dy^{3+} ions, the ED transition has a stronger emission, indicating that the optically active ions are located in the non-inversion environment.

The color emitted by the glasses doped with Eu^{3+}/Dy^{3+} ions can be described by the x and y chromaticity coordinates and presented in the form of CIE diagrams. The CIE chromaticity coordinates of glasses excited at λ_{ex} = 365 nm is presented in Fig. 8. The detailed corresponding chromaticity parameters (x,y) and color temperature CCT values calculated according to equation (1) are shown in Table 6 [50].

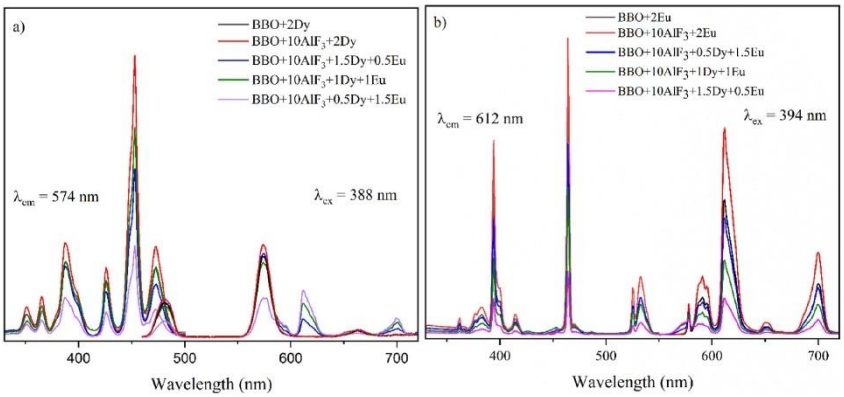

Fig. 6. Excitation and emission spectra of BBO glasses doped with Dy^{3+} (a) and Eu^{3+} ions (b).

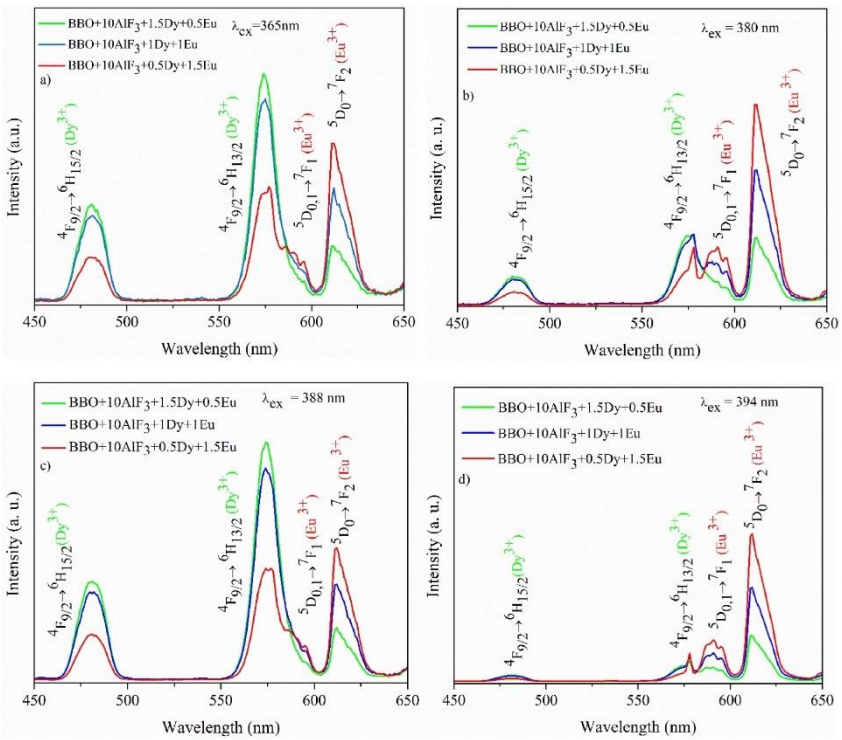

Fig. 7. Emission spectra of glass samples doubly doped with Eu^{3+}/Dy^{3-} under a) λ_{ex} = 365 nm, b) λ_{ex} = 380 nm, c) λ_{ex} = 388 nm, d) λ_{ex} = 394 nm.

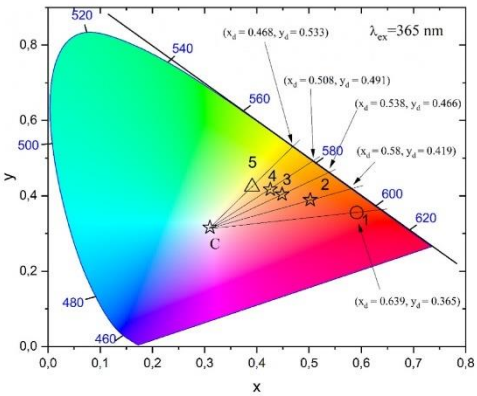

Fig. 8. Chromaticity coordinates in CIE1931 diagram of overall emissions from the BBO+10AlF$_3$+2Dy (1), BBO+10AlF3:Ln3 (2), BBO+10AlF$_3$:Ln2 (3), BBO+10AlF$_3$:Ln1 (4), BBO+10AlF$_3$+2Dy (5) glasses excited at λ_{ex} = 365 nm. Additionally, straight lines connecting the phosphor and C illuminant point(s) are shown with x_d, y_d coordinates for each sample.

$$CCT = -449n^3 + 3525n^2 - 6823n + 5520.33 \quad (2)$$

Where $n = (x-x_c)/(y-y_c)$ with $x_c = 0.332$ and $y_c = 0.186$.

For glass doped only with Eu^{3+} ions (black circle) excited at λ_{ex} = 394 nm, the emitted color is red. With the addition of Dy^{3+} ions, emission shifts from reddish-orange to yellowish-orange for the BBO+10AlF$_3$+2Dy glass sample (black triangle). The corresponding color temperature varies from 1932K (BBO+10AlF$_3$+2Eu) to 3352 and 4032 for BBO+10AlF$_3$+1.5Dy+0.5Eu and BBO+10AlF$_3$+2Dy, respectively. For BBO+10AlF$_3$+2Dy and BBO+10AlF$_3$+1.5Dy+0.5Eu samples emission close to daylight was obtained. It can be clearly seen that the emission color can be tuned by varying the molar ratios of the Eu^{3+}/Dy^{3+}ions and by changing the excitation wavelength. The tendency to shift toward yellowish–orange emission of samples doped with high values of Dy^{3+}ions is consistent with the luminescence analysis and can be explained by the fact that the Dy^{3+} ions mainly occupy the non-inversion symmetry sites. This promotes stronger emission at the 574 nm (yellow) band instead of 488 (blue) nm. As mentioned earlier, Eu^{3+} ions are also incorporated into non-inversion symmetry sites, which has a strong influence on the overall reddish-orange emission of the samples [24].

Additionally, the color purity (CP) compared to the CIE1931 standard source C (x_i = 0.3101, y_i = 0.3162) coordinates were calculated from the weighted average of the sample emission color coordinates (x, y) relative to the illuminant coordinates (x_i, y_i) and the dominant wavelength coordinates (x_d, y_d) relative to (x_i, y_i) coordinates, according to the equation [52]:

$$CP = \frac{\sqrt{(x - x_i)^2 + (y - y_i)^2}}{\sqrt{(x_d - x_i)^2 + (y_d - y_i)^2}} \times 100\% \quad (3)$$

with the dominant wavelength (λ_d) defined as a monochromatic wavelength of the spectrum, which coordinates are placed on the straight line connecting the phosphor with the C point. For BBO+10AlF$_3$+2Dy sample with the dominant wavelength at 573 nm and 50.25 % color purity, BBO+10AlF$_3$:Ln1 glass, due to a significant 580 nm yellowish orange color purity of 58.17 %. Next, close to orange light emission in BBO+10AlF$_3$:Ln2 glass considering a 585 nm close to orange light dominant emission with color purity 62.25 % and orange light in BBO+10AlF$_3$:Ln3 glass sample, due to the 591 nm color purity of 71.05 %. The BBO+10AlF$_3$+2Eu sample with the high red light emission at 606 nm color purity of 85.77 %.

3.2.2. Energy transfer in doped Eu^{3+}/Dy^{3+} glasses

The possibility of energy transfer between rare-earth ions has been investigated in the BBO+10AlF$_3$+Eu, BBO+10AlF$_3$+Dy, and BBO+10AlF$_3$+Eu + Dy glass samples. The main condition under which this phenomenon can be present is the overlap of the absorption spectra of Eu^{3+} acting as acceptor and donor fluorescence (Dy^{3+}) [14,53]. In the case of the studied glasses, a partial overlap of the spectra in the range of 450–470 nm is observed (Fig. 9). The $^7F_0 \rightarrow {}^5D_2$ absorption band of Eu^{3+} ions at 464 nm overlapped with the $^4F_{9/2} \rightarrow {}^6H_{15/2}$ (484 nm) of Dy^{3+} ions Thus, this can indicate that energy transfer may occur from Dy^{3+} ions to Eu^{3+} ions in borate bismuth glasses [54].

Fig. 10 a shows the emission spectra of Eu^{3+}/Dy^{3+} codoped glass

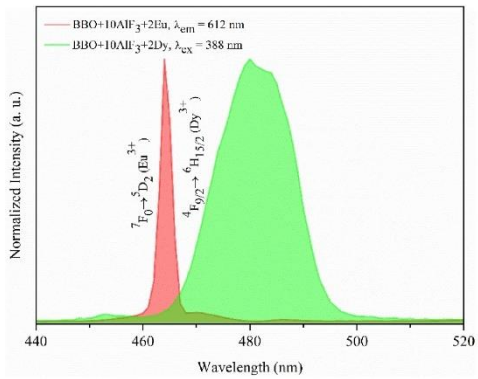

Fig. 9. Partially overlap of the emission spectrum of BBO+10AlF$_3$+2Dy at λ_{ex} = 388 nm and the excitation spectrum of BBO+10AlF$_3$+2Eu at λ_{em} = 612 nm.

Table 6
CIE1931 color coordinates (x, y), correlated color temperature (CCT), dominant wavelength (λ_d), dominant wavelength coordinates (x_d, y_d) and color purity (CP) for λ_{ex} = 365 nm excitation of prepared samples and examples for other glasses doped with rare earth ions.

Sample	(x, y)	CCT(K)	λ_d (nm)	(x_d, y_d)	CP (%)
BBO+10AlF$_3$+2Dy	(0.391, 0.424)	4050	573	(0.468, 0.533)	50.25 %
BBO+10AlF$_3$:Ln1	(0.426, 0.417)	3294	579	(0.508, 0.491)	58.17 %
BBO+10AlF3:Ln2	(0.449, 0.404)	2806	585	(0.538, 0.466)	60.25 %
BBO+10AlF$_3$:Ln3	(0.502, 0.389)	2015	591	(0.58, 0.419)	71.05 %
BBO+10AlF$_3$+2Eu	(0.591, 0.356)	1875	606	(0.639, 0.365)	85.77 %
Standard white	(0.31, 0.336)	5455 [51]			
CdO-GeO$_2$-TeO$_2$: Dy^{3+}/Eu^{3+} glass	(0.382, 0.407)	4153 [23]			
Y_2O_3–Al_2O_3–Bi_2O_3–B_2O_3–SiO_2: Dy^{3+}/Eu^{3+} glass	(0.332, 0.342)	5520 [4]			

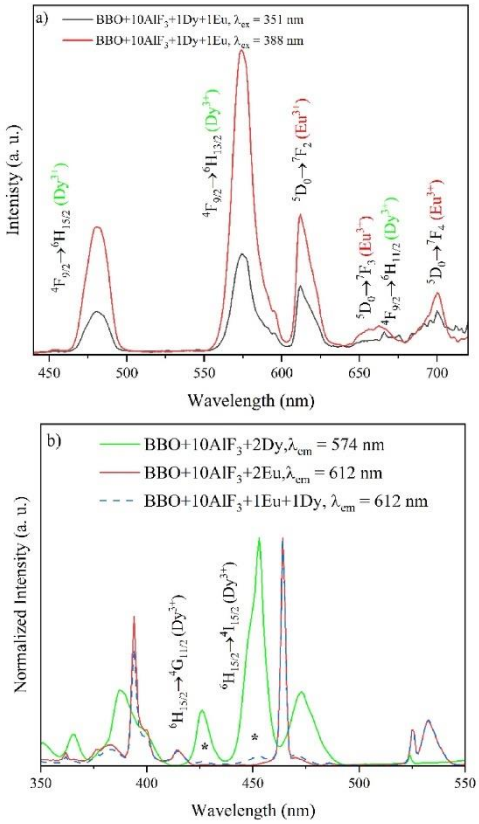

Fig. 10. (a) Emission spectra of Eu^{3+}/Dy^{3+} codoped glass upon 351 nm and 388 nm excitation, (b) excitation spectra of BBO+10AlF$_3$+2Eu and BBO-+10AlF$_3$+1Dy+1Eu glasses monitored at λ_{em} = 612 nm and BBO+10AlF$_3$+2Dy monitored at λ_{em} = 574 nm.

upon 351 nm and 388 nm excitation, corresponding to Dy^{3+} ions, where the Eu^{3+} ions should not be excited [55]. However, the emission spectra, apart from the bands characteristic for Dy^{3+} ions, also reveal the europium $^5D_0 \rightarrow {}^7F_2$ and $^5D_0 \rightarrow {}^7F_4$ transitions. Thus means that Eu^{3+} ions are sensitized by Dy^{3+} ions [55]. In Fig. 10 b, the excitation spectrum of the glass doped with Dy^{3+} ions monitored at the $^4F_{9/2} \rightarrow {}^6H_{13/2}$ transition (Dy^{3+}), shows bands that can be assigned only to the transitions of Dy^{3+} ions. In the same way, the spectrum of the sample singly doped with Eu^{3+} ions monitored at 612 nm ($^5D_0 \rightarrow {}^7F_2$) contains only peaks originating from transitions of Eu^{3+} ions. However, the spectrum of Eu^{3+} and Dy^{3+} codoped glass (BBO+10AlF$_3$+1Dy+1Eu) monitored at the $^5D_0 \rightarrow {}^7F_2$ Eu^{3+} transition reveals additional bands that are observed in the Dy^{3+} single doped glass monitored at 574 nm. Therefore, the excitation upon 351 nm through Dy^{3+} ions (Fig. 10a) and the presence of Dy^{3+} bands in Dy^{3+}/Eu^{3+} excitation spectrum at 612 nm suggest that the energy transfer from Dy^{3+} to Eu^{3+} ions occurs. This can be supported by the spectral overlap of the Eu^{3+} absorption band and Dy^{3+} emission band seen in Fig. 9.

This behavior suggested that the energy transfer from Dy^{3+} to Eu^{3+} ions occurs and the excitation of Dy^{3+} ions can contribute to the emission spectrum of the codoped glasses. Fig. 11 presents energy level diagram of Eu^{3+} and Dy^{3+} ions and possible energy transfer mechanism between both ions in the codoped glasses. This energy transfer mechanism can be described as follows:

$$^7F_0\ (Eu^{3+}) + {}^4F_{9/2}\ (Dy^{3+}) \rightarrow {}^5D_2\ (Eu^{3+}) + {}^6H_{15/2}\ (Dy^{3+})\ (1)$$

Concretely, after excitation at 388 nm Dy^{3+} ions are excited from the $^6F_{15/2}$ ground state to the $^4I_{13/2}$ excited state and then relaxed non-radiatively to the $^4F_{9/2}$ level. From this level, the glass shows radiatively emissions to the $^6H_{15/2}$ (480 nm), $^6H_{13/2}$ (574 nm) and $^6H_{11/2}$ (662 nm). Additionally, part of the energy can be transferred non-radiatively from $^4F_{9/2}$ energy level of Dy^{3+} to the $^5D_2$ excited level of Eu^{3+}. Then the excited Eu^{3+} ions relaxed non-radiatively to the $^5D_0$ and next by radiative transitions to the $^5D_0$, $^7F_1$, $^7F_2$, $^7F_3$, and $^7F_4$ occur.

3.2.3. Time resolved luminescence

To get better insight into the luminescence properties of Eu^{3+} and Dy^{3+} doped glasses, luminescence decay curves were measured (Fig. 12). The obtained decay curves can be described as two-exponential decays, by the following equation [54]:

$$I\ (t) = A_1 \exp\ (-t/\tau_1) + A_1 \exp\ (-t/\tau_2) \quad (4)$$

Where A_1 and A_2 are the amplitudes of the two decay components, τ_1, and τ_2 are the short and long luminescence lifetimes, respectively. The τ_1 is attributed to the rare-earth ions placed in low symmetry environment, while the τ_2 is a component related to the RE^{3+} in higher symmetry crystal field. Both, τ_1 and τ_2 are components of the average lifetime $<\tau_{avg}>$, which was calculated using equation (3) [24]. The calculated values can be seen in Table 7.

$$\tau_{-}(<\mathrm{avg}>) = \left(A_{-}()\ 1\tau_1^2 + A2\tau_2^2\right) \ / \ \left(A_{-}(1)\ \tau_{-}(1) + A_{-}(1)\ \tau_{-}(1)\right) \quad (5)$$

The average lifetimes of the Dy^{3+}: $^4F_{9/2} \rightarrow {}^6H_{13/2}$ transition were found to be strongly related to the concentration of Eu^{3+} and Dy^{3+} ions. The lifetimes of dysprosium increase with decreasing Dy^{3+} content from 420 μs for BBO+10AlF$_3$+1.5Eu+0.5Dy sample to 320 μs for BBO+10AlF$_3$+0.5Eu+1.5Dy. This agrees with other previous studies [14,24]. The highest value is obtained for glass doped with 1.5 % of europium. This indicates that the lifetimes of Dy^{3+} increase with increasing europium content, which may be evidence of $Eu^{3+} \rightarrow Dy^{3+}$ energy transfer occurrence in the borate-bismuth glass system [26]. Additionally, to determine the influence of AlF$_3$ addition, lifetime measurements of single doped glasses were conducted. The BBO+2Eu and BBO+10AlF$_3$+2Eu glasses were excited at λ_{exc} = 394 nm and observed around 612 nm (Fig. 12 b). The sample BBO+2Dy and BBO+10AlF$_3$+2Dy were monitored at 388 m excitation wavelength and observed at around 574 nm (Fig. 12 b). Single exponential decay was observed in Eu^{3+} doped glasses and two exponential decay was observed in glasses doped with Dy^{3+} ions. Similar behavior was observed by T. Lewandowski et al. [13]. This behavior can be explained by the fact, that decay times of Dy^{3+} ions in glass matrix is strongly related to the Dy^{3+} ions concentration. It was found that in glasses with higher Dy^{3+} concentration the double-exponential decay was observed [4,18,56–58].

The calculated parameters are presented in Table 8. In the case of glasses doped with Eu^{3+} the decay times did not differ much from each other. However, in Dy^{3+} doped samples the 40 μs increase can be seen, due to the addition of AlF$_3$.

4. Conclusions

The B_2O_3–Bi_2O_3 glass system doped with AlF$_3$ and Eu^{3+}/Dy^{3+} ions in different molar ratios was successfully synthesized using a conventional melt quenching technique. Rare earth ions present in the studied glasses are placed mostly in low-symmetry crystallographic sites, without an inversion center. Color-tunable emission was achieved due to the

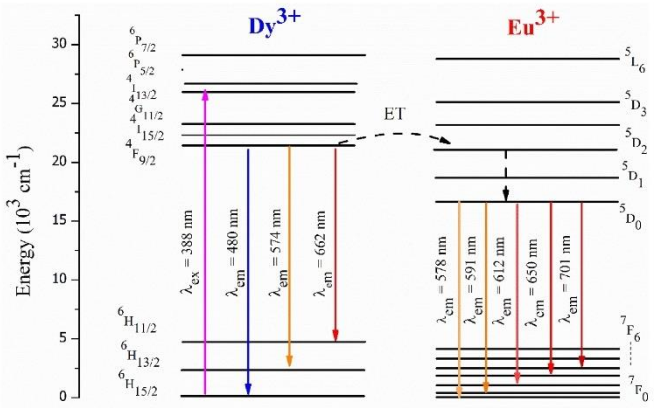

Fig. 11. Energy levels of Eu^{3+} and Dy^{3+} ions.

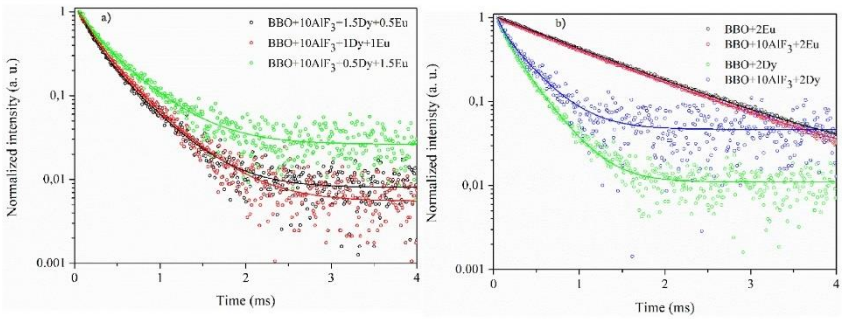

Fig. 12. The luminescence decay times for (a) double and single (b) BBO glasses doped with Eu^{3+}/Dy^{3+} ions.

Table 7
Calculated parameters of luminescence decays of glasses doped with Eu^{3+}/Dy^{3-} at $\lambda_{ex} = 388$ nm and observation at $\lambda_{em} = 574$ nm.

Sample	τ_1 (μs)	τ_2 (μs)	$<\tau_{avg}>$ (μs)
BBO+10AlF3+1.5Eu+0.5 Dy	130	470	420
BBO+10AlF3+1Eu−1Dy	180	450	350
BBO+10AlF3+0.5Eu+1.5 Dy	150	410	320
BBO+10AlF3+2Dy	60	330	300

Table 8
Calculated parameters of luminescence decays of glasses doped with Eu^{3-}/Dy^{3+}.

	τ_1 (μs)	τ_2 (μs)	τ_{avg} (μs)
$\lambda_{ex} = 394$ nm, $\lambda_{obs} = 612$ nm,			
BBO+2Eu	1120		
BBO+10AlF$_3$+2Eu	1110		
$\lambda_{ex} = 388$ nm, $\lambda_{obs} = 574$ nm,			
BBO+2Dy	80	290	260
BBO+10AlF$_3$+2Dy	60	330	300

different ratios of Eu^{3+}/Dy^{3+} addition. Glasses singly doped with Eu^{3+} under excitation at 394 nm emitted a reddish-orange color. The addition of dysprosium ions changes the emitted color to a warm yellowish-orange color, close to daylight. Luminescence results indicated that the energy transfer from Dy^{3-} to Eu^{3+} ions occurs in the proposed glass system. However, the decay times of the luminescence measurements indicate that the back transfer from Eu^{3+} to Dy^{3+} may also be present in glass samples. Moreover, the addition of AlF_3 has a strong influence on the luminescence properties of Eu^{3+}/Dy^{3-} doped glasses. Samples doped with 10 mol % of aluminum fluoride are characterized by luminescence enhancement in comparison to undoped ones. Additionally, all prepared samples were transparent, making them appropriate materials for optical applications. It can be concluded that synthesized borate-bismuth glasses doped with AlF_3 and Eu^{3+}/Dy^{3+} can be used as phosphors for solid-state lighting devices.

Author contributions

Dušan Galusek: Resources. José J. Velázquez: Conceptualization, Investigation, Writing – review & editing. Michal Žitňan: Data curation, Investigation, Writing – review & editing. Michał Maciejewski: Data curation, Investigation. Wojciech Sadowski: Resources, Supervision. Barbara Kościelska: Conceptualization, Supervision, Validation, Writing

– review & editing. Karolina Milewska: Conceptualization, Data curation, Formal analysis, Investigation, Methodology, Project administration, Validation, Visualization, Writing – original draft

Declaration of competing interest

The authors declare that they have no known competing financial interests or personal relationships that could have appeared to influence the work reported in this paper.

Data availability

I have shared the link to data

Acknowledgements

This paper is a part of the dissemination activities of project "FunGlass" (Centre for Functional and Surface Functionalized Glass). This project has received funding from the European Union's Horizon 2020 research and innovation programme under grant agreement no. 739566. The authors also gratefully acknowledge the financial support from the Slovak Grant Agency of the Ministry of Education, Science, Research and Sport, VEGA No 1/0844/21.

References

[1] X. Zhang, Q. Tan, S. Hu, J. Yang, Hydrothermal synthesis of $ScVO_4$:Ln^{3+} (Ln = Eu, Dy, Eu/Dy) microcrystals with controllable morphology, energy transfer and multicolor luminescence, Mater. Chem. Phys. 215 (2018) 259–268, https://doi.org/10.1016/j.matchemphys.2018.05.030.

[2] P.P. Pawar, S.R. Munishwar, S. Gautam, R.S. Gedam, Physical, thermal, structural and optical properties of Dy^{3+} doped lithium alumino-borate glasses for bright W-LED, J. Lumin. 183 (2017) 79–88, https://doi.org/10.1016/j.jlumin.2016.11.027.

[3] J. Dahiyaa, A. Hoodaa, A. Agarwalb, S. Khasa, Tuneable colour flexibility in Dy^{3+}&Eu^{3+}co-doped lithium fluoride bismuth borate glass system for solid state lighting applications, J. Non Cryst. Solids 576 (2022) 121237, https://doi.org/10.1016/j.jnoncrysol.2021.121237.

[4] D.V. Krishna Reddy, T. Sambasiva Rao, Sk Taherunnisa, A. Suchocki, Y. Zhydachevskyy, M. Piaseckic, M. Rami Reddya, Tunable white light by varying excitations in yttrium alumino bismuth borosilicate glasses co-doped with Dy^{3+}-Eu^{3+} for cool WLED applications, J. Non-Cryst. Solids 513 (2019) 167–182, https://doi.org/10.1016/j.jnoncrysol.2019.03.011.

[5] J. An, S. Zhang, R. Liu, G. Hu, Z. Zhang, Y. Qiu, Y. Zhou, F. Zeng, Z. Su, Luminescent properties of Dy^{3+}/Eu^{3+} doped fluorescent glass for white LED based on oxyfluoride matrix, J. Rare Earths 39 (2021) 26–32, https://doi.org/10.1016/j.jre.2020.01.013.

[6] J. Yanga, I. Sohn, Compositional dependence of thermophysical properties in binary alkaline earth borate melts: insights from structure in short range and intermediate range order, J. Mater. Sci. Technol. 131 (2022) 195–203, https://doi.org/10.1016/j.jmst.2022.05.037.

[7] A. Jha, B. Richards, G. Jose, T. Teddy-Fernandez, P. Joshi, X. Jiang, Rare-earth ion doped TeO_2 and GeO_2 glasses as laser materials, Prog. Mater. Sci. 57 (2012) 1426–1491, https://doi.org/10.1016/j.pmatsci.2012.04.003.

[8] G. Lakshminarayana, H. Yang, J. Qiu, White light emission from Tm^{3+}/Dy^{3+} co-doped oxyfluoride germanate glasses under UV light excitation, J. Solid State Chem. 182 (2009) 669–676, https://doi.org/10.1016/j.jssc.2008.11.020.

[9] J. Sun, X. Zhang, Z. Xia, H. Du, Synthesis and luminescence properties of novel $LiSrPO_4$:Dy^{3+} phosphor, Mater. Res. Bull. 46 (2011) 2179–2182, https://doi.org/10.1016/j.materresbull.2011.07.033.

[10] Ch Zhu, Y. Yang, X. Liang, S. Yuan, G. Chen, Rare earth ions doped full-color luminescence glasses for white LED, J. Lumin. 126 (2007) 707–710, https://doi.org/10.1016/j.jlumin.2006.10.028.

[11] G. Zissis, Energy consumption and environmental and economic impact of lighting: the current situation, in: R. Karlicek, C.C. Sun, G. Zissis, R. Ma (Eds.), Handbook of Advanced Lighting Technology, Springer, Cham, 2016, https://doi.org/10.1007/978-3-319-00295-8_40-1.

[12] E. Erol, N. Vahedigharehchopogh, O. Kibrisli, M.C. Ersundu, A.E. Ersundu, Recent progress in lanthanide-dopedluminescent glasses for solid-state lighting applications—a review, J. Phys. Condens. Matter 33 (2021) 483001, https://doi.org/10.1088/1361-648X/ac22d9.

[13] T. Lewandowskia, C. Seweryński, M. Walasa, M. Łapiński, A. Synak, W. Sadowski, B. Kościelska, Structural and luminescent study of TeO_2-BaO-Bi_2O_3-Ag glass systemdoped with Eu^{3+} and Dy^{3+} for possible color-tunable phosphor, Opt. Mater. 79 (2018) 390–396, https://doi.org/10.1016/j.optmat.2018.03.031.

[14] D. Rajesh, K. Brahmachary, Y.C. Ratnakaram, N. Kiran, A.P. Baker, G.G. Wang, Energy transfer based emission analysis of Dy^{3+}/Eu^{3+} co-doped ZANP glasses for white LED applications, J. Alloys Compd. 646 (2015) 1096–1103, https://doi.org/10.1016/j.jallcom.2015.05.138.

[15] L.A. Diaz-Torres, E. De la Rosa, P. Salas, V.H. Romero, C. Angeles-Chavez, Efficient photoluminescence of Dy^{3+} at low concentrations in nanocrystalline ZrO_2, J. Solid State Chem. 181 (2008) 75–80, https://doi.org/10.1016/j.jssc.2007.09.033.

[16] G. Blasse, B.C. Grabmaier, Luminescent Materials, Springer, Berlin Heidelberg, 1994.

[17] M. Fhoula, T. Koubaa, M. Dammak, White photoluminescence and energy transfer properties of Dysprosium and Europium singly and codoped $Na_2ZnP_2O_7$ phosphors Optics and Laser Technology, 130, 2020, https://doi.org/10.1016/j.optlastec.2020.106352.

[18] K. Griebenow, M. Phuong-Truong, F. Munoz, R. Klement, D. Galusek, Tuning the fluorescence of Dy^{3+} via the structure of borophosphate glasses, Sci. Rep. (2023), https://doi.org/10.1038/s41598-023-28941-1.

[19] K. Griebenow, F. Munoz, N.S. Tagiara, R. Klement, A. Prnova, B. Wolfrum, E. I. Kamitsos, A. Duran, D. Galusek, Structure and fluorescence properties of Dy-doped alkaline earth borophosphate glasses, Int. J. Appl. Glass Sci. 12 (2021) 472–484, https://doi.org/10.1111/ijag.16105.

[20] G. Ramakrishna, R. Naik, H. Nagabhushana, R.B. Basavaraj, S.C. Prashantha, S. C. Sharma, K.S. Anantharaju, White light emission and energy transfer (Dy^{3+}→Eu^{3+}) in combustion synthesized YSO:Dy^{3+},Eu^{3+} nanophosphors, Optik 127 (2016) 2939–2945, https://doi.org/10.1016/j.ijleo.2015.11.234.

[21] M. Kemere, U. Rogulis, J. Sperga, Luminescence and energy transfer in Dy^{3+}/Eu^{3+} co doped aluminosilicate oxyfluoride glasses and glass ceramics, J. Alloys Compd. 735 (2018) 1253–1261, https://doi.org/10.1016/j.jallcom.2017.11.077.

[22] P. Du, J.S. Yu, Energy transfer mechanism and color controllable luminescence in Dy^{3+}/Eu^{3+}-codoped $NaLa(MoO_4)_2$ phosphors, J. Alloys Compd. 653 (2015) 468–473, https://doi.org/10.1016/j.jallcom.2015.08.256.

[23] D.A. Rodríguez-Carvajal, A.N. Meza Rocha, U. Caldiño, R. Lozada Morales, E. Alvarez, MaE. Zayas, Reddish orange, neutral and warm white emissions in Eu^{3+}, Dy^{3+} and Dy^{3+}/Eu^{3+} doped CdO-GeO2-TeO_2 glasses, Solid State Sci. 61 (2016) 70–76, https://doi.org/10.1016/j.solidstatesciences.2016.09.009.

[24] M. Walas, M. Lisowska, T. Lewandowskia, A.I. Becerro, M. Łapinski, A. Synak, W. Sadowski, B. Koscielsk, From structure to luminescence investigation of oxyfluoride transparent glasses and glass ceramics doped with Eu^{3+}/Dy^{3+} ions, J. Alloys Compd. 805 (2019) 1410–1418, https://doi.org/10.1016/j.jallcom.2019.07.017.

[25] S. Mukamil, C. Sarumaha, S.M. Wabaidur, M.A. Islam, S.A. Khattak, S. Kothan, M. Shoaib, I. Khan, I. Ullah, J. Kaewkhao, G. Rooh, Investigation of color tunability of Dy^{3+} & Eu^{3+} Co-doped bismuth borate glasses for lighting applications, Mater. Chem. Phys. 288 (2022) 126422, https://doi.org/10.1016/j.matchemphys.2022.126422.

[26] A.N. Meza Rocha, A. Speghini, M. Bettinelli, U. Caldiñ, White light generation through $Zn(PO_3)_2$ glass activated with Eu^{3+} and Dy^{3+}, J. Lumin. 176 (2016) 235–239, https://doi.org/10.1016/j.jlumin.2016.03.035.

[27] Y. Yang, Y. Liu, P. Cai, R. Maalej, H.J. Seo, Thermal stability and spectroscopic properties of Ho3+ doped tellurite-borate glasses, J. Rare Earths 33 (2015) 939–945, https://doi.org/10.1016/S1002-0721(14)60509-3.

[28] M. Saad, M. Poulain, Glass forming ability criterion, Proceedings of the Materials Science Forum 19–20 (1987) 11–18, https://doi.org/10.4028/www.scientific.net/msf.19-20.11.

[29] E.R. Shaaban, M. Shapaan, Y.B. Saddeek, Structural and thermal stability criteria of Bi2O3-B2O3 glasses, J. Phys. Condens. Matter 20 (2008) 155108, https://doi.org/10.1088/0953-8984/20/15/155108.

[30] N. Mary, M. Rebours, E. Castel, S. Vaishnav, W. Deng, A.M.T. Bell, F. Clegg, B. L. Allsopp, A. Scrimshire, P.A. Bingham, Enhanced thermal stability of highbismuth borate glasses by addition of iron, J. Non Cryst. Solids 500 (2018) 149–157, https://doi.org/10.1016/j.jnoncrysol.2018.07.061.

[31] K. Milewska, M. Maciejewski, M. Łapiński, A. Synak, M. Behrendt, W. Sadowski, B. Kościelska, Structural and luminescence properties of B_2O_3-Bi_2O_3-AlF_3 glass doped with Eu^{3+}, Tb^{3+} and Tm^{3+} ions, J. Non-Cryst. Solids 605 (2023) 122169, https://doi.org/10.1016/j.jnoncrysol.2023.122169.

[32] S. Thakur, V. Thakur, A. Kaur, L. Singh, Structural, optical and thermal properties of nickel doped bismuth borate glasses, J. Non-Cryst. Solids 512 (2019) 60–67, https://doi.org/10.1016/j.jnoncrysol.2019.02.012.

[33] L. Singh, V. Thakur, R. Punia, R.S. Kundu, A. Singh, Structural and optical properties of barium titanate modified bismuth borate glasses, Solid State Sci. 37 (2014) 64–71, https://doi.org/10.1016/j.solidstatesciences.2014.08.010.

[34] V. Thakur, et al., Effect of $BaTiO_3$ on the structural and optical properties of lithium borate glasses, Ceram. Int. 41 (2015) 10957–10965, https://doi.org/10.1016/j.ceramint.2015.05.039.

[35] M. Veeramohan Rao, V.V. Ravi Kanth Kumar, Nk Shihab, D. Narayana Rao, Z-Scan studies of barium bismuth borate glasses, Opt. Mater. 84 (2018) 178–183, https://doi.org/10.1016/j.optmat.2018.06.066.

[36] K. Chandra Sekhar, B. Kavitha, N. Narsimlu, V. Sathe, M.A. Alothman, I. O. Olarinoye, M.S. Al-Buriahi, Md Shareefuddin, Enhancement of shielding ability using PbF_2 in Fe reinforced bismuth borate glasses, J. Mater. Sci. Mater. Electron. 32 (2021) 23047–23065, https://doi.org/10.1007/s10854-021-06788-4.

[37] D. Rajesh, Y.C. Ratnakaram, M. Seshadri, A. Balakrishna, T. Satya Krishna, Structural and luminescence properties of Dy^{3+} ion in strontium lithium bismuth borate glasses, J. Lumin. 132 (2012) 841–849, https://doi.org/10.1016/j.jlumin.2011.08.050.

[38] V. Thakur, et al., Effect of $BaTiO_3$ on the structural and optical properties of lithium borate glasses, Ceram. Int. 41 (2015) 10957–10965, https://doi.org/10.1016/j.ceramint.2015.05.039.

[39] B. Karthikeyan, C.S. Suchand Sandeep, J. Cha, H. Takebe, R. Philip, S. Mohan, Optical properties and ultrafast optical nonlinearity of Yb^{3+} doped sodium borate

and bismuthate glasses, J. Appl. Phys. 103 (2008) 103509, https://doi.org/10.1063/1.2931029.
[40] S. Tanabe, J. Kang, T. Hanada, N. Soga, Yellow/blue luminescences of Dy^{3+}-doped borate glasses and their anomalous temperature variations, J. Non-Cryst. Solids 239 (1998) 170–175, https://doi.org/10.1016/S0022-3093(98)00734-0.
[41] N. Deopa, M.K. Sahu, P.R. Ranic, R. Punia, A.S. Rao, Realization of warm white light and energy transfer studies of Dy^{3+}/Eu^{3+} co-doped Li_2O-PbO-Al_2O_3-B_2O_3 glasses for lighting applications, J. Lumin. 222 (2020) 117166, https://doi.org/10.1016/j.jlumin.2020.117166.
[42] K. Anilkumar, S. Damodaraiah, S. Babu, V. Reddy Prasad, Y.C. Ratnakaram, Emission spectra and energy transfer studies in Dy^{3+} and Dy^{3+}/Eu^{3+} co-doped potassium fluorophosphate glasses for white light applications, J. Lumin. 205 (2019) 190–196, https://doi.org/10.1016/j.jlumin.2018.09.007.
[43] A.J. Silversmith, A.P. Beyler, K.E. Arpino, D.M. Boye, K.R. Hoffman, Mechanisms of fluorescence enhancement in rare earth sol–gel glass containing Al^{3+}, J. Lumin. 131 (2011) 457–460, https://doi.org/10.1016/j.jlumin.2010.11.018.
[44] S. Rai, A.L. Fanai, Optical properties of Ho^{3+} in sol-gel silica glass co-doped with Aluminium, J. Non-Cryst. Solids 449 (2016) 113–118, https://doi.org/10.1016/j.jnoncrysol.2016.07.023.
[45] A. Monteil, S. Chaussedent, G. Alombert-Goget, N. Gaumer, J. Obriot, S.J. L. Ribeiro, Y. Messaddeq, A. Chiasera, M. Ferrari, Clustering of rare earth in glasses, aluminum effect: experiments and modeling, J. Non-Cryst. Solids 348 (2004) 44–50, https://doi.org/10.1016/j.jnoncrysol.2004.08.124.
[46] M.J. Lochhead, K.L. Bray, Rare-earth clustering and aluminum codoping in sol—gel silica: investigation using Europium (III) fluorescence spectroscopy, Chem. Mater. 7 (1995) 572, https://doi.org/10.1021/cm00051a019.
[47] M. Fhoula, T. Koubaa, M. Dammak, White photoluminescence and energy transfer properties of Dysprosium and Europium singly and codoped $Na_2ZnP_2O_7$ phosphors, Opt. Laser Technol. 130 (2020) 106352, https://doi.org/10.1016/j.optlastec.2020.106352.
[48] K. Milewska, M. Maciejewski, A. Synak, M. Łapiński, A. Mielewczyk-Gryń, W. Sadowski, B. Kościelska, From structure to luminescent properties of B_2O_3-Bi_2O_3-SrF_2 glass and glass-ceramics doped with Eu^{3+} ions, Materials 14 (2021) 4490, https://doi.org/10.3390/ma14164490.
[49] F. Kang, Y. Hu, H. Wu, G. Ju, Z. Mu, N. Li, Luminescence investigation of Eu^{3+}-Bi^{3+} co-doped $CaMoO_4$ phosphor, J. Rare Earths 29 (2011) 837–842, https://doi.org/10.1016/S1002-0721(10)60552-2.
[50] C.S. McCamy, Correlated color temperature as an explicit function of chromaticity coordinates, Color Res. Appl. 17 (1992) 142, https://doi.org/10.1002/col.5080170211.
[51] L. Mishra, A. Sharma, A.K. Vishwakarma, K. Jha, M. Jayasimhadri, B.V. Ratnam, K. Jang, A.S. Rao, R.K. Sinha, White light emission and color tunability of dysprosium doped barium silicate glasses, J. Lumin. 169 (2016) 121–127, https://doi.org/10.1016/j.jlumin.2015.08.063.
[52] A.N. Meza-Rocha, I. Camarillo, R. Lozada-Morales, U. Caldiño, Reddish-orange and neutral/warm white light emitting phosphors: Eu^{3+}, Dy^{3+} and Dy^{3+}/Eu^{3+} in potassium-zinc phosphate glasses, J. Lumin. 183 (2017) 341–347, https://doi.org/10.1016/j.jlumin.2016.11.068.
[53] J. Wan, L. Cheng, J. Sun, H. Zhong, X. Li, W. Lu, Y. Tian, H. Lin, B. Chen, Energy transfer and colorimetric properties of Eu^{3+}/Dy^{3+} co-doped $Gd_2(MoO_4)_3$ phosphors, J. Alloys Compd. 496 (2010) 331–334, https://doi.org/10.1016/j.jallcom.2010.02.006.
[54] Ch Yu, Z. Yang, A. Huang, Z. Chai, J. Qiu, Z. Song, D. Zhou, Photoluminescence properties of tellurite glasses doped Dy^{3+} and Eu^{3+} for the UV and blue converted WLEDs, J. Non-Cryst. Solids 457 (2017) 1–8, https://doi.org/10.1016/j.jnoncrysol.2016.11.025.
[55] U. Caldiño, A. Lira, A.N. Meza-Rocha, I. Camarillo, R. Lozada-Morales, Development of sodium-zinc phosphate glasses doped with Dy^{3+}, Eu^{3+} and Dy^{3+}/Eu^{3+} for yellow laser medium, reddish-orange and white phosphor applications, J. Lumin. 194 (2018) 231–239, https://doi.org/10.1016/j.jlumin.2017.10.02.
[56] P. Ramakrishna, S. Panda, P. Vinodkumar, R.K. Padhi, H. Jena, B.S. Panigrahi, Structural and optical properties of cerium and dysprosium coactivated borophosphate glasses for cool white light application, J. Non-Cryst. Solids 566 (2021) 120883, https://doi.org/10.1016/j.jnoncrysol.2021.120883.
[57] S.A. Saleem, B.C. Jamalaiah, M. Jayasimhadri, A. Srinivasa Rao, Kiwan Jang, L. Rama Moorthy, Luminescent studies of Dy^{3+} ion in alkali lead tellurofluoroborate glasses, J. Quant. Spectrosc. Radiat. Transfer 112 (2011) 78–84, https://doi.org/10.1016/j.jqsrt.2010.08.017.
[57] J. Pisarska, Luminescence behavior of Dy^{3+} ions in lead borate glasses, Opt. Mater. 31 (2009) 1784–1786, https://doi.org/10.1016/j.optmat.2008.11.028.

[III]Karolina Milewska, Michał Maciejewski, Anna Synak, Marcin Łapiński, Aleksandra Mielewczyk-Gryń, Wojciech Sadowski, Barbara Kościelska, From Structure to Luminescent Properties of B_2O_3-Bi_2O_3-SrF_2 Glass and Glass-Ceramics Doped with Eu^{3+} Ions. Materials, 14, 4490. (IF = **3,748**)

materials MDPI

Article

From Structure to Luminescent Properties of B_2O_3-Bi_2O_3-SrF_2 Glass and Glass-Ceramics Doped with Eu^{3+} Ions

Karolina Milewska [1,*], Michał Maciejewski [1], Anna Synak [2], Marcin Łapiński [1], Aleksandra Mielewczyk-Gryń [1], Wojciech Sadowski [1] and Barbara Kościelska [1,*]

[1] Faculty of Applied Physics and Mathematics, Institute of Nanotechnology and Materials Engineering, Gdańsk University of Technology, ul. Gabriela Narutowicza 11/12, 80-233 Gdańsk, Poland; michal.maciejewski@pg.edu.pl (M.M.); marcin.lapinski@pg.edu.pl (M.Ł.); alegryn@pg.edu.pl (A.M.-G.); wojciech.sadowski@pg.edu.pl (W.S.)

[2] Faculty of Mathematics, Physics and Informatics, Institute of Experimental Physics, University of Gdańsk, ul. Wita Stwosza 57/246, 80-952 Gdańsk, Poland; anna.synak@ug.edu.pl

* Correspondence: karolina.milewska@pg.edu.pl (K.M.); barbara.koscielska@pg.edu.pl (B.K.)

Abstract: Glass-ceramics with the composition B_2O_3-Bi_2O_3-SrF_2 were synthesized by the conventional melt-quenching technique and subsequent crystallization of the parental glasses. The temperature at which the ceramization was carried out was selected based on differential scanning calorimetry (DSC) analysis. The structure of the studied materials and the formation of SrF_2 nanocrystals were confirmed by the Fourier-transform infrared spectroscopy (FTIR), X-ray diffraction (XRD), and X-ray photoelectron spectroscopy (XPS) techniques. It was found that the amount of strontium fluoride introduced into the parental borate-bismuth glass has a significant impact on the growth of SrF_2 nanocrystals. In particular, the influence of the crystalline SrF_2 phase on luminescence intensity and kinetics was studied using Eu_2O_3-doped samples. An increase in luminescence intensity was observed in the samples in which SrF_2 nanocrystals were formed. This is most likely related to the fact that some of the Eu^{3+} ions were (after annealing of the glass) located in the crystalline structure of strontium fluoride. This was confirmed both by the luminescence lifetime obtained based on the luminescence decay curves and the calculated Judd–Ofelt parameters, Ω_2 and Ω_4. The results achieved confirm that the glasses and glass-ceramics described in this work could be considered as a new phosphor for light-emitting diodes (LEDs).

Keywords: glass; glass-ceramics; luminescence; nanocrystals

check for updates

Citation: Milewska, K.; Maciejewski, M.; Synak, A.; Łapiński, M.; Mielewczyk-Gryń, A.; Sadowski, W.; Kościelska, B. From Structure to Luminescent Properties of B_2O_3-Bi_2O_3-SrF_2 Glass and Glass-Ceramics Doped with Eu^{3+} Ions. *Materials* **2021**, *14*, 4490. https://doi.org/10.3390/ma14164490

Academic Editor: Gregorio Bottaro

Received: 30 June 2021
Accepted: 7 August 2021
Published: 10 August 2021

1. Introduction

Glass as a material for applications in optics and optoelectronics has enjoyed unflagging interest for many years. In particular, a lot of research is related to glasses and glass-ceramics with optically active dopants such as rare-earth ions, which are promising materials for use in white LEDs [1–3]. This is because of their unique combination of properties for excellent transmission in the visible and infrared spectral range, high refractive index, and good chemical and mechanical stability [4,5]. Glasses that are the matrix for the rare-earth ions should also have low phonon energy, which decreases the risk of multi-phonon relaxation processes and, consequently, of non-radiative transitions [6]. When we consider glasses for these applications, borate glasses seem to have great potential. Boron oxide as a glass former is characterized by a wide glass formation range, high transparency, and high thermal stability [7]. Unfortunately, the addition of some network modifiers to boron oxide, usually alkali oxides, can lead to a change of coordination number of some of the boron atoms from 3 to 4, changing the properties of borate glass. Interestingly, the property change does not occur linearly with the amount of modifier. This phenomenon is known as the borate anomaly [8–10]. The modifier that allows very good optical properties of borate glasses to be obtained is bismuth oxide. Borate-bismuth

glasses are characterized by high density and high refractive indices and, importantly due to their preparation, are glasses with a comparatively low melting point in a wide glass formation range (20–80 mol % Bi_2O_3) [11]. The choice of bismuth oxide over lead oxide, which has often been used in glasses in recent years, seems particularly good, as it breaks down the toxic material while leaving the glass with the desired properties. However, the addition of Bi_2O_3 to borate oxide also changes the coordination number of the boron atoms [10,12,13], changing the properties of the resulting glass.

Borate glasses were often used as matrices for RE^{3+} ions [12,14,15]. However, research devoted to this subject has shown that an interesting alternative to glasses are glass-ceramics, especially those containing metal fluoride nanocrystals. Optical transparency of glass-ceramics can be reached if the crystallite diameter does not exceed 30 nm [16]. Crystal lattice, especially when the crystalline phase is fluoride, prevents them from luminescence concentration quenching due to clusters of RE^{3+} ions forming [17–19]. Furthermore, if there are heavy atoms in the structure of the nanocrystals, an additional factor appears in the amorphous matrix that reduces the phonon energy of the matrix what consequently promotes RE^{3+} radiative transitions, keeping all the benefits of the glass matrix at the same time [17,20–23]. Much research has been related to the existence of PbF_2 nanocrystals in the borate matrix [14,15]. However, as mentioned earlier, lead is being phased out due to its toxicity. Among various fluoride nanocrystals, which are more environmentally friendly than lead compounds, strontium fluoride SrF_2 seems to be a very good choice in terms of materials for optical applications. This is because SrF_2 exhibits a wide bandgap, low phonon energy, and relatively low hygroscopic properties [24]. On the other hand, to the best of our knowledge, there is no information in the literature on the possibility of crystallization of SrF_2 in a borate-bismuth matrix. SrF_2 nanocrystals are usually grown in glasses by annealing them at a suitable temperature above the glass transition temperature (T_g). The size of nanocrystals can be then controlled by changing heat treatment parameters, but it also depends on the type of glass structure [23–27]. In the case of borate-bismuth glass, the problem is more complicated because in this glass it is possible to obtain at least five stable crystalline phases of Bi_2O_3-B_2O_3 [11] and metastable bismuth orthoborate phases [28]. They can also crystallize in the matrix during annealing, leading to the crystallization of the SrF_2 phase. Nevertheless, due to the optical properties of borane-bismuth glasses and the known beneficial effect of SrF_2 nanocrystals on the luminescence of rare-earth ions, it is worth undertaking such research.

This work is devoted to the synthesis of borate-bismuth glasses and glass-ceramics containing SrF_2 nanocrystals. We present here the results of structural studies of the above materials, as well as the impact of annealing the glasses on the luminescent properties of Eu^{3+} ions incorporated in them. The research was carried out to assess these materials as potential candidates for LED phosphors.

2. Materials and Methods

Borate-bismuth glasses with a nominal composition (in mol%) of $50B_2O_3$-$50Bi_2O_3$ (BBO), $45B_2O_3$-$45Bi_2O_3$-$10SrF_2$ (BBO+$10SrF_2$), and $40B_2O_3$-$40Bi_2O_3$-$20SrF_2$ (BBO+$20SrF_2$) were synthesized using the conventional melt quenching technique. Moreover, glasses doped with Eu_2O_3 (2 mol %) were prepared: BBO+Eu, BBO+$10SrF_2$+Eu, and BBO+$20SrF_2$+Eu. Well-mixed starting raw materials H_3BO_3, $Bi_5OH(OH)_9(NO_3)_4$, SrF_2, and $Eu(NO_3)_3$ were melted in a porcelain crucible at 1100 °C for 15 min. After that, melts were poured onto a steel hot plate (~250 °C) and immediately pressed by another plate, and then cooled down to room temperature. To investigate the effect of annealing the glasses on the crystallization of SrF_2 nanocrystals, the samples were annealed in the interval of 450–590 °C for 1 h and 24 h in an air atmosphere.

Thermal properties of as-prepared glasses were studied on a Netzsch Simultaneous Thermal Analyzer, STA 449 F1, in the platinum-rhodium crucible in an air atmosphere, with a heating rate of 10 K/min. Before each measurement, a blank calibration run was conducted to account for the buoyancy effect. Differential scanning calorimetry (DSC)

allowed the characteristic temperatures to be determined, such as the glass transition temperature Tg and crystallization temperature Tc.

The amorphous nature of the glasses as well as the presence of crystalline phases present in them as a result of annealing was confirmed in X-ray diffraction (XRD) studies. XRD measurements were performed on powder samples on a Philips X'PERT PLUS diffractometer with Cu-Kα radiation.

To determinate the types of structural units present in the samples, Fourier transform infrared spectroscopy (FTIR) measurements were carried out. The measurements were performed on a Perkin-Elmer Frontier MIR/FIR spectrometer with a TGS detector on pellet samples mixed with potassium bromide KBr in a weight ratio (Sample:KBr) of 1:100.

X-ray photoelectron spectroscopy (XPS) analysis confirming the valence states of ions present in the samples was carried out with an Omnicron NanoTechnology spectrometer with a 128-channel collector. XPS measurements were performed in ultra-high vacuum conditions, below 1.1×10^{-8} mBar. The photoelectrons were excited by an Mg-Kα X-ray source with X-ray anode operated at 15 keV and 300 W.

Luminescence emission and excitation spectra of the samples were collected by a SCINCO FluoroMate FS-2 fluorescence spectrometer using pellet samples mixed with KBr in a weight ratio of 1:1. The single measurement results were obtained as a quasi-three-dimensional, colorful flat image, with the wavelength in the horizontal axis, the time in the vertical axis, and the intensity expressed by a range of colors.

Time-resolved emission spectra (TRES) were acquired using a pulsed spectrofluorometer described in detail [27]. The laser system PL2251-20 with an Nd:YAG laser and a PG 401/SH optical parametric generator emitting pulses of FWHMz30 ps from EXSPLA was used as the excitation light source. The emission signal was analyzed by a Bruker Optics 2501S spectrograph and the Hammamatsu streak camera C4334-01 model. All operations were fully automated and controlled by the original Hamamatsu HPDTA software, which allows for real-time data analysis. By slicing the streak camera image at a certain time interval, the time decays were obtained.

3. Results and Discussion

3.1. DSC Analysis

To analyze the thermal properties and the thermal stability of the prepared glasses, DSC measurements were performed. The results are presented in Figure 1. One can observe that the glass transition temperature depended on the SrF_2 content. T_g was located around 424 °C, 456 °C, and 459 °C for BBO, BBO+10SrF_2, and BBO+20SrF_2 glasses, respectively. Interestingly, the exothermic maximum associated with crystallization was only visible for the BBO sample. The onset of crystallization peak temperature (T_x) was located at 534 °C, which is well below the crystallization temperatures of the possible crystalline phases [11]. The glass stability region ΔT, defined as the difference between T_x and T_g, for BBO glass was equal to 110 °C. This is a wide range, but even a small quantity of B_2O_3 may have a positive effect on the thermal stability of this glass [29]. Taking into account the crystallization of the glasses, the thermal stability S parameter describing the glass resistance against devitrification was also determined [30]:

$$S = \frac{(T_c - T_x)(T_c - T_g)}{T_g} \quad (1)$$

In studied BBO glass, the calculated value of S is 8.72. For comparison, the values of S found in the literature for other borate glasses was even about 1 (50B_2O_3-50Bi_2O_3 [31], 50Li_2O-50B_2O [32]). Unfortunately, such a significant difference between these values and the value obtained for our glass was not clear to us. As can be seen, the addition of SrF_2 to the base BBO composition led to the disappearance of the crystallization peak. Therefore, it can be said that it prevented the crystallization of the matrix. Unfortunately, no effect related to the crystallization of the SrF_2 phase in the BBO matrix was observed in these glasses.

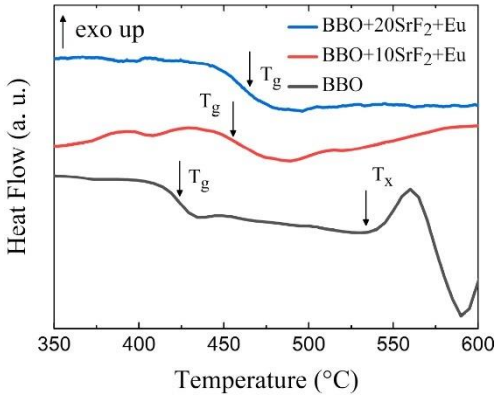

Figure 1. DSC curves of BBO, BBO+10SrF_2, and BBO+20SrF_2 glasses.

3.2. XRD Analysis

The amorphous character of as-prepared glasses was confirmed by XRD studies. Figure 2 shows the diffraction patterns of BBO, BBO+10SrF_2, and BBO+20SrF_2 glass samples. Only broad halos associated with amorphous materials can be seen.

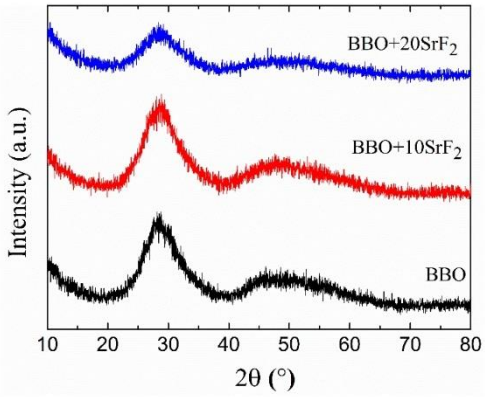

Figure 2. XRD patterns of as-prepared BBO, BBO+10SrF_2, and BBO+20SrF_2 glasses.

The effect of the annealing temperature on the structure of the BBO+10SrF_2 and BBO+20SrF_2 glasses is shown in Figures 3 and 4. In Figure 3, X-ray diffractograms for the BBO+10SrF_2 and BBO+20SrF_2 glasses annealed at temperatures ranging from 560 to 590 °C for 1 h are presented. Figure 4 presents XRD patterns of these glasses after heat treatment in the same temperature range, but for 24 h. The aim of the thermal treatment was the growth of SrF_2 nanocrystals in the glass matrix. XRD patterns of the samples annealed at 560 °C did not differ from the patterns of the unannealed samples and showed a lack of long-range order. It should be noted, however, that in the presented XRD results a small amount of the nano-sized crystalline phase could have gone unnoticed, especially since the amorphous phase in which the nanocrystals were dispersed gives a broad halo in the range of 25–35 (2θ), in which there may be major reflections derived from the crystalline phases. Clear differences between BBO+10SrF_2 and BBO+20SrF_2 samples appeared after

annealing at 570 °C. XRD patterns of the BBO+10SrF_2 sample showed crystallization mainly in the $BiBO_3$ phase (Ref.Code 96-720-9482), but there were also visible low-intensity reflections corresponding to the SrF_2 phase (Ref.Code 96-900-9044). Unfortunately, there were also unidentified peaks in the diffractograms that were likely related to bismuth oxides, but crystalline borates sometimes have highly unusual stoichiometries [8]; therefore, it is difficult to fully characterize the presented diffraction pattern. On the other hand, BBO+20SrF_2 samples showed only the peaks characteristic of the SrF_2 crystalline phase (Ref.Code 96-900-9044). As can be seen, with the increase in the annealing temperature, the amount of $BiBO_3$ crystalline phase in the BBO+10SrF_2 samples decreased, whereas a weak reflection of the SrF2 phase was already present in the sample annealed at 580 °C. In the case of the annealed BBO+20SrF_2 glass, the SrF_2 phase crystallized regardless of the temperature increase. The obtained diffractograms confirm the conclusion drawn based on DSC studies that the presence of SrF_2 in the BBO matrix prevented its crystallization. Unfortunately, annealing the samples at temperatures of 570 °C and higher caused them to begin to lose their transparency. Therefore, 560 °C was chosen as the temperature, providing a compromise between the transparency of the sample and the presence of a crystalline phase in it. At this temperature, only samples heated for 24 h became opaque.

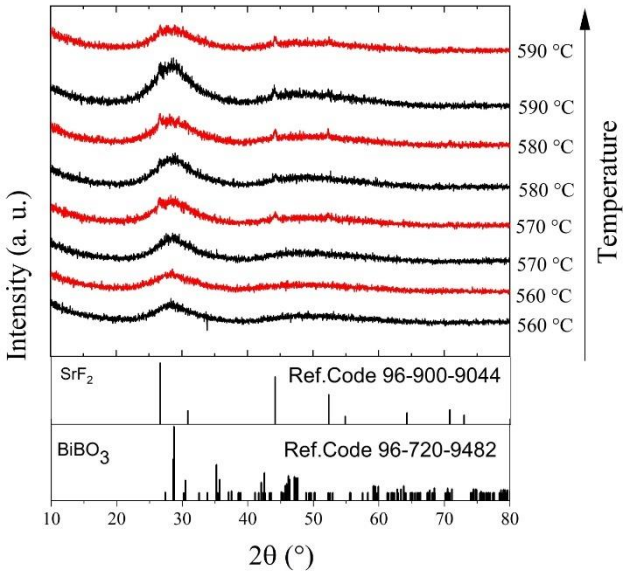

Figure 3. XRD patterns of BBO+10SrF_2 (black) and BBO+20SrF_2 (red) glasses after annealing in the temperature range of 560–590 °C for 1 h.

3.3. FTIR Analysis

Changes in the structure of the studied glasses occurring due to annealing were also visible in the FTIR spectra. The FTIR spectra obtained for BBO+10SrF_2 and BBO+20SrF_2 glasses and glass-ceramics are shown in Figure 5a,b, respectively. For comparison, the spectrum of as-prepared BBO glass was added to each figure. It is well known that the network of borate glasses is mainly constructed from [BO_3] triangular structural units, which under the influence of the modifier can transform into [BO_4] tetrahedral units. Such a change can also occur under the influence of Bi_2O_3 [12]. The broad absorption bands in the region of 680–720 cm^{-1} and 1100–1250 cm^{-1} are usually assigned to deformation and stretching

vibrations of $[BO_3]$ groups [10,13,33]. In addition, the band at about 1200–1400 cm^{-1} can be attributed to the stretching vibration of $[BO_3]$. On the other hand, the presence of $[BO_4]$ groups may be indicated by the band at 900–1100 cm^{-1} [13,33]. However, it should be noted that these bands may shift under the influence of Bi_2O_3 and overlap with the Bi_2O_3 peaks and shoulders [33]. Looking at the spectra presented in Figure 5, it can be concluded that the annealing did not significantly affect them.

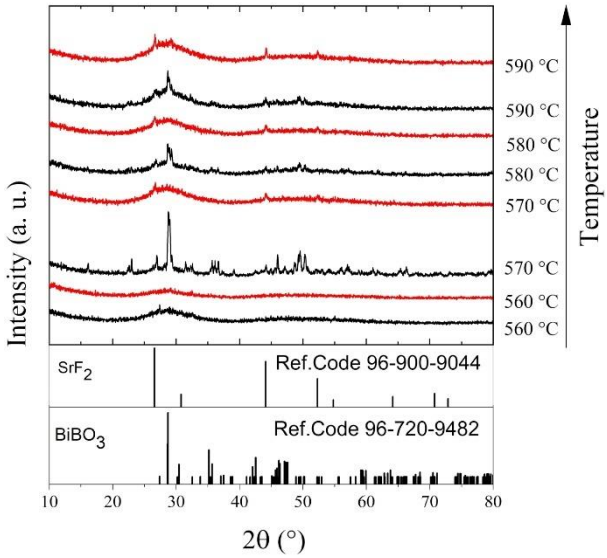

Figure 4. XRD patterns of BBO+10SrF_2 (black) and BBO+20SrF_2 (red) glasses after annealing in the temperature range of 560–590 °C for 24 h.

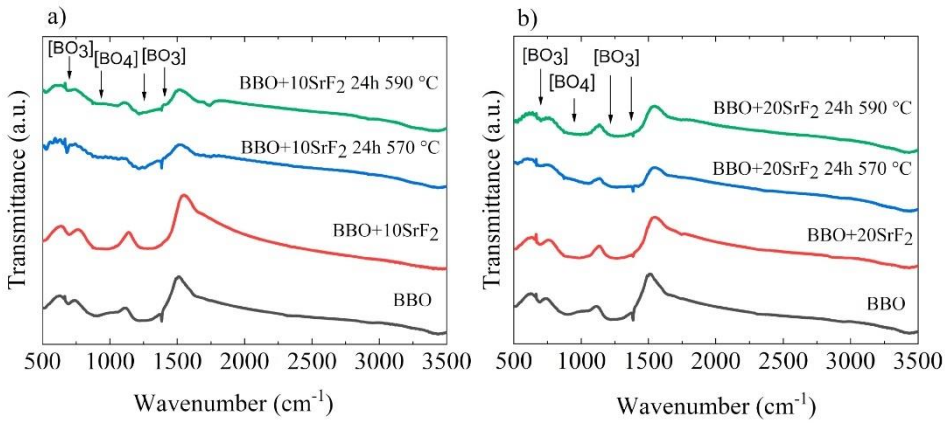

Figure 5. FTIR spectra of BBO+10SrF2 (**a**) and BBO+20SrF2 (**b**) as-prepared glasses and glasses after annealing at 570 °C and 590 °C. For comparison, the spectrum of as-prepared BBO glass was added to each figure.

3.4. XPS Analysis

XPS analysis was performed to provide additional information about the valence states of the elements of which the samples consisted. Particular emphasis was placed on the study of the valence states of Eu and Bi ions, as well as the chemical states of Sr that could indicate Sr chemical bonds with both fluorine and oxygen [24,34,35]. As research has shown, both Eu and Bi ions are in the 3+ valence state. Exemplary spectra of the Sr region of BBO+10SrF_2 and BBO+20SrF_2 glasses and glass ceramics after annealing at 560 °C for 24 h are shown in Figure 6. All spectra consisted of the Sr 3d spin-orbit doublet, but a detailed analysis of these peaks suggests the presence of more than one chemical state of Sr in all samples. Peaks at 133.5 and 135.5 eV could be assigned to the Sr $3d_{5/2}$ and Sr $3d_{3/2}$ in Sr-O [34,35], whereas peaks with energies equal to 134.0 and 136.0 eV could be attributed to Sr $3d_{5/2}$ and Sr $3d_{3/2}$ in Sr-F [34,35]. The contribution of Sr-O and Sr-F doublets in the glasses was 59% and 41% (BBO+10SrF_2) and 67% and 33% (BBO+20SrF_2), respectively. The contribution of Sr-O and Sr-F doublets after annealing was, respectively, 80% and 20% (BBO+10SrF_2) and 52% and 48% (BBO+20SrF_2). Therefore, as can be seen, annealing did not change the ratio of the doublets in the same way in both samples. The increase in the contribution of the Sr-F doublet, which in turn indicated an increase in the amount of the SrF_2 crystal phase in the matrix, only took place in samples containing 20 mol % SrF_2. However, as the analysis of the X-ray diffractograms showed, SrF_2 as the only crystalline phase was also present only in the samples containing 20 mol % SrF_2. Therefore, it can be concluded from both of these methods that the formation of SrF_2 nanocrystals hindered the crystallization of the matrix.

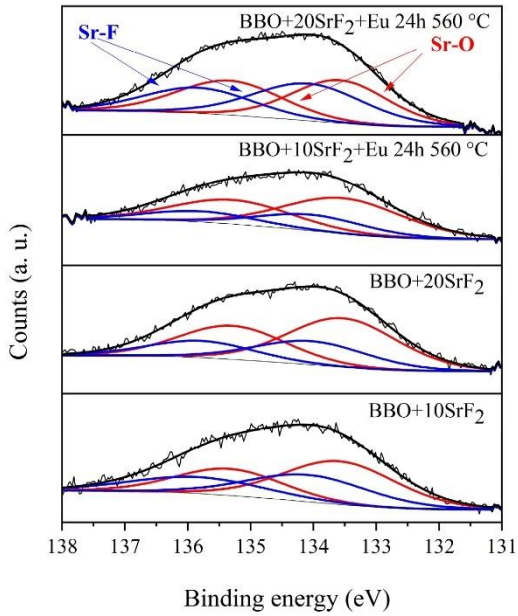

Figure 6. Sr 3D region of XPS spectra of BBO+10SrF_2 and BBO+20SrF_2 as-prepared glasses and glasses after annealing at 560 °C for 24 h.

3.5. Luminescence Analysis

Luminescence properties of Eu-doped BBO, BBO+10SrF_2, and BBO+20SrF_2 glasses and glass-ceramics were investigated to determine the influence of SrF_2 on the luminescence intensity of Eu^{3+} ions. Figures 7a and 8a show the excitation spectra of as-prepared BBO+10SrF_2+Eu and BBO+20SrF_2+Eu glasses monitored at the wavelength of λ_{em} = 615 nm, which corresponds to $^5D_0 \rightarrow {}^7F_2$ transition of Eu^{3+} ions [3,36]. Several characteristics for 4f-4f transition peaks were visible in the spectrum. Excitation bands at 382 and 465 nm may have been assigned to $^7F_0 \rightarrow {}^5G_4$, $^5D_2$ transitions, whereas bands at 396, 415, and 533 nm originated from $^7F_0 \rightarrow {}^5L_6$, $^5D_3$, and $^5D_1$ transitions, respectively [3,36]. A wavelength of 465 nm was selected for the observation of the emission spectra. This is the line with the highest intensity in the excitation spectrum. Emission spectra of BBO+10SrF_2+Eu glass and glass-ceramics crystallized at 560 °C (Figure 7b) consisted of several bands corresponding to Eu^{3+} radiative transitions at 581 nm ($^5D_0 \rightarrow {}^7F_0$), 594 nm ($^5D_0 \rightarrow {}^7F_1$), 615 nm ($^5D_0 \rightarrow {}^7F_2$), 655 nm ($^5D_0 \rightarrow {}^7F_3$), and 703 nm ($^5D_0 \rightarrow {}^7F_4$) [3,36]. As can be seen, there were no significant differences between the intensity of the bands corresponding to the BBO+Eu glass and the glass with the addition of 10 mol % of SrF_2. In addition, annealing of the BBO+10SrF_2+Eu samples did not change the intensity of the spectral lines. However, if we look at the results concerning the structure of the annealed samples, the crystallization of the borane-bismuth matrix, apart from the SrF_2 crystal phase, cannot be ruled out. Assuming that this is the case, the emitted radiation could undergo scattering on defects. Looking at the emission spectra corresponding to the BBO+20SrF_2+Eu samples (Figure 8b), it can be noticed that the emission bands were at the same wavelengths as for the samples with 10 mol % of SrF_2. In addition, it is evident that annealing affected the intensity of Eu^{3+} ions emission. It is worth noticing that the SrF_2 crystalline phase was characterized by considerably lower phonon energy compared to the oxide materials. Therefore, if Eu^{3+} ions are located in the SrF_2 nanocrystals, this leads to a decrease in multi-phonon relaxation probability, and consequently to an increase in emission efficiency. This was also the case with other strontium fluoride-containing glass ceramics [25,37].

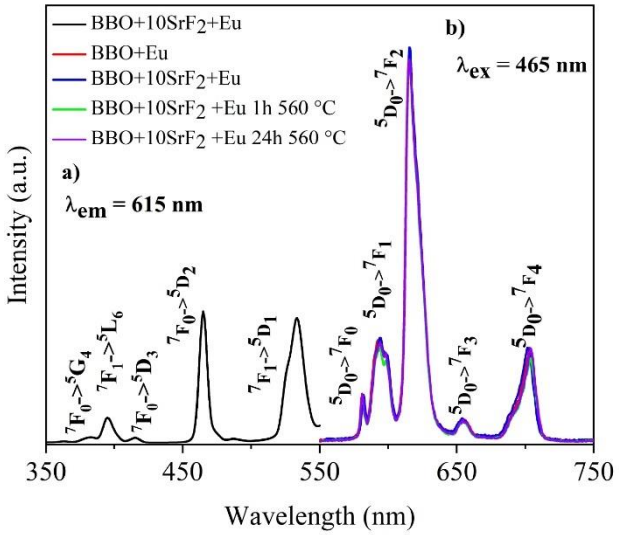

Figure 7. The excitation spectrum of BBO+10SrF_2+Eu glass (**a**), and the emission spectra of BBO+Eu glass, and BBO+10SrF_2+Eu glass and glass-ceramics after annealing at 560 °C for 1 h and 24 h (**b**).

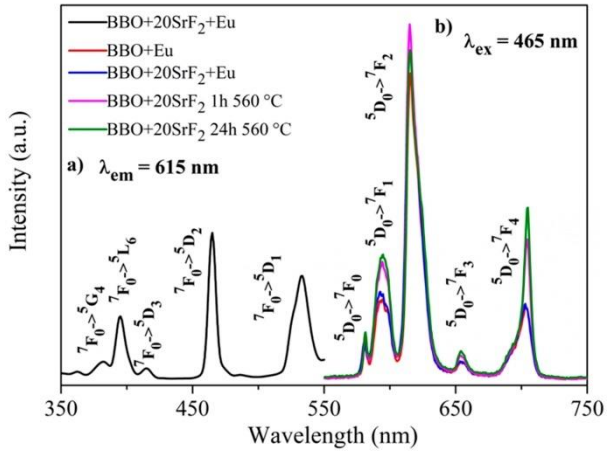

Figure 8. The excitation spectrum of BBO+20SrF_2+Eu glass (**a**), and the emission spectra of BBO+Eu glass, and BBO+20SrF_2+Eu glass and glass-ceramics after annealing at 560 °C for 1 h and 24 h (**b**).

3.6. Luminescence Decay and Judd–Ofelt Analysis

Luminescence decay analysis was performed on as-prepared Eu doped BBO, BBO+10SrF_2 and BBO+20SrF_2 glasses and glass-ceramics. The decay curves were obtained by monitoring $^5D_0 \rightarrow {}^7F_2$ emission line (λ_{em} = 615 nm) upon excitation at λ_{exc} = 465 nm ($^7F_0 \rightarrow {}^5D_2$ transition) and are shown in Figure 9a,b.

It was found that luminescence decays in both cases can be described as two-exponential decays according to the following equation [38]:

$$I(t) = A_1 \exp\left(\frac{-t}{\tau_1}\right) + A_2 \exp\left(\frac{-t}{\tau_2}\right) \quad (2)$$

where τ_1 and τ_2 are long and short luminescence lifetime components contributing to the average lifetime $\langle\tau_{avg}\rangle$, and A_1 and A_2 are amplitudes of respective decay components. The lifetimes τ_1 and τ_2, amplitudes, and average lifetime calculated for the luminescence decay curves presented in Figure 9 are collected in Table 1.

Table 1. Fitting parameters of the luminescence decays, calculated Judd–Ofelt parameters, and luminescence intensity ratios.

	BBO+Eu	BBO+10SrF_2+E	BBO+20SrF_2+Eu	BBO+10SrF_2+Eu 1 h 560 °C	BBO+10SrF2+Eu 24 h 560 °C	BBO+20SrF2+Eu 1 h 560 °C	BBO+20SrF2+Eu 24 h 560 °C
A_1	3913	4148	4267	3297	3431	3440	3338
A_2	3237	3115	2951	3893	3387	3046	2692
τ_1 (ms)	1.2	1.18	1.28	1.24	1.22	1.45	1.48
τ_2 (ms)	0.56	0.5	0.52	0.58	0.56	0.66	0.65
$<\tau_{avg}>$ (ms)	1	1	1.1	1	1	1.2	1.2
Ω_2	5.64	5.15	5.54	6.06	5.86	4.48	5.11
Ω_4	3.89	3.74	3.59	3.78	3.85	3.86	4.07
R/O	3.76	3.45	3.69	4.04	3.90	3.06	2.73

This double-exponential nature of the decay curves indicates the presence of two different surroundings of Eu^{3+} ions. Long lifetime (τ_1) is correlated with higher symmetry of the crystal field, whereas short lifetime (τ_2) is associated with lower symmetry of the Eu^{3+} surroundings. Thus, in glasses containing SrF_2 or PbF_2 nanocrystals, a long

lifetime is attributed to Eu^{3+} ions, which are located in the nanocrystals, and short lifetimes correspond to the ions incorporated into the amorphous matrix [24,25,37,39].

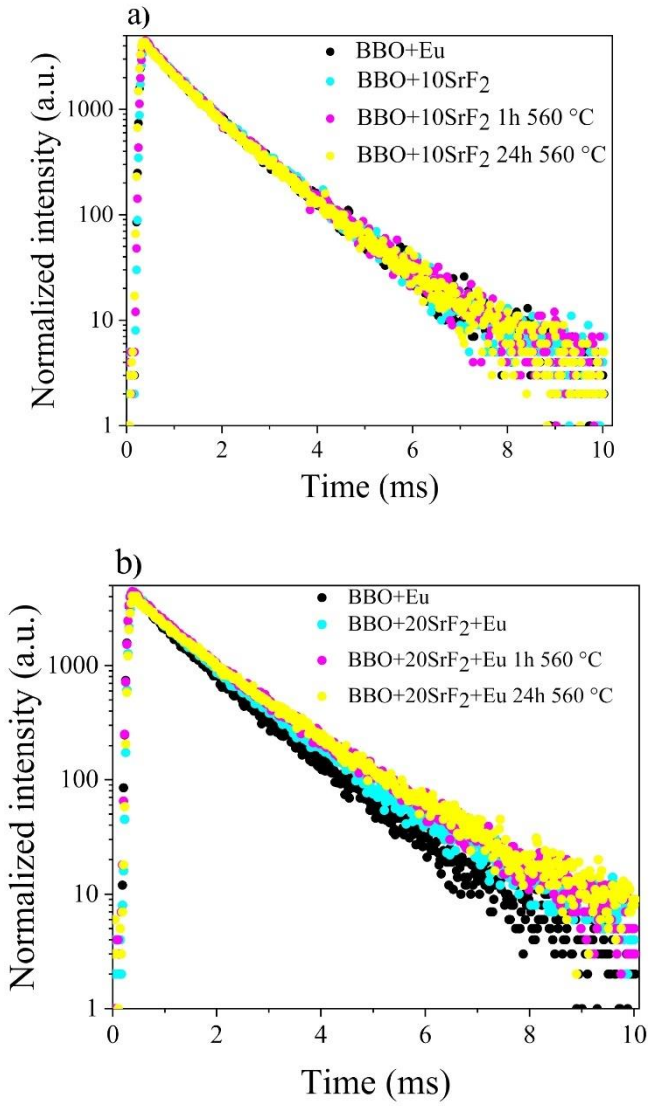

Figure 9. Luminescence decay curves of Eu-doped BBO and BBO+10SrF_2 samples (**a**) Eu-doped BBO and BBO+20SrF_2 samples (**b**).

Concerning the tested samples, it can therefore be said that τ_1 represents the lifetime of Eu^{3+} ions incorporated into the SrF_2 nanocrystals, whereas τ_2 corresponded to ions

surrounded by the glass matrix. However, in the case of the studied samples, the situation seems to be more complicated. Two lifetimes were also observed in BBO+Eu glass, which did not contain strontium fluoride, and if to compare the results obtained for this glass with the values calculated for the BBO+10SrF_2 sample, the lifetimes are not much different. This means that the tested glass may have contained nanocrystalline areas that were formed during the glass preparation process, which are not visible in diffraction studies. Especially in borate glasses with various dopants, single exponential decay curves are usually observed [40,41]. As can be seen, the longest τ_2 lifetime was observed for the BBO+20SrF_2 samples, especially those annealed for 24 h at 560 °C. It seems that in these samples the amount of Eu^{3+} ions incorporated into SrF_2 nanocrystals increased. This result is in line with the results obtained with the XRD. They show that SrF_2 as the only crystalline phase in the glass was present at 20 mol% of SrF_2, whereas at 10 mol% the matrix crystallization also took place.

Changes in symmetry in the surroundings of the europium ions, as well as changes in the degree of covalence of bonds of these ions, can be observed based on Judd–Ofelt parameters. The Judd–Ofelt parameters Ω_2 and Ω_4 were calculated based on luminescence emission spectra using JOES application software and are presented in Table 1. Detailed information regarding software and calculations can be found in reference [42]. The Ω_6 parameter was not determined in this study due to the unregistered emission band, located in the NIR range of wavelength, that corresponds to the $^5D_0 \rightarrow {}^7F_6$ transition band. The Ω_2 parameter is known to be structure sensitive and also depends on the covalence of Eu^{3+} bonds with the ligand [43–46]. It is determined from $^5D_0 \rightarrow {}^7F_2$ hypersensitive transition. The high value of the Ω_2 parameter ($\Omega_2 > \Omega_4$) suggests that Eu^{3+} ions occupied mostly low-symmetry sites. This corresponds to the situation where Eu^{3+} ions were mainly located in the glassy matrix. On the other hand, the Eu-O bond in the glasses was highly covalent, which was also reflected in the high Ω_2 coefficients. In turn, the Ω_4 parameter is related to the rigidity of glasses and is often attributed to the emergence of long-range effects related to crystal lattice [19]. Therefore, the processes of crystallization of glasses should consequently lead to an increase in this parameter. This behavior was observed, for example, in tellurite glass-ceramics containing SrF_2 nanocrystals [25]. The parameters Ω_2 and Ω_4 calculated for the BBO+10SrF_2 and BBO+20SrF_2 glasses before and after annealing were different, but the change due to crystallization depended on the initial amount of SrF_2. In the BBO+10SrF_2 sample, both Ω_2 and Ω_4 were higher in the annealed samples. Nevertheless, it is a sample where it was difficult to say that SrF_2 was the only crystalline phase in the glass matrix and it was, therefore, difficult to analyze the influence of the appearance of SrF_2 nanocrystals on luminescence. On the other hand, in the case of the BBO+20SrF_2 sample, after crystallization the parameter Ω_2 was lower and Ω_4 was higher than in as-prepared glass. However, in the BBO glass containing 20 mol% of SrF_2, no additional crystallization of the matrix was observed after annealing; hence, it can be concluded that the observed change in the values of Ω_2 and Ω_4 parameters, as well as the increase in τ_1 time, are because Eu^{3+} ions were located in SrF_2 nanocrystals.

These results follow the luminescence intensity ratio R (asymmetry ratio), which in the case of Eu^{3+} ions can be calculated from the expression [45]:

$$R = \frac{I(^5D_0 \rightarrow {}^7F_2)}{I(^5D_0 \rightarrow {}^7F_1)} \quad (3)$$

The transition $^5D_0 \rightarrow {}^7F_1$ occurs via magnetic dipole and is independent of the host matrix, whereas $^5D_0 \rightarrow {}^7F_2$ has a pure electric dipole moment origin and is hypersensitive to changes in the crystal field around Eu^{3+} ions. In other words, a more intense $^5D_0 \rightarrow {}^7F_2$ transition indicates that the Eu^{3+} ions mainly occupy positions without an inversion center, whereas a more intense $^5D_0 \rightarrow {}^7F_1$ transition shows that the Eu^{3+} ions are located at sites with higher symmetry. Therefore, with the change in site symmetry of Eu^{3+} ions, when they take positions with higher symmetry, the asymmetry ratio coefficient should decrease. The intensity ratios calculated for the as-prepared BBO+20SrF_2 sample and

the samples after annealing at 560 °C decreased with an increase in the annealing time (resulting in the growth of SrF_2 nanocrystals). This means that some of the Eu^{3+} ions were located in the structure of nanocrystals. Unfortunately, as shown earlier, BBO glass initially containing 10 mol % of SrF_2 may behave differently, which is most likely related to the not-completely-amorphous (after annealing) borate-bismuth matrix.

4. Conclusions

In summary, borate-bismuth glass-ceramics doped with Eu^{3+} ions, with SrF_2 nanocrystals, were obtained. The structural modifications of parental glass, leading to SrF_2 nanostructure crystallization, depend strongly on the initial amount of strontium fluoride. In the case of borate-bismuth glass, it is possible to obtain at least five stable crystalline phases of Bi_2O_3-B_2O_3 [11], and 10 mol % of SrF_2 introduced into the glass is insufficient to block crystallization of the matrix. This has a strong influence on the luminescent properties. The expected increase in the intensity of emission bands was not observed in such glass ceramics, which was probably related to the scattering of the emitted radiation on various types of defects occurring during the annealing of the glasses. The increase in luminescence intensity was observed after annealing in samples containing 20 mol% SrF_2. The luminescence lifetimes obtained for these glass-ceramics indicate that some of the Eu^{3+} ions were located in SrF_2 nanocrystals. This was also confirmed by the analysis of the Judd–Ofelt parameters Ω_2 and Ω_4, and luminescence intensity ratio R. It can therefore be concluded that the glasses and glass-ceramics described in this work could be considered as potential candidates for LED phosphors.

Author Contributions: Conceptualization, B.K. and K.M.; methodology, K.M., M.M., A.S.; M.Ł., A.M.-G., W.S., and B.K.; formal analysis, K.M. and B.K.; investigation, K.M. and B.K.; data curation, K.M. and B.K.; writing—original draft preparation, B.K. and K.M.; writing—review and editing, K.M., M.M., A.S., M.Ł., W.S., and B.K.; supervision, B.K. All authors have read and agreed to the published version of the manuscript.

Funding: This research received no external funding.

Data Availability Statement: The data presented in this study (FTIR and luminescence) are openly available at: https://mostwiedzy.pl/pl/open-research-data/luminescence-and-ftir-measurements-of-b2o3-bi2o3-srf2-glass-and-glass-ceramics-doped-with-eu3-ions,629025230630285-0 (accessed on 30 June 2020).

Acknowledgments: The authors would like to thank Leon Murawski for the fruitful discussions.

Conflicts of Interest: The authors declare no conflict of interest.

References

1. El-Mallawany, R. *Tellurite Glass Smart Materials, Applications in Optics and Beyond*; Springer International Publishing AG, Part of Springer Nature: Cham, Switzerland, 2018; ISBN 978-3-319-76567-9. [CrossRef]
2. Nagaraja Naick, B.; Damodaraiah, S.; Reddy Prasad, V.; Vijaya Lakshmi, R.P.; Ratnakaram, Y.C. Judd-Ofelt analysis and luminescence studies on Dy^{3+} -doped different phosphate glasses for white light emitting material applications. *Opt. Int. J. Light Electron Opt.* **2019**, *192*, 162980. [CrossRef]
3. Zhao, C.; Cai, J.; Li, R.; Tie, S.; Wan, X.; Shen, J. White light emission from $Eu^{3+}/Tb^{3+}/Tm^{3+}$ triply-doped aluminoborate glass excited by UV light. *J. Non-Cryst. Solids* **2012**, *358*, 604–608. [CrossRef]
4. Gonçalves, M.C.; Santos, L.F.; Almeida, R.M. Rare-earth-doped transparent glass ceramics. *C. R. Chim.* **2002**, *5*, 845–854. [CrossRef]
5. Dumbaugh, W.H.; Lapp, J.C. Heavy-metal oxide glasses. *J. Am. Ceram. Soc.* **1992**, *75*, 2315–2326. [CrossRef]
6. Fan, H.; Gao, G.; Wang, G.; Hu, J.; Hu, L. Tm^{3+} doped Bi_2O_3–GeO_2–Na_2O glasses for 1.8 μm fluorescence. *Opt. Mater.* **2010**, *32*, 627–631. [CrossRef]
7. Majérus, O.; Trégouët, H.; Caurant, D.; Pytalev, D. Comparative study of the rare earth environment in rare earth metaborate glass (REB_3O_6, RE = La, Nd) and in sodium borate glasses. *J. Non-Cryst. Solids* **2015**, *425*, 91–102. [CrossRef]
8. Wright, A.C. My Borate Life: An Enigmatic Journey. *Int. J. Appl. Glass Sci.* **2015**, *6*, 45–63. [CrossRef]
9. Wright, A.C. Borate structures: Crystalline and vitreous. *Phys. Chem. Glasses* **2010**, *51*, 1–39.
10. Bobkova, N.M. Properties and Structure of Bismuth-Borate Glasses. *Glass Ceram.* **2016**, *72*, 360–365. [CrossRef]
11. Bajaj, A.; Khanna, A. Crystallization of bismuth borate glasses. *J. Phys. Condens. Matter* **2009**, *21*, 035112. [CrossRef] [PubMed]

12. Bobkova, N.M. Characteristic of the Structure State of Bismuth Ions in Bismuth-Borate Glasses. *Glass Ceram.* **2019**, *75*, 383–386. [CrossRef]
13. Pascuta, P.; Pop, L.; Rada, S.; Bosca, M.; Culea, E. The local structure of bismuth borate glasses doped with europium ions evidenced by FTIR spectroscopy. *J. Mater Sci. Mater. Electron.* **2008**, *19*, 424–428. [CrossRef]
14. Pisarski, W.A.; Pisarska, J.; Mączka, M.; Lisiecki, R.; Grobelny, Ł.; Goryczka, T.; Dominiak-Dzik, G.; Ryba-Romanowski, W. Rare eart-doped lead borate glasses and transparent glass-ceramics: Structure-property relationship. *Spectrochim. Acta Part A* **2011**, *27*, 696–700. [CrossRef] [PubMed]
15. Pisarski, W.A.; Pisarska, J.; Ryba-Romanowski, W. Structural role of rare earth ions in lead borate glasses evidenced by infrared spectroscopy: $BO_3 \leftrightarrow BO_4$ conversion. *J. Mol. Struct.* **2005**, *744*, 515–520. [CrossRef]
16. Hopper, R.W. Stochastic theory of scattering from idealized spinodal structures: II. Scattering in general and for the basic late stage model. *J. Non-Cryst. Solids* **1985**, *70*, 111–142. [CrossRef]
17. Mattarelli, M.; Tikhomirov, V.K.; Seddon, A.B.; Montagna, M.; Moserm, E.; Chiasera, A.; Chaussedent, S.; Conti, G.N.; Pelli, G.L.; Righini, C.; et al. Tm^{3+}- activated transparent oxy-fluoride glass-ceramics: Structural and spectroscopic properties. *J. Non-Cryst. Solids* **2004**, *346*, 354–358. [CrossRef]
18. Boulard, B.; Péron, O.; Jestin, Y.; Ferrari, M.; Duverger-Arfuso, C. Characterization of Er^{3+}-doped fluoride glass ceramics waveguides containing LaF_3 nanocrystals. *J. Lumin.* **2009**, *129*, 1637–1640. [CrossRef]
19. Rodríguez, V.D.; Lavín, V.; Rodríguez-Mendoza, U.R.; Martín, I.R. Spectroscopy of rare earth ions of fluoride glasses for laser applications. *Opt. Mater.* **1990**, *13*, 1–7. [CrossRef]
20. Gao, Y.; Hu, Y.; Zhou, D.; Qiu, J. Effect of heat treatment mechanism on upconversion luminescence in Er^{3+}/Yb^{3+} co-doped NaYF4 oxyfluoride glass-ceramics. *J. Alloys. Compd.* **2017**, *699*, 303–307. [CrossRef]
21. Bae, S.R.; Choi, Y.G.; Bin, W.I.; Lee, K.S.; Chung, W.J. Rare earth doped silicate-oxyfluoride glass ceramics incorporating LaF_3 nano-crystals for UV-LED color conversion. *Opt. Mater* **2013**, *35*, 2034–2038. [CrossRef]
22. Zur, L.; Thi, L.; Tran, N.; Meneghetti, M.; Thanh, V.T.; Righini, G.C. Tin-dioxide nanocrystals as Er^{3+} luminescence sensitizers: Formation of glass-ceramic thin films and their characterization. *Opt. Mater.* **2017**, *63*, 95–100. [CrossRef]
23. Chen, D.; Xiang, W.; Liang, X.; Zhong, J.; Yu, H.; Ding, M.; Lu, H.; Ji, Z. Advances in transparent glass-ceramic phosphors for white light-emitting diodes—A review. *J. Eur. Ceram. Soc.* **2015**, *35*, 859–869. [CrossRef]
24. Walas, M.; Lewandowski, T.; Synak, A.; Łapiński, M.; Sadowski, W.; Kościelska, B. Eu^{3+} doped tellurite glass ceramics containing SrF_2 nanocrystals: Preparation, structure and luminescence properties. *J. Alloys Compd.* **2017**, *696*, 619–626. [CrossRef]
25. Walas, M.; Lisowska, M.; Lewandowski, T.; Becerro, A.I.; Łapiński, M.; Synak, A.; Sadowski, W.; Kościelska, B. From structure to luminescence investigation of oxyfluoride transparent glasses and glass-ceramics doped with Eu^{3+}/Dy^{3+} ions. *J. Alloys Compd.* **2019**, *806*, 1410–1418. [CrossRef]
26. Miguel, A.; Morea, R.; Arriandiaga, M.A.; Hernandez, M.; Ferrer, F.J.; Domingo, C.; Fernandez-Navarro, J.M.; Gonzalo, J.; Fernandez, J.; Balda, R. Structural, optical, and spectroscopic properties of Er^{3+}-doped TeO_2–ZnO–ZnF_2 glass-ceramics. *J. Eur. Ceram. Soc.* **2014**, *34*, 3959–3968. [CrossRef]
27. Grobelna, B.; Bojarski, P.; Kuklinski, B.; Kubicki, A.A.; Synak, A. Optical properties and luminescence kinetics of $Ln_{1.9}Pr_{0.1}(WO_4)_3$ (where Ln = Gd, La) immobilized in silica xerogel. *Opt. Mater.* **2011**, *34*, 103–108. [CrossRef]
28. Becker, P.; Fröhlich, R.Z. Crystal Growth and Crystal Structure of the Metastable Bismuth Orthoborate $BiBO_3$. *Naturforsch* **2004**, *59b*, 256–258. [CrossRef]
29. Yanmin, Y.; Yanzhou, L.; Peiqing, C.; Maalej, R.; Seo, H.J. Thermal stability and spectroscopic properties of Ho^{3+} doped tellurite-borate glasses. *J. Rare Earths* **2015**, *33*, 939–945. [CrossRef]
30. Saad, M.; Poulain, M. Glass Forming Ability Criterion. *Mater. Sci. Forum.* **1987**, *19–20*, 1–18. [CrossRef]
31. Ferreira, E.B.; Zanotto, E.D.; Feller, S.; Lodden, G.; Banerjee, J.; Edwards, T.; Affatigato, M. Critical Analysis of Glass Stability Parameters and Application to Lithium Borate Glasses. *J. Am. Ceram. Soc.* **2011**, *94*, 3833–3841. [CrossRef]
32. Mary, N.; Rebours, M.; Castel, E.; Vaishnav, S.; Deng, W.; Bell, A.M.; Clegg, F.; Allsopp, B.L.; Scrimshire, A.; Bingham, P.A. Enhanced thermal stability of high-bismuth borate glasses by addition of iron. *J. Non-Cryst. Solids* **2018**, *500*, 149–157. [CrossRef]
33. Ali, A.A.; Rammahb, Y.S.; El-Mallawany, R.; Souri, D. FTIR and UV spectra of pentaternary borate glasses. *Measurement* **2017**, *105*, 72–77. [CrossRef]
34. Yagoub, M.Y.A.; Swart, H.C.; Noto, L.L.; O'Connel, J.H.; Lee, M.E.; Coetsee, E. The effects of Eu-concentrations on the luminescent properties of SrF_2: Eu nanophosphor. *J. Lumin.* **2014**, *156*, 150–156. [CrossRef]
35. Yagoub, M.Y.A.; Swart, H.C.; Coetsee, E. Concentration quenching, surface and spectral analyses of SrF_2:Pr^{3+} prepared by different synthesis techniques. *Opt. Mater.* **2015**, *42*, 204–209. [CrossRef]
36. Sontakke, A.D.; Tarafder, A.; Biswas, K.; Annapurna, K. Sensitized red luminescence from Bi^{3+} co-doped Eu^{3+}: ZnO–B_2O_3 glasses. *Phys. B Condens. Matter* **2009**, *404*, 3525–3529. [CrossRef]
37. Luo, Q.; Qiao, X.; Fan, X.; Liu, S.; Yang, H.; Zhang, X. Reduction and luminescence of europium ions in glass ceramics containing SrF_2 nanocrystals. *J. Non-Cryst. Solids* **2008**, *354*, 4691–4694. [CrossRef]
38. Yu, C.; Yang, X.; Huang, A.; Chai, Z.; Qiu, J.; Song, Z.; Zhou, D. Photoluminescence properties of tellurite glasses doped Dy^{3+} and Eu^{3+} for the UV and blue converted WLEDs. *J. Non-Cryst. Solids* **2017**, *457*, 1–8. [CrossRef]
39. Szpikowska-Sroka, B.; Pawlik, N.; Goryczka, T.; Pisarski, W.A. Effect of the initial reagents concentration on final crystals size and luminescence properties of PbF_2:Eu^{3+} phosphors. *J. Alloys Compd.* **2008**, *730*, 150–160. [CrossRef]

40. Jamalaiah, B.C.; Suresh Kumar, J.; Mohan Babu, A.; Rama Moorthy, L. Spectroscopic studies of Eu^{3+} ions in LBTAF glasses. *J. Alloys Compd.* **2009**, *478*, 63–67. [CrossRef]
41. Venkatramu, V.; Babu, P.; Jayasankar, C.K. Fluorescence properties of Eu^{3+} ions doped borate and fluoroborate glasses containing lithium, zinc and lead. *Spectrochim. Acta Part A* **2006**, *63*, 276–281. [CrossRef]
42. Ćirić, A.; Stojadinović, S.; Sekulić, M.; Dramićanin, M.D. JOES: An application software for Judd-Ofelt analysis from Eu^{3+} emission spectra. *J. Lumin.* **2019**, *205*, 351–356. [CrossRef]
43. Haouari, M.; Ben Slimen, F.; Maaoui, A.; Gaumer, N. Structural and spectroscopic properties of Eu^{3+} doped tellurite glass containing silver nanoparticles. *J. Alloys Compd.* **2018**, *743*, 586–596. [CrossRef]
44. Liang, H.; Yang, Z.; Xiao, L.; Xie, F. Radiative transition propability of a europium (III) chelating polymer. *Optoelecton. Adv. Mater. Rapid Commun.* **2010**, *4*, 1396–1399.
45. Bebars, S.; Gadallah, A.S.; Khedr, M.A.; Abou Kana, M.T.H. Photoluminescent properties of the europium and terbium complexes covalently bonded to functionalized mesoporous material PABA-MCM-41. *J. Lumin.* **2017**, *192*, 949–956. [CrossRef]
46. Kumar, J.S.; Pavani, K.; Babu, A.M.; Giri, N.K.; Rai, S.B.; Moorthy, L.R. Fluorescence characteristics of Dy^{3+} ions in calcium fluoroborate glasses. *J. Lumin.* **2010**, *130*, 1916–1923. [CrossRef]